Novel Efficient Precoding Techniques for Multiuser MIMO Systems

This thesis is submitted in partial fulfilment of the requirements for Doctor of Philosophy (Ph.D.)

Keke Zu

Communications Research Group

Department of Electronics

University of York

May 2013

Abstract

In Multiuser MIMO (MU-MIMO) systems, precoding is essential to eliminate or minimize the multiuser interference (MUI). However, the design of a suitable precoding algorithm with good overall performance and low computational complexity at the same time is quite challenging, especially with the increase of system dimensions. In this thesis, we explore the art of novel low-complexity high-performance precoding algorithms with both linear and non-linear processing strategies.

Block diagonalization (BD)-type based precoding techniques are well-known linear precoding strategies for MU-MIMO systems. By employing BD-type precoding algorithms at the transmit side, the MU-MIMO broadcast channel is decomposed into multiple independent parallel SU-MIMO channels and achieves the maximum diversity order at high data rates. The main computational complexity of BD-type precoding algorithms comes from two singular value decomposition (SVD) operations, which depend on the number of users and the dimensions of each user's channel matrix. In this thesis, two categories of low-complexity precoding algorithms are proposed to reduce the computational complexity and improve the performance of BD-type precoding algorithms. One is based on multiple LQ decompositions and lattice reductions. The other one is based on a channel inversion technique, QR decompositions, and lattice reductions to decouple the MU-MIMO channel into equivalent SU-MIMO channels. Both of the two proposed precoding algorithms can achieve a comparable sum-rate performance as BD-type precoding algorithms, substantial bit error rate (BER) performance gains, and a simplified receiver structure, while requiring a much lower complexity.

Tomlinson-Harashima precoding (THP) is a prominent nonlinear processing technique employed at the transmit side and is a dual to the successive interference cancelation (SIC) detection at the receive side. Like SIC detection, the performance of THP strongly depends on the ordering of the precoded symbols. The optimal ordering algorithm, however, is impractical for MU-MIMO systems with multiple receive antennas. We propose a multi-branch THP (MB-THP) scheme and algorithms that employ multiple transmit processing and ordering strategies along with a selection scheme to mitigate interference

in MU-MIMO systems. Two types of multi-branch THP (MB-THP) structures are proposed. The first one employs a decentralized strategy with diagonal weighted filters at the receivers of the users and the second uses a diagonal weighted filter at the transmitter. The MB-MMSE-THP algorithms are also derived based on an extended system model with the aid of an LQ decomposition, which is much simpler compared to the conventional MMSE-THP algorithms. Simulation results show that a better BER performance can be achieved by the proposed MB-MMSE-THP precoder with a small computational complexity increase.

Contents

List of Figures

List of Tables

Acknowledgements

First and foremost, I would like to express my deepest gratitude to my supervisor, Prof. Rodrigo C. de Lamare for his professional guidance and unconditional support throughout my years at York. I thank him for the countless hours he spent with me, discussing everything from research to career choice, reading my papers, giving comments and suggestions. I am also thankful to Prof. Martin Haardt for his great advice and professional suggestions. Special thanks are also extended to my thesis advisor Dr. Yuriy Zakharov for his time and valuable comments. I have benefited a lot from the discussions and insightful conversations with them.

I feel happy to be part of the Communications Research Group, the staff here is so nice and kind. I still remember the pleasant experience to work with Dr. Paul D Mitchell as the assistant of ISWCS 2010 International Conference. I am also very grateful for the help from the IT support team. Every time Mr Paul Breslin will bring some jokes to subside the boring software installation time. But, if you could give me the administrative password, I will be more than happy. Thank you for all the lectures of Introduction to Communications, Introduction to Signal Processing, Digital Filter, Signal Processing for Communications, Adaptive Filter, Detection and Estimation, DSP Architectures, Maths for Music Technology. I am not only got a good memory to work with you as the demonstrator but also I improved my understanding of these subjects by teaching the students.

My deepest gratitude is expressed to my parents for their selfless support. The encouragement from them is always my forward momentum. Finally, I would also take this chance

to thank all the staff, colleagues, and friends who are not listed, for all your kind concern, support and help!

Declaration

Some of the work presented in this thesis has been published at academic conferences, journals or submitted to journals. These publications are listed at the end of Chapter 1.

To the best knowledge of the author, all work in this thesis claimed as original is so. Any research not original is clearly stated, and references and acknowledgements to other researchers have been given as appropriate.

Symbols

$\approx$	approximately equal to
$\lfloor x+y \rfloor$	floor function
$\lceil x+y \rceil$	ceiling function
$\lceil \cdot \rfloor$	round function
$\sum$	summation
$\bigotimes$	Kronecker product
$\min$	minimum
$\max$	maximum
$\mathbf{0}_m$	$m \times m$ all zeros matrix
$\boldsymbol{I}_m$	$m \times m$ identity matrix
$\boldsymbol{A}^T$	transpose of $\boldsymbol{A}$
$\boldsymbol{A}^H$	conjugate transpose of $\boldsymbol{A}$
$\boldsymbol{A}^{-1}$	inverse of $\boldsymbol{A}$
$\boldsymbol{A}^\dagger$	Moore-Penrose inverse (pseudoinverse) of $\boldsymbol{A}$
$\|\boldsymbol{A}\|^2$	squared Frobenius norm of $\boldsymbol{A}$
$\det(\boldsymbol{A})$	determinant of the matrix $\boldsymbol{A}$
$\mathrm{r}(\boldsymbol{A})$	rank of the matrix $\boldsymbol{A}$
$\mathrm{Tr}(\boldsymbol{A})$	trace of the matrix $\boldsymbol{A}$
$\mathrm{diag}\{\boldsymbol{A}_1, \boldsymbol{A}_2, \ldots, \boldsymbol{A}_K\}$	creates a block diagonal matrix with $\boldsymbol{A}_k$ on the main diagonal
$\Re(\cdot)$ and $\Im(\cdot)$	real and the imaginary parts of $\boldsymbol{A}$, respectively

Glossary

3G	Third Generation
4G	Fourth Generation
3GPP	3rd Generation Partnership Project
AOA	Angle of Arrival
BD	Block Diagonalization
BER	Bit Error Rate
BS	Base Station
CDF	Cumulative Distribution Function
CDMA	Code Division Multiple Access
CLLL	Complex LLL
CLR	Complex Lattice Reduction
CSI	Channel State Information
DPC	Dirty Paper Coding
FDD	Frequency Division Duplexing
FDMA	Frequency Division Multiple Access
GSM	Global System for Mobile Communications
IEEE	Institute of Electrical and Electronics Engineers
ISI	Inter-symbol Interference
LLL	Lenstra Lenstra Lovsz
LR	Lattice Reduction
MAP	Maximum A Posteriori Algorithm
MIMO	Multiple Input Multiple Output
MISO	Multiple Input Single Output
ML	Maximum Likelihood
MLD	Maximum Likelihood Detection
MMSE	Minimum Mean Square Error
MSE	Mean Squared Error
MSI	Multi Stream Interference
MUI	Multi User Interference
MU-MIMO	Multiple User MIMO

NP-hard	Non-deterministic Polynomial-time hard
OFDM	Orthogonal Frequency Division Multiplexing
OSIC	Ordered Successive Interference Cancelation
PBD	Partial Block Diagonalization
PDF	Probability Distribution Function
QAM	Quadrature Amplitude Modulation
QoS	Quality of Service
QPSK	Quadrature Phase Shift Keying
SD	Sphere Decoding
SDMA	Space Division Multiple Access
SIC	Successive Interference Cancelation
SIMO	Single Input Multiple Output
SISO	Single Input Single Output
SINR	Signal to Interference and Noise Ratio
SM	Spatial Multiplexing
SNR	Signal-to-Noise Ratio
SO-THP	Successive Optimization THP
ST	Space Time
SU-MIMO	Single User MIMO
SVD	Singular Value Decomposition
TDD	Time Division Duplexing
TDMA	Time Division Multiple Access
THP	Tomlinson-Harashima precoding
TS	Tree Search
UE	User Equipment
UT	User Terminal
V-BLAST	Vertical-Bell Laboratory Layered Space-Time
WCDMA	Wideband Code Division Multiple Access
WiMAX	Worldwide Interoperability for Microwave Access
WLAN	Wireless Local Area Network
ZF	Zero Forcing

Chapter 1

Introduction

1.1 Current Trends of Wireless Communications

The origins of radio date back to 1861 when Maxwell, while at King's College in London, proposed a mathematical theory of electromagnetic waves [1]. A practical demonstration of the existence of such waves was performed by Hertz in 1887 at the University of Karlsruhe using stationary waves [2]. After this, the radio technique was applied in various areas. One of the best-known examples is the commercial wireless communication systems, with more than 7 billion devices connected globally by 2013 and predicted to reach over 10 billion devices by the end of 2016 [3]. According to a white paper from Cisco [3], the mobile data traffic will grow at a *Compound Annual Growth Rate* (CAGR) of 66 percent from 2012 to 2017, reaching 11.2 exabytes per month by 2017.

In order to meet the dramatically increased data traffic, the mobile communication industry is moving rapidly toward *fourth-generation* (4G) wireless systems, which include mobile WiMAX and *Long-Term Evolution* Advanced (LTE Advanced). Currently, a number of major operators such as Verizon have already initiated LTE service [4] and the 4G connections represent 0.9 percent of mobile connections today. With 4G networks, wireless internet connectivity will be faster and more affordable which will result in a substantial increase in wireless internet usage.

The emergence of extremely high rate applications such as high-definition video conference, however, presents new challenges to wireless networks. One issue that needs to be

addressed is how to meet the requirement of extremely high data rates. Another issue is that with the rapidly increasing demand for wireless data traffic, a massive network densification is required which is neither economically nor ecologically viable with the current cellular system architectures [5]. With these challenges, 5G wireless systems with virtually ubiquitous coverage are under discussion [6, 7]. Japanese operator NTT Docomo has successfully tested uplink packet transmissions at an ultra-fast 10Gbps based on a 16×8 *Multiple-Input Multiple-Output* (MIMO) system in December of 2012 [8]. In summary, the growth of global 4G deployments and the development of the beyond 4G (5G) techniques are the current general trends of wireless communication systems.

1.2 Problems of MU-MIMO Systems

The main problems faced by wireless communication systems can be attributed to two major aspects, namely, the limited radio spectrum resource and the complicated wireless propagation environment. With the continued development of industry and business, the requirement for radio spectrum is increasingly strong, and thus the suitable radio spectrum is becoming scarcer and more expensive. Meanwhile, wireless systems are inevitably faced with a complicated propagation environment. The three impact factors are noise, fading and interference. For noise, communication systems usually use the matched filtering method to maximize the *Signal-to-Noise-Ratio* (SNR) [9]. The way to overcome the fading effects mainly relies on equalization and diversity techniques. The art of dealing with interference is closely related with multiple access techniques [10], such as *Frequency Division Multiple Access* (FDMA), *Time Division Multiple Access* (TDMA), *Code Division Multiple Access* (CDMA), *Space Division Multiple Access* (SDMA), etc.

Because of its tremendous potential in addressing the limited spectrum resource and the system performance problems, *Multiple-Input Multiple-Output* (MIMO) technique have attracted intense research efforts in the wireless communications field. By producing multiple transmitting channels in space, the spectrum efficiency has been greatly increased without additional bandwidth or increased transmit power. MIMO systems have already been employed in the existing 802.11n [11] and 802.16e [12] standards, and are among the core techniques in the next generation wireless systems [13, 14]. The research works

in [15–17] pointed out that for the independent and identically distributed (i.i.d.) Gaussian noise channel, the capacity of *Single-User MIMO* (SU-MIMO) systems can grow linearly with the number of transmit or receive antennas. For the capacity of *Multiuser-MIMO* (MU-MIMO) systems, it was showed that similar capacity scaling can be achieved by using *Dirty Paper Coding* (DPC) techniques [18]. The vision for next generation cellular networks includes data rates approaching 100 Mb/s for highly mobile users and up to 1 Gb/s for low mobile or stationary users. This calls for efficient use of the existing spectrum and MU-MIMO systems are expected to play a key role in this context [19].

Some advantages of MU-MIMO systems can be obtained with the aid of precoding techniques. By precoding we mean all methods applied at the transmitter that facilitate detection at the receiver [20]. Although precoding is not a new concept and has been used in SU-MIMO systems as well, it was optional and used only to improve the SNR at the receiver [21]. However, in MU-MIMO systems precoding is essential to eliminate or minimize *Multiuser Interference* (MUI).

Precoding techniques are performed with the help of downlink *Channel State Information* (CSI). The assumption that full CSI is available at the transmit side is valid in *Time-Division Duplex* (TDD) systems because the uplink and downlink share the same frequency band. For *Frequency-Division Duplex* (FDD) systems, however, the CSI needs to be estimated at the receiver and fed back to the transmitter. With precoding techniques employed at the transmit side, the required computational effort for each user's receiver can be reduced and eventually the receiver structure can be simplified [22]. There are mainly two types of precoding techniques, linear and non-linear. Linear precoding is characterized by its simplicity since the data signal is linearly transformed at the transmitter. The nonlinear precoding is named from its nonlinear processing, and a superior performance is achieved compared to the linear precoding algorithms. A number of different techniques to address the issue of MU-MIMO downlink transmission and reception have been proposed [2, 22]. Currently, there are some challenges and problems for MU-MIMO precoding techniques in the following aspects:

- BER and sum-rate performance

  Unlike the received signal in SU-MIMO systems, the received signals of different

users in MU-MIMO systems not only suffer from the noise and the inter-antenna interference but are also affected by MUI. The conventional precoding techniques such as *Zero Forcing* (ZF) and *Minimum Mean Squared Error* (MMSE) precoding [20] can still be used for MU-MIMO systems, but they result in a reduced throughput and BER performance due to a higher transmit power required at transmit side.

- Computational complexity

  Because of the existence of MUI, the MU-MIMO broadcast channel needs to be decomposed into multiple independent parallel SU-MIMO channels first to achieve the maximum transmit diversity order or maximum sum-rate capacity. The conventional ways to achieve the parallel channels result in considerable computational complexity cost. It is a challenge to design a suitable precoding algorithm with good overall performance and low computational complexity at the same time for MU-MIMO systems.

- Distributed receive antennas

  In the MU-MIMO scenarios, the users are geographically distributed. This creates a challenge in decoding the received symbols since joint decoding requires each user to have the data received from all the receive antennas of all the users. It is impractical to achieve this level of coordination between all users.

- Scalability for a large number of antennas

  A configuration of up to 8 transmit antennas for the downlink is suggested in the LTE standard. A new amendment for the W-LAN standard IEEE 802.11ac also recommends up to 8 MIMO spatial streams. Configurations with dozens of antennas are now being considered [23]. High-dimensional MIMO systems or large MIMO systems are very promising for the next generation of wireless communication systems due to their potential to improve rate and reliability dramatically [24]. However, the applicability and scalability of the proposed precoding algorithms in the literature to the large MIMO systems is an issue.

1.3 Motivation

The conflict between performance and complexity of precoding algorithms becomes dramatically intense for large MU-MIMO systems, which implies novel efficient precoding techniques should be developed.

For traditional precoding, an important performance bound corresponds to the DPC. It has shown in [18] that the capacity of systems with i.i.d Gaussian interference is equal to that of interference free systems by utilizing DPC. However, it requires infinitely long codewords, which cannot be implemented in practice [25]. *Vector Perturbation* (VP) [26] can achieve near ideal DPC performance by minimizing the transmit power for each transmitted symbol. Again, the method requires the joint search of the optimal perturbation vector based on the *Sphere Decoding* (SD) algorithm [27, 28], which is a *Nondeterministic Polynomial* time (NP)-hard problem. In contrast, linear precoding algorithms, such as ZF, MMSE precoding, have much lower complexity but their performance can suffer dramatically due to noise enhancement if the channel matrix $\boldsymbol{H}$ is near singular.

As a generalization of the ZF precoding algorithm, *Block Diagonalization* (BD) and *Regularized Block Diagonalization* (RBD) based linear precoding algorithms have been proposed in [29, 30] for MU-MIMO systems. We term the BD and RBD based precoding schemes as BD-type precoding algorithms in this work for convenience. However, a relatively high computational complexity is required by the BD-type based precoding algorithms due to two *Singular Value Decomposition* (SVD) operations, which depend on the number of users and the dimensions of each user's channel matrix. Moreover, BD-type precoding cannot achieve the maximum transmit diversity order. The relatively high cost and limited BER performance of the BD-type precoding algorithms suggest that precoding algorithms for MU-MIMO with lower complexity and superior BER performance should be investigated.

The nonlinear *Tomlinson-Harashima Precoding* (THP) is another technique that can decompose the MU-MIMO channel into parallel channels by utilizing a successive preprocessing cancelation at the transmit side [20]. Because of MUI is canceled out successively, the performance of THP strongly depends on the ordering of the precoded symbols. The conventional THP algorithms, however, are mainly focused on the case of users with a

single receive antenna. For the case of users with multiple receive antennas, there are currently very few works in the literature. Furthermore, most of the ordering schemes for THP algorithms with single receive antenna are impractical for the users with multiple receive antennas due to the fact that the users are physically distributed. It is worth to further explore the structures of THP especially for the users equipped with multiple antennas.

1.4 Summary of Contributions

Based on the previously discussed problems and motivation, the contributions of this thesis are summarized below:

- A low-complexity LC-RBD-LR precoding algorithm is proposed for the replacement of the RBD algorithm. Simulation results show that the proposed algorithm can achieve almost the same sum-rate as RBD while offering a lower complexity and substantial BER gains with perfect as well as imperfect channel state information at the transmit side.

- A simple strategy based on a channel inversion technique, QR decompositions, and lattice reductions to decouple the MU-MIMO channel into equivalent SU-MIMO channels is proposed. Analytical and simulation results show that the proposed LR-S-GMI precoding algorithms can achieve a comparable sum-rate performance as BD-type precoding algorithms, substantial bit error rate (BER) performance gains, and a simplified receiver structure, while requiring a much lower complexity.

- A *Multi-Branch THP* (MB-THP) scheme and algorithms that employ multiple transmit processing and ordering strategies along with a selection scheme to mitigate interference in MU-MIMO systems is developed in this thesis. The MB-MMSE-THP algorithms are also derived based on an extended system model with the aid of an LQ decomposition, which is much simpler compared to the conventional MMSE-THP algorithms. Simulation results show that a better bit error rate (BER) performance can be achieved by the proposed MB-MMSE-THP precoder with a small computational complexity increase.

1.5 Thesis Outline

The thesis is organized into six Chapters as listed below:

- Chapter 2 conducts a literature review on the fundamentals of MIMO, including capacity aspects, detection techniques, and especially a comprehensive survey of the precoding algorithms reported in the literature so far, such as ZF, MMSE, B-D, RBD, DPC, THP, *Vector Perturbation* (VP), and *Lattice Reduction (LR) aided precoding*. The theoretical and methodological contributions to the MU-MIMO precoding are summarized. The chapter provides the MU-MIMO system model that will be used in the remainder for this thesis. Moreover, the characteristics, performance and complexity of these algorithms are described and compared, which provides a technical context for this thesis.

- In Chapter 3, we focus on the low-complexity replacement of RBD algorithm by building the equivalence between the SVD and QR decomposition. Simulation results of the proposed LC-RBD-LR precoding algorithm are given with perfect as well as imperfect CSI at the transmit side.

- In Chapter 4, we consider to reduce the computational complexity of BD-type precoding further. This leads us to employ a channel inversion scheme, instead of the first SVD operation, to obtain the equivalent parallel SU-MIMO channels. The proposed LR-S-GMI type precoding algorithms are derived and their behavior in terms of BER, sum-rate and computational complexity are analyzed.

- In Chapter 5, we consider the development of non-linear THP algorithms. Novel MB-THP algorithms are developed based on two basic THP structures. A comprehensive performance analysis is carried out in terms of error covariance matrix, sum-rate and computational complexity.

- In Chapter 6, conclusions and a discussion on possibilities for future work are presented.

1.6 List of Publications

Journal Papers

- K. Zu, R. C. de Lamare and M. Haardt, "Multi-Branch Tomlinson-Harashima Precoding Design for MU-MIMO Systems: Theory and Algorithms", (2nd round Review) IEEE Transactions on Communications, 2013.
- K. Zu, R. C. de Lamare and M. Haardt, "Low-Complexity Generalized Design of Block Diagonalization Type Precoding Algorithms for Multiuser MIMO Systems", Accepted for publication in IEEE Transactions on Communications, 2013.
- K. Zu and R. C. de Lamare, "Low-Complexity Lattice Reduction-Aided Regularized Block Diagonalization for MU-MIMO Systems", IEEE Communications Letters, vol. 16, no. 6, Jun. 2012.

Conference Papers

- K. Zu, R. C. de Lamare and M. Haardt, "Low-Complexity Lattice Reduction-Aided Channel Inversion Methods for Large Multi-User MIMO Systems", IEEE Asilomar Conference on Signals, Systems and Computers, Pacific Grove, USA, Oct. 2012.
- K. Zu, R. C. de Lamare and M. Haardt, "Lattice Reduction-Aided Regularized Block Diagonalization for Multiuser MIMO Systems", IEEE Wireless Communications and Networking Conference (WCNC), Paris, France, Apr. 2012.
- K. Zu and R. C. de Lamare, "Pre-Sorted Multiple-Branch Successive Interference Cancelation Detection for High-Dimensional MIMO Systems", ITG/IEEE Workshop on Smart Antennas, Dresden, Germany, Mar. 2012.
- K. Zu, R. C. de Lamare and M. Haardt, "Multi-Branch Tomlinson-Harashima Precoding for Single-User MIMO Systems", ITG/IEEE Workshop on Smart Antennas, Dresden, Germany, Mar. 2012.
- K. Zu and R. C. de Lamare "Switched Lattice Reduction-Aided Detection Techniques for MIMO Systems", Sensor Signal Processing for Defence Conference, London, UK, Sep. 2011.

- K. Zu, R. C. de Lamare, ”Lattice Reduction-Aided Preprocessing and Detection Techniques for MU-MIMO in Broadcast”, European Wireless Conference, Vienna, Austria, April. 2011.

Chapter 2

Literature Review

Contents

2.1 MIMO Systems

MIMO techniques were first investigated in point to point or SU-MIMO scenarios, that is, the *Base Station* (BS) or transmitter equipped with multiple transmit antennas and the *User Equipment* (UE) or receiver equipped with multiple receive antennas. Winters [16], Foschini [31], and Telatar [32] predicted that remarkable spectral efficiencies for wireless systems with multiple antennas when the channel exhibits rich scattering can be accurately obtained. SU-MIMO is one of the key techniques in *Long Term Evolution* (LTE) Release 8, which requires 300 Mb/s for *Downlink* (DL) and 75 Mb/s for *Uplink* (UL) throughput [21]. However, the LTE Release 10, also known as LTE-Advanced, targets the achievement of 1 Gb/s for DL and 500 Mb/s for UL. One of the key enabling features to meet this DL requirement is MU-MIMO. MU-MIMO systems refer to the case where a

BS or a transmitter with multiple antennas services multiple users simultaneously. The benefits offered by MIMO systems are built on two underlying gains *Spatial Diversity* (SD) and *Spatial Multiplexing* (SM), which come with the increased cost for *Radio Frequency* (RF) hardware.

2.1.1 Multiplexing and Diversity

Compared with the conventional *Single-Input Single-Output* (SISO) systems, MIMO systems have more degrees of freedom regarding the signal transmission. There are three major transmission models: Diversity [33, 34], Multiplexing [35], and Diversity mixed with Multiplexing [36].

2.1.1.1 MIMO Diversity

Wireless channels severely suffer from fading phenomena, which causes unreliability in data decoding. Fundamentally, the spatial diversity scheme sends multiple copies through multiple transmit antennas, so that the probability that all the signal components fade simultaneously is reduced. Therefore, the reliability of the data reception is enhanced and improved [2].

Receive diversity can be used in *Single-Input Multiple-Output* (SIMO) channels. The receive antennas see independently faded versions of the same signal. The receiver combines these signals so that the resultant signal exhibits considerably reduced fading [37]. The receive diversity order is characterized by the number of independently fading branches, and the maximum receive diversity order is equal to the number of receive antennas in SIMO channels. The transmit diversity is applicable to *Multiple-Input Single-Output* (MISO) channels [9, 10]. The typical transmit diversity transmission is Alamouti *Space Time* (ST) coding [33]. The transmit diversity order corresponds to the number of independently faded paths that a symbol passes through. Therefore, the maximum transmit diversity order of SIMO system is equal to the number of transmit antennas. For a general MIMO system with N_r receive antennas and N_t transmit antennas, the max-

imum diversity order that can be achieved is

$$D = N_r \times N_t, \tag{2.1}$$

where the channel between each transmit-receive antenna pair is assumed to fade independently.

2.1.1.2 MIMO Multiplexing

In spatial multiplexing, a high rate signal is split into multiple lower rate streams and each stream is transmitted from a different transmit antenna in the same frequency channel. Foschini [31] has shown that in the high-SNR regime, the capacity of a channel with *independent and identically distributed* (i.i.d.) Rayleigh fading between each transmit-receive antenna pair is given by

$$C(\mathrm{SNR}) = \min\{N_r, N_t\}\log(\mathrm{SNR}) + O(1), \tag{2.2}$$

where SNR is the signal to noise ratio. The spatial multiplexing transmission offers a linear increase with the number of receive or transmit antennas in the transmission rate for the same bandwidth and with no additional power expenditure [2]. spatial multiplexing is only possible in MIMO channels and compared with the spatial diversity transmission, the spatial multiplexing transmission aims to maximize the system capacity. One typical spatial multiplexing transmission model is the *Bell Laboratory Layered Space-Time* (BLAST) system [35]. The maximum multiplexing gain of the BLAST system is

$$r = \min(N_r, N_t), \tag{2.3}$$

where r is the multiplexing gain. The spatial multiplexing configuration can also be applied in a multiuser format. This allows a capacity increase proportional to the smaller value between the number of transmit antennas and the total number of receive antennas.

2.2 Channel Modeling

The main characteristic of wireless communication is that it is open to various fading, and usually communicate with mobile users. Thus, the transmission channel is time varying.

In land mobile communication systems, the radio wave may encounter buildings, trees, mountains, etc, and the transmitted signals will be reflected, scattered and diffracted. Then the received signals will fluctuate in amplitude, phase and angle, this is the so-called multi-path fading. On the other hand, because of the mobility of the UE, the time varying nature of the wireless channel is exacerbated further.

2.2.1 Environment of Wireless Transmission

The propagation loss when a radio wave is transmitted in the space can be summarized into three categories [9, 10]. They are path loss, shadow fading and multipath fading. The loss of received power is proportional to the distance [37]. The path loss exponent varies from 2.5 to 6 depending on the terrain and foliage [2]. Several empirically based path loss models have been developed such as Okumura, Hata, COST-231 and Erceg [38–41] models. Shadow fading represents the log term variation of the received signal power level and is also called large scale fading. The shadow fading is usually caused by shadowing effects of buildings or nature features and is determined by the local mean of a fast fading signal [2]. The multi-path fading is the rapid and tiny fluctuation generated by the signal scattering off objects between the transmitter and receiver, and it is also called small scale fading. The central limit theorem holds if there is sufficiently large scattering, which means the channel impulse response will be well-modeled as a Gaussian process irrespective of the distribution of the wave components. The envelope of the received signal has a Rayleigh density function given by [2]

$$f(x) = \frac{2x}{\Omega} e^{-\frac{x^2}{\Omega}} u(x), \tag{2.4}$$

where Ω is the average received power and $u(x)$ is the unit step function. If there is a direct or a *Line-of-Sight* (LOS) path present between the transmitter and the receiver, the distribution of the signal amplitude is Ricean

$$f(x) = \frac{2x(K+1)}{\Omega} e^{\left(-K-\frac{(K+1)x^2}{\Omega}\right)} I_0(2x\sqrt{\frac{K(K+1)}{\Omega}}) u(x), \tag{2.5}$$

where K is the Ricean factor which is the ratio of the power in the mean component of the channel to the power scattered component and $I_0(x)$ is the zero-order modified

Bessel function. We restrict the channel model to Rayleigh or Ricean fading in this work, however, more sophisticated Nakagami distribution can be found in [42].

The impact of small scale fading on the signal is mainly in three aspects: frequency selective fading, time selective fading, and space selective fading. In wireless communication systems, the coverage is mainly determined by the path loss and shadow fading, while the multipath fading is closely related to the quality of the transmission. So, if the system designers want to implement efficient and reliable communication, the multipath fading must be deeply studied.

2.2.2 Frequency Selective Fading

In a multipath propagation environment, several delayed and scaled versions of the transmitted signal arrive at the receiver. If a narrow impulse signal $\delta(t)$ was transmitted, the arrival time will be varied among the multipath signals. Thus, the received signal $r(t)$ will be composed of various impulse signals which have different time delays as described by

$$r(t) = \sum_{l}^{n} \alpha_l(t)\delta[(t - \tau_l(t))], \tag{2.6}$$

where the quantity $\alpha_l(t)$ is the fading factor of the lth path and $\tau_l(t)$ is the time delay of the lth path. The time difference between the last and first arrived resolvable delay signal is defined as the delay spread, denoted as $\tau_{\max}$ [9, 10]. However, it is more common to adopt the coherence bandwidth B_c to describe the impact of multipath fading, which is usually defined as

$$B_c = \frac{1}{\tau_{\max}}. \tag{2.7}$$

Then, the impact of multipath fading can be measured by the coherence bandwidth B_c. If the signal bandwidth B_s is smaller than B_c, it means all the multipath components arrived within the symbol duration. In other words, the frequency components in $r(t)$ undergo the same attenuation and phase shift in transmission through the channel, it is called frequency-nonselective or flat fading channel. Otherwise, if the signal bandwidth is greater than B_c, the arrived multipath components would go beyond the symbol duration, then, the symbols would be overlapped by each other and finally the *Inter Symbol*

Interference (ISI) would be generated, which results in the so called frequency selective fading.

2.2.3 Time Selective Fading

In wireless communication systems, the channel will be changed by every move from the receive side or transmit side. The frequency dispersion is used to describe the time selective fading, correspondingly, the two important parameters are Doppler frequency shift and coherence time. When the receiver is moving, the received signal frequency will be shifted compared with its original transmitted signal. The additional frequency shift is known as Doppler frequency shift, which can be described as follows

$$f = \frac{v}{\lambda}\cos(\theta), \tag{2.8}$$

where the quantity v is the velocity of the mobile station, λ is the carrier wavelength, θ is the angle between the incident radio wave and the direction of the mobile station. The maximum value of f is known as the maximum Doppler frequency shift f_m.

Because of the frequency spread of the channel, the impulse response of the channel will be randomly fluctuated, this phenomenon is known as time selective fading. The coherence time is typically defined as the time lag for which the signal autocorrelation coefficient reduces to 0.7, and it is inversely proportional to the Doppler spread [2], i.e.,

$$T_c = \frac{1}{f_m}. \tag{2.9}$$

If the transmission time is greater than T_c, the amplitude and phase change imposed by the channel varies considerably over the period of the transmission time, which is known as fast fading. Conversely, if the transmission time is less than the channel coherence time, the amplitude and phase change imposed by the channel can be considered roughly constant over the period of use, this is known as slow fading.

2.2.4 Space Selective Fading

In wireless communication with multiple antennas, the signals are scattered by various objects through the transmission paths. Angle spread at the receiver refers to the spread

in *Angle of Arrive* (AOA)s of the multipath components at the receive antenna array. With the presence of the angle spread, the antennas with different spatial location at the receive side will experience different angle spreads, which is known as the space selective fading [2].

The space selective fading is described by the coherence space D_c which is the maximum spatial separation when the channel is strongly correlated. When the distance d between the receive antennas is shorter than D_c the received signals will be considered to have a strong correlation between each other. Otherwise, the received signals will be considered as low correlation.

2.3 MIMO Channel Model

The main features of wireless channels are discussed in Section 2.2. In this Section, the discussion is around the MIMO channel model. The spatial channel model for MIMO systems with detailed parameters are given in 3GPP standards [43]. In this report, we focus on the general MIMO channel model and the descriptions for SU-MIMO and MU-MIMO systems are respectively addressed.

2.3.1 SU-MIMO Channel Model

The typical SU-MIMO channel is shown as follows in Figure 2.1, where $\boldsymbol{N}_b$ is the total

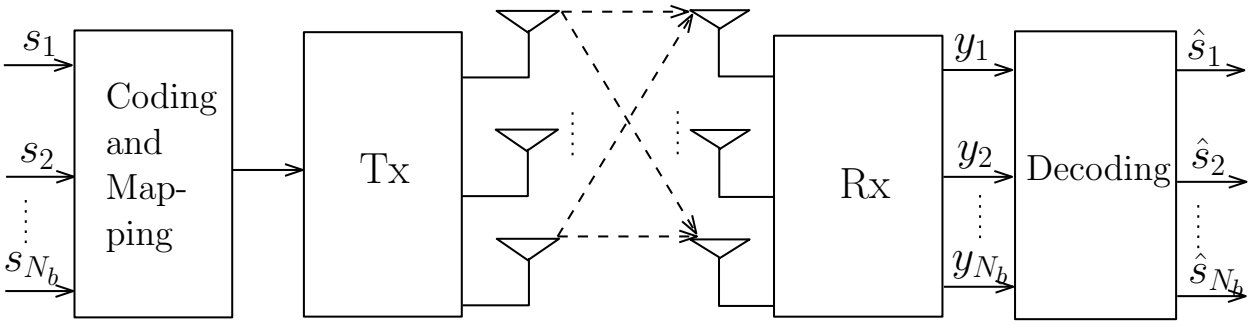

Figure 2.1: SU-MIMO Channel Model

number of transmit streams, the vector $\boldsymbol{s}$ is the transmit data, $\boldsymbol{y}$ denotes the received

signal, and $\hat{\boldsymbol{s}}$ is the estimated data.

We assume that the transmit antenna number is N_t, the receive antenna number is N_r and the maximum number of multipaths between the BS and UE is L. The channel statistical model can be expressed as [44]

$$\boldsymbol{H}(\tau, t) = \sum_{l=0}^{L-1} \boldsymbol{A}_l(t)\delta(\tau - \tau_l), \tag{2.10}$$

where the quantity $\boldsymbol{A}_l(t) \in \mathbb{C}^{N_r \times N_t}$ represents the lth path between the transmitter and receiver. If we adopt $h_{i,j}(\tau, t)$ to represent the impulse response between the jth transmit and the ith receive antenna, the channel matrix of SU-MIMO can be rewritten as

$$\boldsymbol{H}(\tau, t) = \begin{bmatrix} h_{1,1}(\tau,t) & h_{1,2}(\tau,t) & \dots & h_{1,N_t}(\tau,t) \\ h_{2,1}(\tau,t) & h_{2,2}(\tau,t) & \dots & h_{2,N_t}(\tau,t) \\ \vdots & \vdots & \ddots & \vdots \\ h_{N_r,1}(\tau,t) & h_{N_r,2}(\tau,t) & \dots & h_{N_r,N_t}(\tau,t) \end{bmatrix}, \tag{2.11}$$

where $h_{i,j}(\tau, t)$ is the function of time, delay and location of the receive antenna, and also includes the amplitude gain and phase rotation. If the transmitted signal vector is $\boldsymbol{s}(t) \in \mathbb{C}^{N_t \times 1}$, then the received signal vector is obtained as

$$\boldsymbol{y}(t) = \boldsymbol{H}(\tau, t) * \boldsymbol{s}(t) + \boldsymbol{n}(t), \tag{2.12}$$

where $\boldsymbol{n}(t) \in \mathbb{C}^{N_r}$ is the Gaussian noise with i.i.d. entries of zero mean and variance σ_n^2. In the flat fading channel, since the output at any instant of time is independent of inputs at previous times, the received signal can be expressed as

$$\boldsymbol{y} = \boldsymbol{H}\boldsymbol{s} + \boldsymbol{n}. \tag{2.13}$$

Another factor we should take into account is the spatial correlation caused by the scattering and insufficient spacing between adjacent antennas. A correlated channel matrix can be obtained using the Kronecker model [2]

$$\boldsymbol{H}_c = \boldsymbol{R}_r^{\frac{1}{2}} \boldsymbol{H} \boldsymbol{R}_t^{\frac{1}{2}}, \tag{2.14}$$

where $\boldsymbol{R}_r$ and $\boldsymbol{R}_t$ are receive and transmit covariance matrices with $\mathrm{tr}(\boldsymbol{R}_r) = N_r$ and $\mathrm{tr}(\boldsymbol{R}_t) = N_t$. Both $\boldsymbol{R}_r$ and $\boldsymbol{R}_t$ are positive semi-definite Hermitian matrices.

In the presence of receive or transmit correlation, the rank of $\boldsymbol{H}_c$ is constrained by $\min(r(\boldsymbol{R}_r), r(\boldsymbol{R}_t))$. Therefore, the system will suffer both BER and sum-rate performance losses because of the rank deficiency. For the case of an urban wireless environment, the UE is always surrounded by rich scattering objects and the channel is most likely independent Rayleigh fading at the receive side. From the transmitter's point of view, however, the spatial structure of the channel is governed by remote scattering objects and will most likely result in a highly spatially correlated scenario [45]. Hence, we assume $\boldsymbol{R}_r = \boldsymbol{I}_{N_r}$, and we have

$$\boldsymbol{H}_c = \boldsymbol{H}\boldsymbol{R}_t^{\frac{1}{2}}. \tag{2.15}$$

To study the effect of antenna correlations, random realizations of correlated channels are generated according to the exponential correlation model [46] such that the elements of $\boldsymbol{R}_t$ are given by

$$R_t(i,j) = \begin{cases} r^{j-i}, & i \leq j \\ r_{j,i}^*, & i > j \end{cases}, |r| \leq 1, \tag{2.16}$$

where r is the correlation coefficient between any two neighboring antennas. This correlation model is suitable for our study since, in practice, the correlation between neighboring channels is higher than that between distant channels.

2.3.2 MU-MIMO Channel Model

We consider an uncoded MU-MIMO downlink channel, with N_t transmit antennas at the base station (BS) and N_k receive antennas at the kth user equipment (UE). With K users in the system, the total number of receive antennas is $N_r = \sum_{k=1}^{K} N_k$. A block diagram of such a system is illustrated in Figure 2.2. Where the vectors $\boldsymbol{s}_k$, $\boldsymbol{P}_k$, $\boldsymbol{x}_k$, and $\boldsymbol{y}_k$ denote the transmit data, precoding matrix, precoded data, and the received data, respectively.

From the system model, the combined channel matrix $\boldsymbol{H}$ and the joint precoding matrix $\boldsymbol{P}$ are given by

$$\boldsymbol{H} = [\boldsymbol{H}_1^T \ \boldsymbol{H}_2^T \ \ldots \ \boldsymbol{H}_K^T]^T \in \mathbb{C}^{N_r \times N_t}, \tag{2.17}$$

$$\boldsymbol{P} = [\boldsymbol{P}_1 \ \boldsymbol{P}_2 \ \ldots \ \boldsymbol{P}_K] \in \mathbb{C}^{N_t \times N_r}, \tag{2.18}$$

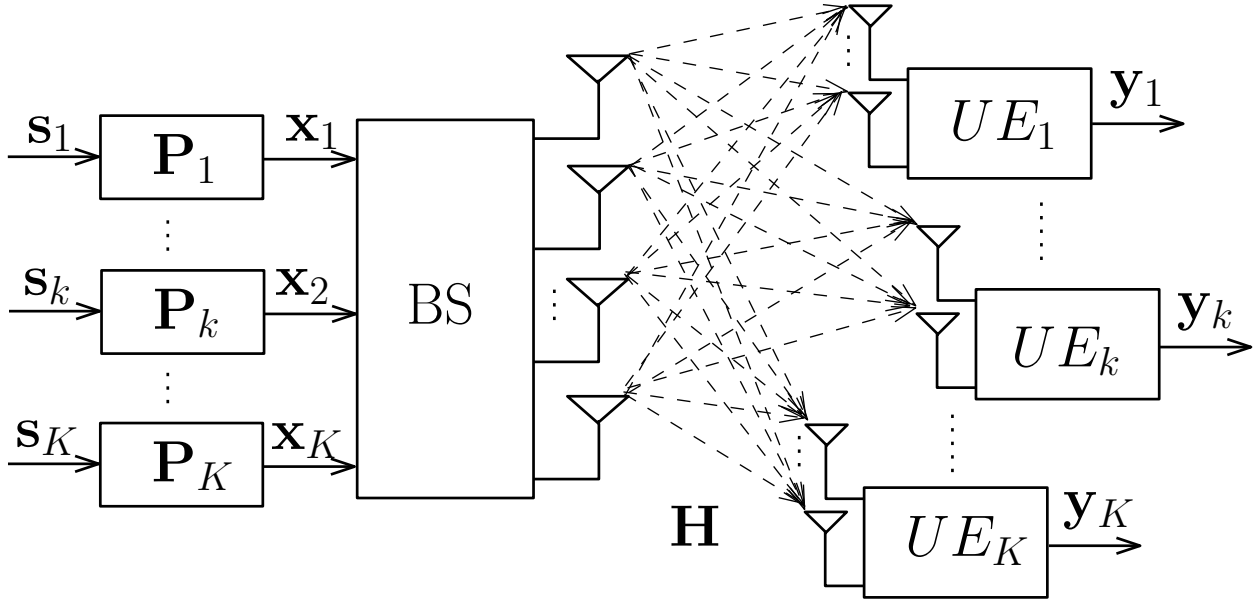

Figure 2.2: MU-MIMO Channel Model

where $\boldsymbol{H}_k \in \mathbb{C}^{N_k \times N_t}$ is the ith user's channel matrix. The quantity $\boldsymbol{P}_k \in \mathbb{C}^{N_t \times N_k}$ is the kth user's precoding matrix. For a flat fading MIMO channel, the received signal $\boldsymbol{y}_k \in \mathbb{C}^{N_k \times 1}$ at the kth user is given by

$$\boldsymbol{y}_k = \boldsymbol{H}_k \boldsymbol{x}_k + \boldsymbol{H}_k \sum_{j=1, j \neq k}^{K} \boldsymbol{x}_j + \boldsymbol{n}_k, \tag{2.19}$$

where the quantity $\boldsymbol{x}_k = \boldsymbol{P}_k \boldsymbol{s}_k \in \mathbb{C}^{N_t \times 1}$ is the kth user's transmitted signal, and $\boldsymbol{n}_k \in \mathbb{C}^{N_k \times 1}$ is the kth user's Gaussian noise with independent and identically distributed (i.i.d.) entries of zero mean and variance σ_n^2.

2.4 Capacity of MIMO Systems

Generally, there are two transmission techniques for MIMO wireless systems as discussed above, spatial diversity and spatial multiplexing. Although the full diversity can be achieved by the *Space Time Block Codes* (STBC), they suffer a loss in terms of capacity or sum-rate [47] since its aim is to enhance reliability and usually the same transmit data are sent by the multiple antennas. The maximum transmission data rate can be achieved by the spatial multiplexing due to the fact that multiple independent data streams are

simultaneously transmitted [2].

2.4.1 SU-MIMO Capacity

For a SU-MIMO system shown in Figure 2.1, with the received signal obtained in (2.13) the channel capacity is expressed as [48]

$$C = \max_{\mathrm{tr}(\boldsymbol{R}_{ss})=N_t} \log_2 \det\Big(\boldsymbol{I}_{N_r} + \frac{E_s}{N_t N_0}\boldsymbol{H}\boldsymbol{R}_{ss}\boldsymbol{H}^H\Big), \tag{2.20}$$

where E_s is the total average transmit energy, N_0 is the noise power, and $\boldsymbol{R}_{ss} = \mathrm{E}\{\boldsymbol{s}\boldsymbol{s}^H\}$ is the autocorrelation of the transmitted signal $\boldsymbol{s}$.

The capacity in (2.20) is dependent on the CSI at the transmit side. The scenario in which CSI is known at the transmit side is termed as *Closed-loop* (CL) system. The *Open-loop* (OL) system is that in which CSI is not known at the transmit side and only the statistics of $\boldsymbol{H}$ are known. For the OL MIMO systems, the transmit energy is equally spread among all the transmit antennas since the channel information is not accessible at the transmit side, that is, $\boldsymbol{R}_{ss} = \boldsymbol{I}_{N_t}$. In this case, the channel capacity of OL MIMO systems is obtained as

$$C = \log_2 \det\Big(\boldsymbol{I}_{N_r} + \frac{E_s}{N_t N_0}\boldsymbol{H}\boldsymbol{H}^H\Big). \tag{2.21}$$

Using the eigne-decomposition $\boldsymbol{H}\boldsymbol{H}^H = \boldsymbol{Q}\boldsymbol{\Lambda}\boldsymbol{Q}^H$ and the identity $\det(\boldsymbol{I}_m + \boldsymbol{A}\boldsymbol{B}) = \det(\boldsymbol{I}_n + \boldsymbol{B}\boldsymbol{A})$ for matrices $\boldsymbol{A} \in \mathbb{C}^{m\times n}$ and $\boldsymbol{B} \in \mathbb{C}^{n\times m}$, the channel capacity in (2.21) is simplified to

$$C = \log_2 \det\Big(\boldsymbol{I}_{N_r} + \frac{E_s}{N_t N_0}\boldsymbol{\Lambda}\Big) = \sum_{i=1}^{r} \log_2\Big(1 + \frac{E_s}{N_t N_0}\lambda_i\Big), \tag{2.22}$$

where $r = \min(N_t, N_r)$ is the rank of the channel matrix and λ_i denotes the ith positive eigenvalues of $\boldsymbol{H}\boldsymbol{H}^H$. Equation (2.22) describes how a MIMO channel is converted into r SISO channels with power gain λ_i and transmit power $\frac{E_s}{N_t}$.

For the CL MIMO system, different transmit energies can be allocated to each transmit antenna according to the CSI at the transmit side. Then, the autocorrelation matrix $\boldsymbol{R}_{ss}$ here is a diagonal matrix with different transmit power γ_i on the diagonal. Using the SVD of $\boldsymbol{H} = \boldsymbol{U}\boldsymbol{\Sigma}\boldsymbol{V}^H$ with $\boldsymbol{U} \in \mathbb{C}^{N_r\times N_r}$ and $\boldsymbol{V} \in \mathbb{C}^{N_t\times N_t}$ unitary matrices, and $\boldsymbol{\Sigma} \in$

$\mathbb{C}^{N_r \times N_t}$ a rectangular matrix, whose main diagonal elements $\sqrt{\lambda_i}$ are singular values of $\boldsymbol{H}$, assuming the rank of the channel matrix is r (2.20) can be rewritten as

$$C = \sum_{i=1}^{r} \log_2\Big(1 + \frac{E_s \gamma_i}{N_t N_0}\lambda_i\Big). \tag{2.23}$$

The capacity in (2.23) can be maximized by solving the power allocation problem below

$$C_{\max} = \max_{\sum_{i=1}^{r}\gamma_i = N_t} \sum_{i=1}^{r} \log_2\Big(1 + \frac{E_s \gamma_i}{N_t N_0}\lambda_i\Big). \tag{2.24}$$

The optimal value $\gamma_i^{(\mathrm{o})}$ for equation (2.24) can be found by the *Water Filling* (WF) algorithm [49, 50] as

$$\begin{aligned} \gamma_i^{(\mathrm{o})} &= \Big(\mu - \frac{N_t N_0}{E_s \lambda_i}\Big)^+, \; i = 1, \cdots, r \\ \sum_{i=1}^{r} \gamma_i^{(\mathrm{o})} &= N_t, \end{aligned} \tag{2.25}$$

where μ is a constant and $(x)^+$ is defined as

$$(x)^+ = \begin{cases} x & if \; x \geq 0 \\ 0 & if \; x < 0. \end{cases} \tag{2.26}$$

Therefore, the resulting capacity of a CL MIMO channel is given by the sum of the individual parallel SISO channel capacities

$$C_{\max} = \sum_{i=1}^{r} \log_2\Big(1 + \frac{E_s \gamma_i^{(\mathrm{o})}}{N_t N_0}\lambda_i\Big). \tag{2.27}$$

Since the rank $r = \min(N_t, N_r)$ in (2.22) and (2.27), the capacity gain of SU-MIMO system is scaled by $\min(N_t, N_r)$, that is

$$C_{SU-MIMO} \propto \min(N_t, N_r). \tag{2.28}$$

2.4.2 MU-MIMO Capacity

In typical cellular systems, the number of receive antennas at the battery powered user is often smaller than the number of transmit antennas at the *Base Station* (BS), which limits the capacity gain in (2.28). MU-MIMO systems have drawn a wide attention recently because of the potential to achieve higher multiplexing gains. A typical MU-MIMO system

is displayed in Figure 2.2, in which K users each with N_k receive antennas are served by a single BS with N_t transmit antennas. The *Downlink* (DL) and *Uplink* (UL) channels are referred as *Broadcast Channel* (BC) and *Multiple Access Channel* (MAC) respectively in the MU-MIMO scenarios.

MAC with two (and also three) input users was first presented by Ahlswede in [51], which can be regarded as one of the first major breakthroughs in the field of multiple-user channels since Shannons paper [52]. The MIMO MAC capacity region with $N_t = N_k = 1$ and $K > 1$ in [51] is equivalent to that of the multiple SISO links

$$C_{\mathrm{MAC}}(N_t = N_k = 1, K > 1) = \left\{ \sum_{k \in S} R_k \leq \log(1 + \sum_{k \in S} P_k |h_k|^2), \forall S \subseteq \{1, \cdots, K\} \right\}, \tag{2.29}$$

where the quantity P_k, and R_k respectively denote the kth user's transmit power, and sum-rate. For the case $N_k = 1$, $N_t > 1$ and $K > 1$, since all data streams of K independent users are available for the BS, the MAC of MU-MIMO is equivalent to the (K, N_t) OL SU-MIMO uplink channel. Similar to the SU-MIMO systems, it is shown in [15] that the sum-rate capacity of MAC is proportional to $\min(K, N_t)$, that is

$$C_{\mathrm{MAC}}(N_k = 1, N_t > 1, K > 1) = \log_2 \det\Big(\boldsymbol{I}_{N_t} + \frac{P}{K} \boldsymbol{H} \boldsymbol{H}^H \Big), \tag{2.30}$$

where the quantity P is the total transmit power and each antenna transmits with power $\frac{P}{K}$. From (2.30), there is no coordination required among users. Another thing can be verified is that the sum capacity in (2.30) is scaled by $\min(K, N_t)$, so the N_t-fold increase in the sum-rate can be obtained as long as K is larger than N_t, which is usually not the case for SU-MIMO systems as N_r is often smaller than N_t.

For the case $N_k > 1$, $N_t > 1$ and $K > 1$, suppose user k transmits using a fixed covariance $\boldsymbol{Q}_k$

$$\boldsymbol{Q}_k = \mathrm{E}[\boldsymbol{s}_k \boldsymbol{s}_k^H]. \tag{2.31}$$

The achieving sum-rate for K users is given by [53]

$$C_{\mathrm{MAC}}(N_k = 1, N_t > 1, K > 1) = \log_2 \det\Big(\boldsymbol{I} + \sum_{j=1}^{K} \frac{1}{N_0} \boldsymbol{H}_j \boldsymbol{Q}_j \boldsymbol{H}_j^H \Big). \tag{2.32}$$

For the maximization of the sum-rate in (2.32), each user needs to determine its optimum covariance by using convex optimization techniques, which requires the information of all the other users' channel [54].

The MIMO BC channels belong to the category of non-degraded vector channels, for which the capacity region remains unknown. However, by using the DPC strategy in [18], a duality between broadcast channels and MAC has been established in [55–57]. The authors in [57] have shown that the dirty paper region is exactly equal to the capacity region of the dual MIMO MAC, with the transmitters having the same sum power constraint as the MIMO BC, which is given by

$$C_{\mathrm{BC}} = \cup_{\sum_{k=1}^{K} P_k \leq P} C_{\mathrm{MAC}}\big(\{\boldsymbol{H}_k\}, \{P_k\}\big). \tag{2.33}$$

Therefore, we can determine weighted sum-rates and transmit covariances in the MAC domain, then determine the BC transmit covariances by using the MAC-BC duality in (2.33).

2.5 Interference Suppression

Spatially multiplexed MIMO (SM-MIMO) systems can transmit higher data-rate than MIMO systems using diversity techniques as we discussed in Section 2.4. For the wireless system engineer, however, two key factors that are responsible for the advantages of SM-MIMO systems are how to design the optimized signal transmission at the transmit side and the appropriate signal detection at the receive side. The detection and precoding strategies are studied in this section.

2.5.1 MIMO Detection Techniques

There are a variety of detectors for MIMO systems, and we focus on the classic MIMO detection algorithms in this section. We begin with the *Maximum Likelihood Detection* (MLD) for the reason that it can achieve a full diversity gain, and the BER performance of MLD can be used as the lower bound to measure the performance of other detection algorithms.

2.5.1.1 MLD and SD

For a $N_r \times N_t$ MIMO system, given the channel matrix $\boldsymbol{H}$ and the transmitted signal $\boldsymbol{s}$, the *Probability Density Function* (PDF) of the received signal $\boldsymbol{y}$ is

$$p(\boldsymbol{y}/\boldsymbol{H}, \boldsymbol{s}) = \frac{1}{(2\pi\sigma_n^2)^{N_r}} \exp(-\frac{\|\boldsymbol{y} - \boldsymbol{H}\boldsymbol{s}\|^2}{2\sigma_n^2}), \tag{2.34}$$

where N_r is the number of receive antennas and σ_n^2 is the variance of the noise. The received signal $\boldsymbol{y}$ in (2.34) is usually known, thus, the MLD problem consists of determining the vector $\boldsymbol{s}$ with the highest a posteriori probability below

$$\tilde{\boldsymbol{s}} = \arg\max \frac{1}{(2\pi\sigma_n^2)^{N_r}} \exp(-\frac{\|\boldsymbol{y} - \boldsymbol{H}\boldsymbol{s}\|^2}{2\sigma_n^2}), \tag{2.35}$$

which is equivalent to solving the following *Integer Least Square* (ILS) problem,

$$\boldsymbol{s}_{\mathrm{MLD}} = \arg \min_{\boldsymbol{s} \in A^{N_r}} \|\boldsymbol{y} - \boldsymbol{H}\boldsymbol{s}\|^2, \tag{2.36}$$

where A is the set of the constellation points. A straightforward method for solving (2.36) would be an exhaustive search over all possible points, which is usually termed as MLD in the wireless communication field. The probability of detection error is minimized by MLD, however, its complexity grows exponentially with the number of constellation points and the number of transmitted streams. Therefore, the MLD is usually impractical for systems with a large number of antennas and a high order modulation.

In order to reduce the computational complexity of MLD, the *Sphere Decoding* (SD) [27, 28] algorithm solves (2.36) by performing a search in a hyper sphere around the received vector $\boldsymbol{y}$, thereby reducing the search space and hence the required computational effort [58, 59]. A point belongs to the sphere if

$$d^2 \geq \|\boldsymbol{y} - \boldsymbol{H}\boldsymbol{s}\|^2, \tag{2.37}$$

where d is the search radius. From (2.36), it is very important to choose an appropriate initial sphere radius. If d is too large, we may obtain too many points and the search may remain exponential in size, whereas if d is too small, we may obtain no points inside the sphere. The search radius d can be chosen based on the statistical properties of the noise such that with a high probability we find a lattice point inside the sphere. The radius is selected to be a scaled variance of the noise in such a way that with a high probability we find a lattice point inside the sphere [58, 60].

2.5.1.2 Linear Detection

In practice, the *Linear Detection* (LD) algorithms are more feasible due to their lower complexity compared to the MLD. This is often observed for a sufficient number of constellation points and antennas. The performance of the linear detectors, however, is inferior to that of the MLD, so they are usually considered a suboptimal detection algorithm [2].

LD algorithms take the received vector $\boldsymbol{y}$ and premultiply it by a matrix $\boldsymbol{G}$. The matrix $\boldsymbol{G}$ can be optimized by using different criteria, two of the most popular are the *Zero Forcing* (ZF) criterion and *Minimum Mean Square Error* (MMSE) criterion. Assuming the channel matrix is reversible, the ZF linear detector is designed to completely eliminate the interference, that is

$$\boldsymbol{G}_{\mathrm{ZF}} = (\boldsymbol{H}^H \boldsymbol{H})^{-1} \boldsymbol{H}^H. \tag{2.38}$$

The ZF detection filter at the receive side is actually the left inverse of the channel matrix $\boldsymbol{H}$ from (2.38). The estimation of the transmitted symbol $\boldsymbol{s}$ is

$$\tilde{\boldsymbol{s}}_{\mathrm{ZF}} = \boldsymbol{s} + \boldsymbol{G}_{\mathrm{ZF}} \boldsymbol{n}. \tag{2.39}$$

Then, the error covariance matrix of ZF detection is obtained as

$$\boldsymbol{\Phi}_{\mathrm{ZF}} = E\{(\tilde{\boldsymbol{s}}_{\mathrm{ZF}} - \boldsymbol{s})(\tilde{\boldsymbol{s}}_{\mathrm{ZF}} - \boldsymbol{s})^H\} = \sigma_n^2 \boldsymbol{G}_{\mathrm{ZF}} {\boldsymbol{G}_{\mathrm{ZF}}}^H. \tag{2.40}$$

From (2.40), the noise power can be significantly increased by $\boldsymbol{G}_{\mathrm{ZF}}$ especially when the channel is ill conditioned. Thus, the BER performance of the ZF detector will be greatly reduced. This phenomenon is termed as *noise enhancement* in wireless communication.

In order to reduce the effects of noise amplification caused by the ZF filter, the MMSE criterion takes the noise term into account and is designed according to

$$\boldsymbol{G}_{\mathrm{MMSE}} = \arg\min_{\boldsymbol{G}} E\{\|\boldsymbol{G}\boldsymbol{y} - \boldsymbol{s}\|\}. \tag{2.41}$$

By utilizing the orthogonality principle $E\{\|\boldsymbol{G}\boldsymbol{y} - \boldsymbol{s}\|\boldsymbol{y}^H\} = \boldsymbol{0}$, the $\boldsymbol{G}_{\mathrm{MMSE}}$ is easily derived as

$$\boldsymbol{G}_{\mathrm{MMSE}} = (\boldsymbol{H}^H \boldsymbol{H} + \sigma^2 \boldsymbol{I}_{N_t})^{-1} \boldsymbol{H}^H. \tag{2.42}$$

As shown in [61], the linear MMSE detector is equivalent to ZF with respect to an extended system model. The extended channel matrix $\underline{\boldsymbol{H}}$ and the extended received signal $\underline{\boldsymbol{y}}$ are given by

$$\underline{\boldsymbol{H}} = \begin{bmatrix} \boldsymbol{H} \\ \sigma_n \boldsymbol{I}_{N_t} \end{bmatrix} \text{ and } \underline{\boldsymbol{y}} = \begin{bmatrix} \boldsymbol{y} \\ \boldsymbol{0}_{N_t,1} \end{bmatrix}, \tag{2.43}$$

The MMSE filter can have a similar format to that of the ZF filter,

$$\boldsymbol{G_{MMSE}} = (\underline{\boldsymbol{H}}^H \underline{\boldsymbol{H}})^{-1} \underline{\boldsymbol{H}}^H, \tag{2.44}$$

From (2.44), it is the property of $\underline{\boldsymbol{H}}$ that determines the noise amplification in the MMSE detection case. A better performance can be obtained by performing the MMSE detection since the MUI mitigation is balanced with noise enhancement.

2.5.1.3 Successive Interference Cancelation

The *Successive Interference Cancelation* (SIC) detection is a good trade-off between the MLD and the LD, in the view of BER performance and computational complexity [62]. The filters employed in SIC detection are mainly based on the linear filters which are discussed above. The key idea of SIC detection is layer peeling, that is, the first symbol is decoded first, and then the decoded symbol is canceled in the next layer peeling. This manipulation is repeated layer by layer until all the symbols are decoded from the received signal. By layer peeling, the interference caused by the already detected symbols is canceled. The conventional structure of the SIC detection has been given in [2, 35], and multiple channel inversion operations are required, which increases the computational complexity. The SIC detection can be equivalently implemented by a QR decomposition [61, 63], which calculates $\boldsymbol{H} = \boldsymbol{QR}$, and then computes $\boldsymbol{y}' = \boldsymbol{Q}^H \boldsymbol{y}$. The computational complexity can be reduced dramatically by the QR decomposition based SIC detection. The detection steps are summarized bellow

$$\begin{aligned} \hat{s}_{N_b} &= Q\left(\frac{y'_{N_b}}{r_{N_b,N_b}}\right), \\ \hat{s}_i &= Q\left(\frac{y'_i - \sum_{j=i+1}^{N_b} r_{i,j}\hat{s}_j}{r_{i,i}}\right), \end{aligned} \tag{2.45}$$

where the function $Q(\cdot)$ quantizes the received signal to the nearest transmitted symbols, the quantity N_b is the number of transmit streams. Finally, the estimated transmit signal $\hat{\boldsymbol{s}} = [\hat{s}_1, ..., \hat{s}_{N_b}]^T$.

From the SIC detection steps in (2.45), it is possible that the first decoded stream is the weakest one among all the streams, and thus it is highly possible that the first decoded symbol $\hat{s}_{N_t}$ is wrong. The error will be passed on layer by layer, resulting in a performance loss of SIC detection. This phenomenon is called *error propagation*. For the reduction of the *error propagation* effect, we can sort the detection order among all the streams. This is the basic idea of the so called *Ordered Successive Interference Cancelation* (OSIC) detection. One of the famous OSIC algorithms is *Vertical-Bell Laboratory Layered Space Time* (V-BLAST) detection [35]. In the V-BLAST detection structure the order is obtained by the minimum row norm, that is, the detection order is determined from the smallest to the largest. The V-BLAST ordering is equivalent to the highest SINR ordering. The optimal detection order can be achieved by the V-BLAST, however, it requires calculation of a matrix inversion at each layer peeling which is computationally intensive for MIMO systems. In order to reduce the computational effort and find a better detection order, the *Sorted QR Decomposition* (SQRD) algorithm is proposed in [63] for SIC detection. The SQR-ZF-SIC algorithm can achieve almost the same performance as V-BLAST with a fraction of the computational effort; the performance of SQR-MMSE-SIC is suboptimal while in [61] a low complexity *post sorting* algorithm for MMSE-SIC (PSA-MMSE-SIC) is proposed which employs unitary transformations to achieve the same performance as MMSE-BLAST.

2.5.1.3 Simulation Results

The BER performance of the detection algorithms discussed above are illustrated in Figure 2.3. A 10×10 SU-MIMO system is considered with a block Rayleigh fading channel. The modulation is uncoded QPSK and the number of trials used to average the curves is 10000 and the packet length is 100 symbols for the simulations. The quantity E_b/N_0 is defined as $E_b/N_0 = \frac{N_r E_s}{N_t N \sigma_n^2}$ with N being the number of information bits transmitted per symbol. As the MMSE approach always offer a better BER performance than ZF, we focus on MMSE-SIC in this simulation. The ML solution computed with the SD algorithm

shows the best BER performance, followed by PSA-MMSE-SIC. The BER performance of MMSE-SIC is quite close to that of PSA-MMSE-SIC at values of low E_b/N_0s and is much better than MMSE and ZF.

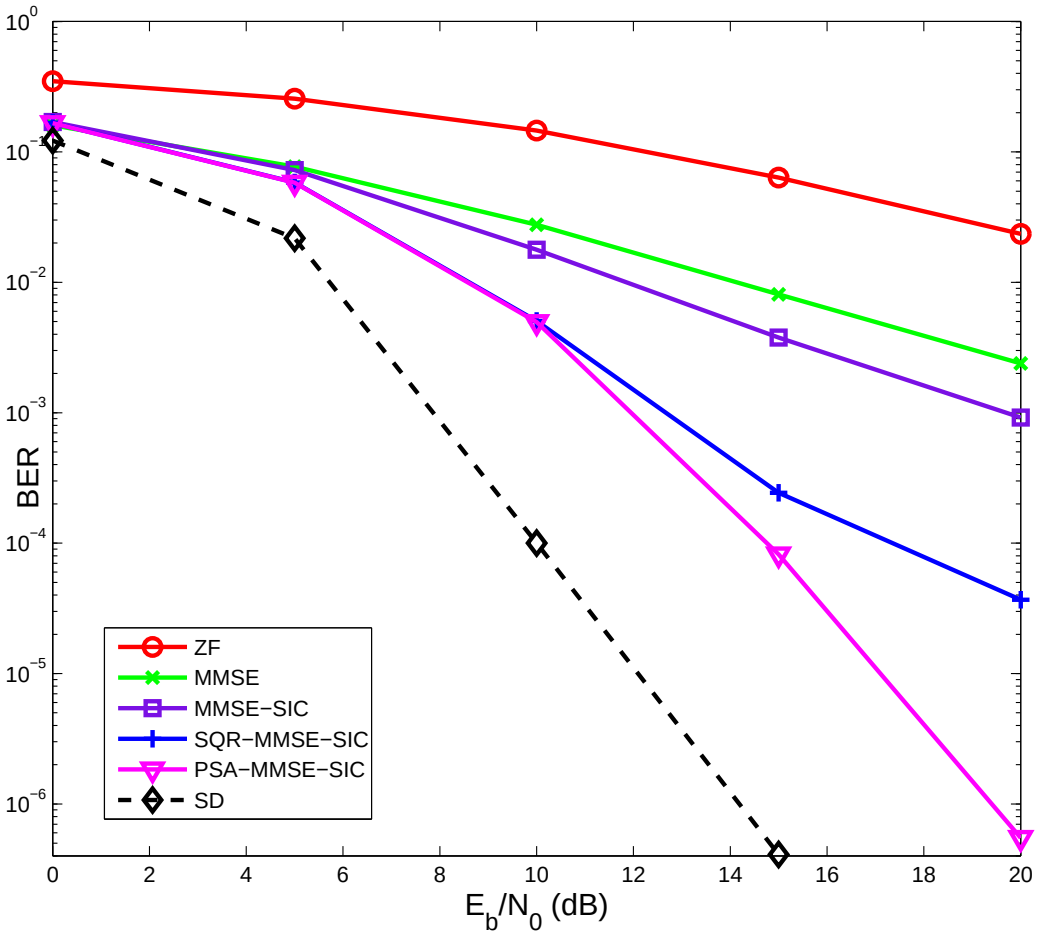

Figure 2.3: The BER Performance of MIMO Detection Algorithms

2.5.2 MIMO Precoding

There are two main reasons that the precoding techniques are so important in wireless MIMO systems. One is that if the precoding techniques are applied at the source signals before they are transmitted it reduces the performance loss caused by interference and channel fading. Thus, the advantage of MIMO system will be enhanced. On the other

hand, it is well known that the BS has more powerful computing ability and the power supply is normally not an issue at the BS. Therefore, if the detection like processing approaches in Section 2.5.1 can be removed from the receive side to the transmit side, the structure of UE would be simplified and a significant amount of power can be saved which is very important considering the mobility of the UE.

2.5.2.1 Linear Precoding

With the CSI available at the transmit side, a simple way to deal with the MUI is to set the constraint so to force all interference terms to zero, the method is known as the *Zero Forcing* (ZF) precoding [20]. Since the transmitted power is limited by E_s, the precoding matrix has to be designed to satisfy the transmit power constraint, that is

$$E\{\|\beta \boldsymbol{P}\boldsymbol{s}\|^2\} = E_s, \tag{2.46}$$

where β is a gain factor to make sure that the transmitted signal power after precoding will not be changed. The estimation of the transmitted signal $\tilde{\boldsymbol{s}}$ at the receiver side is given by

$$\tilde{\boldsymbol{s}} = \beta^{-1}(\beta \boldsymbol{H}\boldsymbol{P}\boldsymbol{s} + \boldsymbol{n}). \tag{2.47}$$

Then, the ZF precoding design problem can be described as follows [64]

$$\{\boldsymbol{P}, \beta\} = \arg_{\{\boldsymbol{P},\beta\}} E\{\|\boldsymbol{s} - \tilde{\boldsymbol{s}}\|^2\}, \text{ s.t.} E\{\|\beta \boldsymbol{P}\boldsymbol{s}\|^2\} = E_s, \ \tilde{\boldsymbol{s}}|_{\boldsymbol{n}=0} = \boldsymbol{s}. \tag{2.48}$$

The solution of the above optimization problem is

$$\boldsymbol{P} = \beta_{\text{ZF}} \boldsymbol{H}^H (\boldsymbol{H}\boldsymbol{H}^H)^{-1}, \tag{2.49}$$

$$\beta_{\text{ZF}} = \sqrt{\frac{E_s}{\text{tr}((\boldsymbol{H}\boldsymbol{H}^H)^{-1}\boldsymbol{R}_s)}}, \tag{2.50}$$

where $\boldsymbol{R}_s = E\{\|\boldsymbol{s}\boldsymbol{s}^H\|\}$.

From (2.50), if the channel matrix $\boldsymbol{H}$ is ill conditioned β_{ZF} will become smaller and the performance of ZF precoding will be poor due to $E\{\|\boldsymbol{s} - \tilde{\boldsymbol{s}}\|^2\} = \beta_{ZF}^{-2}\text{tr}(\boldsymbol{R}_n)$.

In order to reduce the noise enhancement, the second constraint in (2.48) needs to be dropped, that is,

$$\{\boldsymbol{P}, \beta\} = \arg_{\{\boldsymbol{P},\beta\}} \text{Min} E\{\|\boldsymbol{s} - \tilde{\boldsymbol{s}}\|^2\}, \text{ s.t.} E\{\|\beta \boldsymbol{P}\boldsymbol{s}\|^2\} = E_s. \tag{2.51}$$

The above equation (2.51) is the well-known MMSE constraint and its solution is given by

$$\boldsymbol{P} = \beta_{\mathrm{MMSE}}(\boldsymbol{H}^H\boldsymbol{H} + \frac{\mathrm{tr}(\boldsymbol{R}_n)}{E_s}\boldsymbol{I}_b)^{-1}\boldsymbol{H}^H, \tag{2.52}$$

$$\beta_{\mathrm{MMSE}} = \sqrt{\frac{E_s}{\mathrm{tr}((\boldsymbol{H}^H\boldsymbol{H} + \frac{\mathrm{tr}(\boldsymbol{R}_n)}{E_s}\boldsymbol{I}_b)^{-1}\boldsymbol{H}^H\boldsymbol{R}_s\boldsymbol{H})}}. \tag{2.53}$$

ZF and MMSE precoding techniques are attractive due to their simplicity, however, hey result in a reduced throughput or require a higher power at the transmitter in the MU-MIMO scenarios [65]. As a generalization of the ZF precoding algorithm, *Block Diagonalization* (BD) based precoding algorithms have been proposed in [29, 30] for MU-MIMO systems especially for receivers with multiple antennas. However, BD based precoding algorithms only take the MUI into account and thus suffer a performance loss at low SNRs when the noise is the dominant factor. Therefore, a *Regularized Block Diagonalization* (RBD) precoding algorithm which introduces a regularization factor to take the noise term into account has been proposed in [66].

The design of BD-type precoding algorithms is performed in two steps [29, 66]. The first precoding filter is used to completely eliminate (by BD) or balance the MUI with noise (by RBD), then exact (by BD) or approximate (by RBD) parallel SU-MIMO channels are obtained. The second precoding filter is implemented to parallelize each user's streams. Correspondingly, the precoding matrix $\boldsymbol{P}_k$ for the kth user can be rewritten in two parts as

$$\boldsymbol{P}_k = \boldsymbol{P}_k^a\boldsymbol{P}_k^b, \tag{2.54}$$

where $\boldsymbol{P}_k^a \in \mathbb{C}^{N_t\times M_k}$ and $\boldsymbol{P}_k^b \in \mathbb{C}^{M_k\times N_k}$. The parameter M_k denotes the number of streams transmitted by the kth user and is dependent on the specific choice of the precoding algorithm. Therefore, the equivalent combined channel matrix of all users after the first precoding filter is

$$\boldsymbol{H}\boldsymbol{P}^a = \begin{bmatrix} \boldsymbol{H}_1\boldsymbol{P}_1^a & \boldsymbol{H}_1\boldsymbol{P}_2^a & \dots & \boldsymbol{H}_1\boldsymbol{P}_K^a \\ \boldsymbol{H}_2\boldsymbol{P}_1^a & \boldsymbol{H}_2\boldsymbol{P}_2^a & \dots & \boldsymbol{H}_2\boldsymbol{P}_K^a \\ \vdots & \vdots & \ddots & \vdots \\ \boldsymbol{H}_K\boldsymbol{P}_1^a & \boldsymbol{H}_K\boldsymbol{P}_2^a & \dots & \boldsymbol{H}_K\boldsymbol{P}_K^a \end{bmatrix}, \tag{2.55}$$

We exclude the kth user's channel matrix and define $\overline{\boldsymbol{H}}_k$ as

$$\overline{\boldsymbol{H}}_k = [\boldsymbol{H}_1^T \ \ldots \ \boldsymbol{H}_{k-1}^T \ \boldsymbol{H}_{k+1}^T \ \ldots \ \boldsymbol{H}_K^T]^T \in \mathbb{C}^{\overline{N}_k \times N_t}, \tag{2.56}$$

where $\overline{N}_k = N_r - N_k$. Then, the interference generated to the other users is determined by $\overline{\boldsymbol{H}}_k \boldsymbol{P}_k^a$.

In order to eliminate all the MUI, we impose the constraint that

$$\forall i \in (1, \ldots, K) \ \overline{\boldsymbol{H}}_k \boldsymbol{P}_k^a = \mathbf{0} \text{ s.t. } \mathrm{E}\|\boldsymbol{x}_\mathrm{k}\|^2 = \xi_\mathrm{k}, \tag{2.57}$$

where the quantity ξ_k is the average transmit power for each user. We term the formulation (2.57) as the BD constraint. Note that the BD constraint is actually an extension of the ZF constraint in [64] for MU-MIMO with multiple receive antennas. In order to take the noise term into account as well, an RBD constraint is developed in [66] and given by

$$\boldsymbol{P}_k^a = \arg\min_{\boldsymbol{P}_k^a} \mathrm{E}\{\sum_{\mathrm{k}=1}^{\mathrm{K}} \|\overline{\boldsymbol{H}}_\mathrm{k} \boldsymbol{P}_\mathrm{k}^\mathrm{a}\|^2 + \beta_\mathrm{k}\|\boldsymbol{n}_\mathrm{k}\|^2\}$$
$$\text{s.t. } \mathrm{E}\|\boldsymbol{x}_\mathrm{k}\|^2 = \xi_\mathrm{k}. \tag{2.58}$$

Assuming that the rank of $\overline{\boldsymbol{H}}_k$ is $\overline{L}_k$, define the SVD of $\overline{\boldsymbol{H}}_k$

$$\overline{\boldsymbol{H}}_k = \overline{\boldsymbol{U}}_k \overline{\boldsymbol{\Sigma}}_k \overline{\boldsymbol{V}}_k^H = \overline{\boldsymbol{U}}_k \overline{\boldsymbol{\Sigma}}_k [\ \overline{\boldsymbol{V}}_k^{(1)} \quad \overline{\boldsymbol{V}}_k^{(0)}\ ]^H, \tag{2.59}$$

where $\overline{\boldsymbol{U}}_k \in \mathbb{C}^{\overline{N}_k \times \overline{N}_k}$ and $\overline{\boldsymbol{V}}_k \in \mathbb{C}^{N_t \times N_t}$ are unitary matrices. The diagonal matrix $\overline{\boldsymbol{\Sigma}}_k \in \mathbb{C}^{\overline{N}_k \times N_t}$ contains the singular values of the matrix $\overline{\boldsymbol{H}}_k$. Factorizing $\overline{\boldsymbol{V}}_k$ into two parts, $\overline{\boldsymbol{V}}_k^{(1)} \in \mathbb{C}^{N_t \times \overline{L}_k}$ consists of the first $\overline{L}_k$ non-zero singular vectors and $\overline{\boldsymbol{V}}_k^{(0)} \in \mathbb{C}^{N_t \times (N_t - \overline{L}_k)}$ holds the last $N_t - \overline{L}_k$ zero singular vectors. Thus, $\overline{\boldsymbol{V}}_k^{(0)}$ forms an orthogonal basis for the null space of $\overline{\boldsymbol{H}}_k$. The solution for the BD constraint is given by

$$\boldsymbol{P}_k^{a(\mathrm{BD})} = \overline{\boldsymbol{V}}_k^{(0)}. \tag{2.60}$$

As shown in [66], the solution for the RBD constraint can be obtained as

$$\boldsymbol{P}_k^{a(\mathrm{RBD})} = \overline{\boldsymbol{V}}_k (\overline{\boldsymbol{\Sigma}}_k^T \overline{\boldsymbol{\Sigma}}_k + \alpha \boldsymbol{I}_{N_t})^{-1/2}, \tag{2.61}$$

where $\alpha = \frac{N_r \sigma_n^2}{E_s}$ is the regularization parameter with E_s is the whole average transmit power.

After the first precoding process, the MU-MIMO channel is decoupled into a set of K parallel independent SU-MIMO channels by the BD precoding. For the RBD precoding, there are residual interferences between these channels due to the regularization process. However, these interferences tend to zero at high SNRs. Therefore, the second precoding filter $\boldsymbol{P}_k^b$ has the diagonal structure as

$$\boldsymbol{P}^b = \begin{bmatrix} \boldsymbol{P}_1^b & 0 & \dots & 0 \\ 0 & \boldsymbol{P}_2^b & \dots & 0 \\ \vdots & \vdots & \ddots & \vdots \\ 0 & 0 & 0 & \boldsymbol{P}_K^b \end{bmatrix}.$$

And the effective channel matrix for the kth user can be expressed as

$$\boldsymbol{H}_{\text{eff}_k} = \boldsymbol{H}_k \boldsymbol{P}_k^a. \tag{2.62}$$

Define $L_{\text{eff}} = \text{rank}(\boldsymbol{H}_{\text{eff}_k})$ and consider the second SVD operation on the effective channel matrix

$$\boldsymbol{H}_{\text{eff}_k} = \boldsymbol{U}_k \boldsymbol{\Sigma}_k {\boldsymbol{V}_k}^H = \boldsymbol{U}_k \begin{bmatrix} \boldsymbol{\Sigma}_k & 0 \\ 0 & 0 \end{bmatrix} [\ \boldsymbol{V}_k^{(1)} \quad \boldsymbol{V}_k^{(0)}\ ]^H, \tag{2.63}$$

using the unitary matrix $\boldsymbol{U}_k \in \mathbb{C}^{L_{\text{eff}} \times L_{\text{eff}}}$ and $\boldsymbol{V}_k^{(1)}$ contains the first L_{eff} singular vectors. The second precoding filters for BD and RBD precoding can be respectively obtained as

$$\boldsymbol{P}_k^{b\,(\text{BD})} = \boldsymbol{V}_k^{(1)} \boldsymbol{\Lambda}^{(\text{BD})}, \tag{2.64}$$

$$\boldsymbol{P}_k^{b\,(\text{RBD})} = \boldsymbol{V}_k \boldsymbol{\Lambda}^{(\text{RBD})}, \tag{2.65}$$

where $\boldsymbol{\Lambda}$ is the power loading matrix that depends on the optimization criterion. An example of power loading is the *Water Filling* (WF) [2]. The kth user's decoding matrix is obtained as

$$\boldsymbol{G}_k = \boldsymbol{U}_k^H, \tag{2.66}$$

which needs to be known by each user's receiver.

Note that for the conventional BD-type precoding algorithms, there is a dimensionality constraint below to be satisfied

$$N_t > \max\{\text{rank}(\overline{\boldsymbol{H}}_1), \text{rank}(\overline{\boldsymbol{H}}_2), \dots, \text{rank}(\overline{\boldsymbol{H}}_K)\}. \tag{2.67}$$

Then, we can get the matrix dimension relationship as $N_t \geq N_r > \overline{N}_k \geq \overline{L}_k > N_k \geq L_{\text{eff}}$. Note that the first SVD operation in (2.59) needs to be implemented K times on $\overline{\boldsymbol{H}}_k$ with dimension $\overline{N}_k \times N_t$ and the second SVD operation in Equation (2.63) needs to be implemented K times on $\boldsymbol{H}_{\text{eff}_k}$ with dimensions $L_{\text{eff}} \times (N_t - \overline{L}_k)$ for the BD precoding and $L_{\text{eff}} \times N_t$ for the RBD precoding. From the above analysis, most of the computational complexity of the BD-type precoding algorithms comes from the two SVD operations which make the computational complexity of the BD-type precoding algorithms increase with the number of users K and the system dimensions.

2.5.2.2 Tomlinson-Harashima Precoding

The concept of "writing on dirty paper" was introduced by Costa in [18]. The traditional additive Gaussian noise channel is modified to include an additive interference term that is known at the transmitter

$$y = s + i + n, \tag{2.68}$$

where the quantity y, s, i, n is the the received signal, transmitted signal, interference and Gaussian noise, respectively. If the interference i is known deterministically at the transmit side, the transmitted signal s can be set to $s = d - i$, where d is the codeword. The transmitted power, however, is increased by this setting. And thus, a modulo operator, which is defined below, is necessary to make sure the coded signal falls into the boundary of the modulation alphabet.

$$\mathrm{M}_\tau(x) = x - \left\lfloor \frac{\mathrm{Re}(x)}{\tau} + \frac{1}{2} \right\rfloor \tau - j \left\lfloor \frac{\mathrm{Im}(x)}{\tau} + \frac{1}{2} \right\rfloor \tau, \tag{2.69}$$

where $\lfloor \cdots \rfloor$ is the floor function and τ is a constant for the periodic extension of the constellation. Then, the transmitted signal s is obtained as

$$s = \mathrm{M}_\tau(d - i) = d - i - \tau k, \tag{2.70}$$

where k is an integer from the floor function. The modulo function reduces the power of the transmitted signal form as compared to what it would be if the simple method of $s = d - i$ were used. Correspondingly, the received signal regarding the transmitted signal s in (2.70) is

$$\mathrm{M}_\tau(y) = \mathrm{M}_\tau(s + i + n) = \mathrm{M}_\tau(d + n). \tag{2.71}$$

Hence, no additional power is needed to cancel the interference that is used in a nominal additive Gaussian noise channel. Costa proved that the capacity of this channel is the same as if the interference was not present. If the signal has a power constraint $\|s\|^2 \leq \rho$, then the capacity of this system is

$$C_{\mathrm{DPC}} = \log_2(1 + \frac{\rho}{N_0}), \tag{2.72}$$

where N_0 is the noise power. To use Costa's analogy, writing on dirty paper is information theoretically equivalent to writing on clean paper when one knows in advance where the dirt is, this approach is called *Dirty Paper Coding* (DPC).

However, DPC is not suitable for practical use due to the requirement of infinitely long codewords and codebooks [25]. Tomlinson-Harashima precoding (THP) [67, 68] is a pre-equalization technique originally proposed for channels with *Intersymbol Interference* (ISI). Then, the THP technique was extended from temporal equalization to spatial equalization for MIMO precoding in [69]. Although THP suffers a performance loss compared to DPC as shown in [70], it can work as a cost-effective replacement of DPC in practice [71]. As revealed in [69, 72], the THP structure can be seen as the dual of the SIC detection implemented at the receive side. In the literature, there are two basic THP structures according to the positions of the diagonal weighted filter, decentralized filters located at the receivers or centralized filters deployed at the transmitter, which are denoted as dTHP or cTHP, respectively [73].

Based on the knowledge of CSI at the transmit side, the interference of the parallel streams of a MIMO system with spatial multiplexing can be subtracted from the current stream. This SIC technique at the transmit side is known as THP and can be seen as the dual of SIC detection at the receive side. Generally, there are three filters to implement the THP algorithm: the feedback filter $\boldsymbol{B} \in \mathbb{C}^{S\times S}$, the feedforward filter $\boldsymbol{F} \in \mathbb{C}^{S\times S}$, and the scaling matrix $\boldsymbol{G} \in \mathbb{C}^{S\times S}$, where S denotes the total number of transmitted streams. According to the position of $\boldsymbol{G}$, there are two basic THP structures, which are illustrated in Fig. 2.4. The decentralized THP (dTHP) employs $\boldsymbol{G}$ (or submatrices of it) at the receivers, whereas the centralized THP (cTHP) uses $\boldsymbol{G}$ at the transmitter.

The feedback filter $\boldsymbol{B}$ is used to successively cancel the interference caused by the previous streams from the current stream. Therefore, the feedback filter $\boldsymbol{B}$ should be a lower

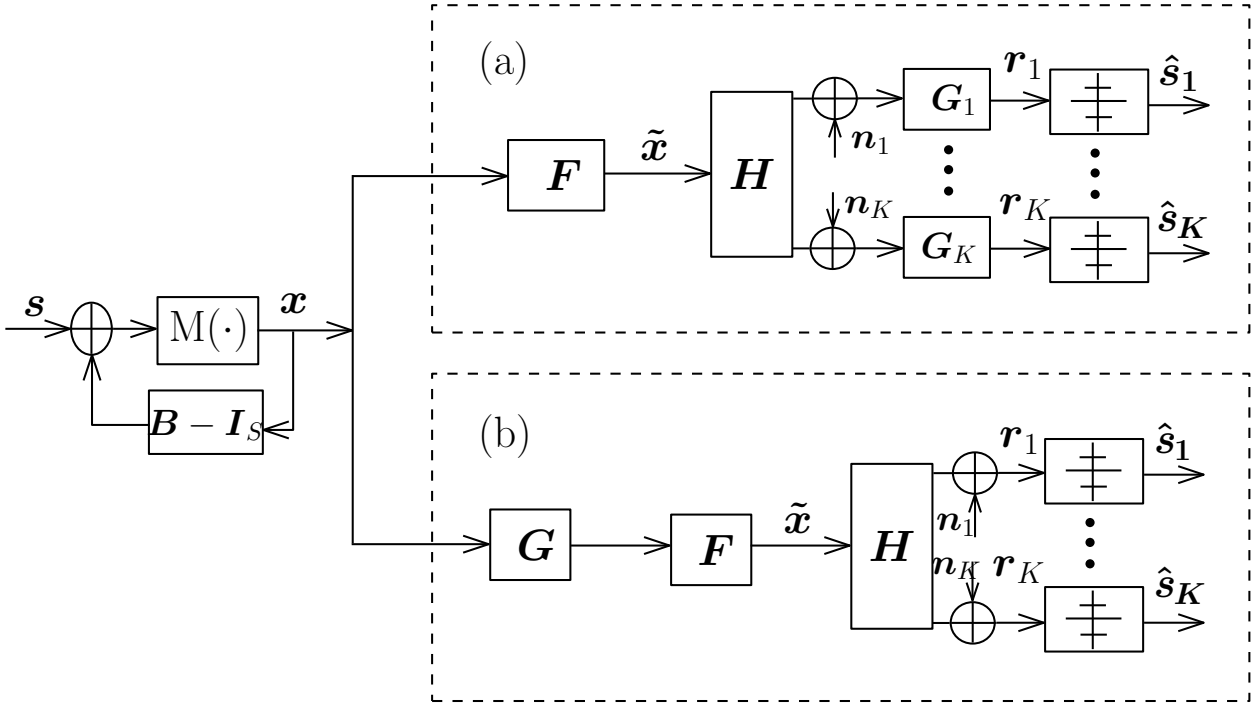

Figure 2.4: The two basic THP structures.(a) Decentralized THP: the scaling matrix $\boldsymbol{G}$ is separately placed at the receivers.(b) Centralized THP: the scaling matrix $\boldsymbol{G}$ is placed at the transmitter.

triangular matrix with ones on the main diagonal [72]. The feedforward filter $\boldsymbol{F}$ is used to enforce the spatial causality and has to be implemented at the transmit side for MU-MIMO systems because the physically distributed users cannot be processed jointly. The scaling filter $\boldsymbol{G}$ contains the corresponding weighted coefficient for each stream and thus it should have a diagonal structure. The quantity $\tilde{\boldsymbol{x}}$ is the channel symbol after the precoding, $\tilde{\boldsymbol{x}} = \boldsymbol{F}\boldsymbol{x}$ for dTHP and $\tilde{\boldsymbol{x}} = \boldsymbol{F}\boldsymbol{G}\boldsymbol{x}$ for cTHP. Finally, the received signal after the feedback, feedforward, and the scaling filter, for the dTHP and cTHP is respectively given by

$$\boldsymbol{r}^{(\mathrm{dTHP})} = \boldsymbol{G}(\boldsymbol{H}\boldsymbol{F}\boldsymbol{x} + \boldsymbol{n}), \tag{2.73}$$

$$\boldsymbol{r}^{(\mathrm{cTHP})} = \beta(\boldsymbol{H} \cdot \frac{1}{\beta}\boldsymbol{F}\boldsymbol{G}\boldsymbol{x} + \boldsymbol{n}), \tag{2.74}$$

where the quantity $\boldsymbol{x} \in \mathbb{C}^{S\times 1}$ is the combined transmit channel signal and $\boldsymbol{n} = [\boldsymbol{n}_1^T, \boldsymbol{n}_2^T, \cdots, \boldsymbol{n}_K^T]^T \in \mathbb{C}^{S\times 1}$ is the combined Gaussian noise vector with i.i.d. entries of zero mean and variance σ_n^2. The factor β is used to impose the power constraint $\mathrm{E}\|\tilde{\boldsymbol{x}}\|^2 = \xi$ with ξ being the average transmit power.

As reported in the literature, SIC detection can be efficiently implemented by a QR decomposition [74], whereas THP can be implemented by an LQ decomposition. By utilizing an LQ decomposition on the channel matrix $\boldsymbol{H}$, we have

$$\boldsymbol{H} = \boldsymbol{L}\boldsymbol{Q}, \tag{2.75}$$

where $\boldsymbol{L}$ is a lower triangular matrix and $\boldsymbol{Q}$ is a unitary matrix. Therefore, the filters for THP algorithm can be obtained as

$$\boldsymbol{F} = \boldsymbol{Q}^H, \tag{2.76}$$

$$\boldsymbol{G} = \mathrm{diag}[l_{1,1}, l_{2,2}, \cdots, l_{S,S}]^{-1}, \tag{2.77}$$

$$\boldsymbol{B}^{(\mathrm{dTHP})} = \boldsymbol{G}\boldsymbol{L}, \boldsymbol{B}^{(\mathrm{cTHP})} = \boldsymbol{L}\boldsymbol{G}, \tag{2.78}$$

where $l_{i,i}$ is the ith diagonal element of the matrix $\boldsymbol{L}$.

From Figure 2.4, the transmitted symbols x_i are successively generated as

$$x_i = s_i - \sum_{j=1}^{i-1} b_{i,j}x_j,\ i = 1, \cdots, S, \tag{2.79}$$

where s_i is the ith transmit data with variance σ_s^2 and $b_{i,j}$ are the elements of $\boldsymbol{B}$ in row i and column j. From the above formulation, the transmit power will be significantly increased as the amplitude of x_i exceeds the modulation boundary by the successive cancelation. In order to reduce the amplitude of the channel symbol x_i to the boundary of the modulation alphabet, a modulo operation $\mathrm{M}(\cdot)$ should be employed which is defined element-wise as

$$\mathrm{M}(x_i) = x_i - \left\lfloor \frac{\mathrm{Re}(x_i)}{\tau} + \frac{1}{2} \right\rfloor \tau - j \left\lfloor \frac{\mathrm{Im}(x_i)}{\tau} + \frac{1}{2} \right\rfloor \tau, \tag{2.80}$$

where τ is a constant for the periodic extension of the constellation. The specific value of τ depends on the chosen modulation alphabet. Common choices for τ are $\tau = 2\sqrt{2}$ for QPSK symbols and $\tau = 8\sqrt{10}$ in case of rectangular 16-QAM when the symbol variance is one [75]. The modulo processing is equivalent to adding a perturbation vector $\boldsymbol{d}$ to the transmit data $\boldsymbol{s}$, such that the modified transmit data are

$$\boldsymbol{v} = \boldsymbol{s} + \boldsymbol{d}. \tag{2.81}$$

Thus, the initial signal constellation is extended periodically and the effective transmit data symbols $\boldsymbol{v}_k$ are taken from the expanded set.

Although the modulo operation is employed to restrict the amplitude of $\boldsymbol{x}$ within the same scale as that of $\boldsymbol{s}$, a power loss is introduced by the nonlinear processing of THP, which can be measured by $\alpha = \frac{M}{M-1}$ for the M-QAM constellations [70, 72]. The power loss is not negligible for small modulation sizes, but for moderate sizes of M it is negligible and vanishes as M increases. Except for the power loss, a modulo loss is also introduced by THP due to the received symbols at the boundary of a constellation may be mistaken for symbols at the opposite boundary [70]. The modulo loss is more significant for the small constellations. We neglect the power and modulo loss in this work since moderate sizes of M are employed. Then, we have $\mathrm{E}\|\boldsymbol{x}\| \approx \mathrm{E}\|\boldsymbol{s}\|$. Since the norm of $\boldsymbol{x}$ is not changed by the multiplication of the unitary matrix $\boldsymbol{F}$, the normalization factor β is not necessary for dTHP. For cTHP, since the power and modulo loss can be neglected, the normalization factor is approximately obtained as

$$\beta = \frac{\mathrm{E}\|\boldsymbol{F}\boldsymbol{G}\boldsymbol{x}\|}{\mathrm{E}\|\boldsymbol{s}\|} \approx \sqrt{\sum_{i=1}^{S} (1/l_{i,i}^2)}. \tag{2.82}$$

Mathematically, the feedback processing is equivalent to an inversion operation $\boldsymbol{B}^{-1}$. Therefore, the transmitted symbol $\boldsymbol{x}$ can be written as

$$\boldsymbol{x} = \boldsymbol{B}^{-1}\boldsymbol{v} = \boldsymbol{B}^{-1}(\boldsymbol{s} + \boldsymbol{d}), \tag{2.83}$$

Then, the received signal for dTHP and cTHP can be respectively expressed as

$$\boldsymbol{r}^{(\mathrm{dTHP})} = \boldsymbol{v} + \boldsymbol{G}\boldsymbol{n}, \tag{2.84}$$

$$\boldsymbol{r}^{(\mathrm{cTHP})} = \boldsymbol{v} + \beta\boldsymbol{n}. \tag{2.85}$$

From (2.84) and (2.85), we can see that the THP can transfer the MU-MIMO channel into equivalent parallel SISO channel as BD-type precoding.

2.5.2.3 Vector Perturbation

A nonlinear vector perturbation (VP) approach, which is based on *Sphere Encoding* (SE) to perturb the data, was proposed in [26]. With the perturbation, a near optimal performance is achieved by VP precoding [76]. Assume the quantity $\boldsymbol{u} \in \mathbb{C}^K$ is the data vector, and $\boldsymbol{u}$ is perturbed

$$\tilde{\boldsymbol{u}} = \boldsymbol{u} + \tau\boldsymbol{\ell}, \tag{2.86}$$

where τ is a positive real number and $\boldsymbol{\ell}$ is a K-dimensional complex integer vector that needs to be decided. For the ZF-VP, the transmitted channel signal is

$$\boldsymbol{x} = \frac{1}{\sqrt{\beta}}\boldsymbol{H}^{\dagger}\tilde{\boldsymbol{u}}, \tag{2.87}$$

with $\boldsymbol{H}^{\dagger} = \boldsymbol{H}^H(\boldsymbol{H}\boldsymbol{H}^H)^{-1}$ and the parameter $\beta = \|\boldsymbol{H}^{-1}\tilde{\boldsymbol{u}}\|^2$. The scalar τ is chosen to make sure that the original transmit data vector $\boldsymbol{u}$ can solely be restored at the receive side by applying the modulo operation in (2.69). Usually, the value of τ is designed according to the chosen constellation

$$\tau = 2(|c|_{\max} + \triangle/2), \tag{2.88}$$

where $|c|_{\max}$ is the absolute value of the constellation symbols with greatest magnitude, and $\triangle$ is the smallest distance between two constellation symbols. The perturbation vector $\boldsymbol{\ell}$ is designed to minimize the transmit power normalization

$$\boldsymbol{\ell} = \mathrm{argmin}_{\boldsymbol{\ell}'}\|\boldsymbol{H}^{-1}\tilde{\boldsymbol{u}}\|^2 = \mathrm{argmin}_{\boldsymbol{\ell}'}\|\boldsymbol{H}^{-1}(\boldsymbol{u} + \tau\boldsymbol{\ell}')\|^2. \tag{2.89}$$

Equation (2.89) is a K-dimensional integer-lattice least-squares problem, for which there exist a large number of algorithms, in particular the *sphere decoder* algorithm [77–79]. As it is applied at the transmit side, it is referred as *sphere encoder* in [26]. The MMSE-VP has been derived in [80]. Note that the THP is a constrained type of VP, however, finding the optimal perturbation vector can be a nondeterministic polynomial time (NP)-hard problem.

2.5.2.4 Limited Feedback Techniques

If we want to adopt a precoding strategy to counteract the MUI or channel fading, the *Channel State Information* (CSI) must be available at the transmit side. In TDD systems, the channel information at the transmit side can be obtained by using the reciprocity principle, that is, the uplink and downlink of the TDD system are sharing the same channel to transmit and receive data. In FDD systems, the uplink and downlink employ different frequencies to transmit and receive signals, thus the channel information need to be estimated and fed back from the receive side to the transmit side in the FDD systems. Furthermore, it is impossible to feed back all the channel information from the receive side to the transmit side due to the fact that the bandwidth of the control channel is limited. Therefore, a reasonable way to feed back the channel information is through *limited feedback* techniques.

The channel $\boldsymbol{H}$ is usually obtained at the receiver through procedures such as training. As pointed out in [81] that allowing the receiver to send a small number of information bits about the channel conditions to the transmitter can allow near optimal channel adaptation. The general idea of *limited feedback* is that the receiver quantizes some function of $\boldsymbol{H}$ using *Vector Quantization* (VQ) techniques. VQ approaches using the Lloyd algorithm [82] have been shown in [83]. Grassmannian line packing approach has been proposed in [84]. The *Random Vector Quantization* (RVQ) was first proposed in [85], which the codebook is randomly generated. With the benefits achieved by the *limited feedback* techniques, the price is the overhead loss. The role of overhead is discussed and analyzed in [86–88].

2.5.2.5 Simulation Results

In this section, a MU-MIMO system with $N_t = 8$ transmit antennas and $K = 4$ users each equipped with $N_k = 2$ receive antennas is considered; this scenario is denoted as the $(2, 2, 2, 2) \times 8$ case. Uncoded QPSK modulation schemes are employed in the simulation. The channel matrix $\boldsymbol{H}$ is assumed to be a complex i.i.d. Gaussian matrix with zero mean and unit variance. The number of simulation trials is 10^6 and the packet length is 10^2 symbols.

As illustrated in Figure 2.5, the BER performance of the BD and RBD precoding algorithms is worse than that of the THP algorithms. For the THP algorithms, a better BER performance is offered by ZF-dTHP over ZF-cTHP, while a much better BER performance is achieved by MMSE-cTHP than MMSE-dTHP. The maximum transmit diversity order is achieved by MMSE-VP.

2.6 Lattice Reduction Techniques

Lattice Reduction (LR) is another preprocessing and detection technique that has recently attracted significant research efforts. Yao and Wornell [89] used the LR algorithm in conjunction with MIMO detection techniques. The symbol error rate curves can parallel the maximum-likelihood detection by using LR-aided detection schemes. For this reason, a great deal of interest has been devoted to exploring the application of LR in MIMO systems. The LR-aided detection schemes with respect to the minimum mean square error criterion have been extended by Wüebben et al [90]. In [91] not only the LR-aided SU-MIMO detection but also the LR-aided SU-MIMO precoding has been investigated. LR-aided MIMO precoding for decentralized receivers was first investigated in [69].

2.6.1 Lattice Reduction Algorithms

The most commonly used LR algorithm is the LLL algorithm which was first proposed by Lenstra, Lenstra, and L. Lovasz in [92]. The essence of the LLL algorithm is to orthogonalize the columns of the channel matrix and reduce its size as well. The LL-

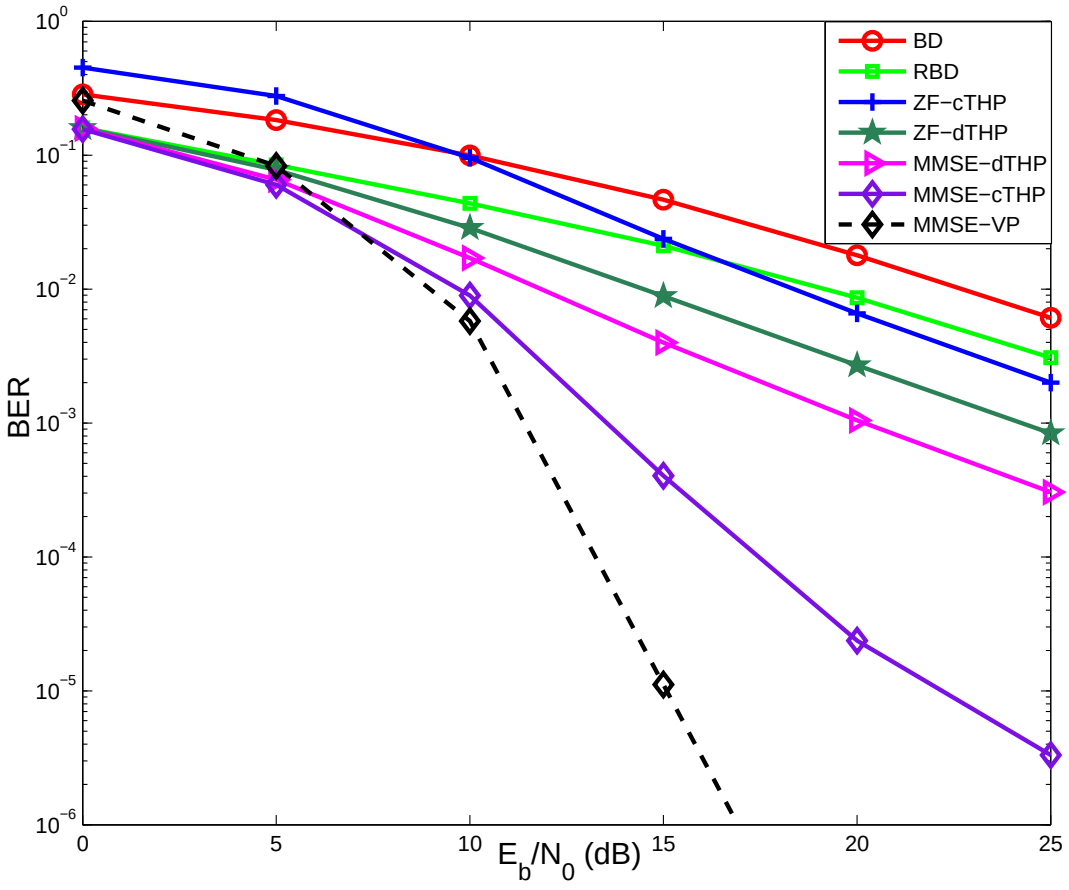

Figure 2.5: The BER performance of MIMO Precoding Algorithms.

L algorithm cannot guarantee to find the optimal lattice basis which can be found by Korkin and Zolotarev (KZ) reduction which is an exponential-time lattice reduction algorithm [93]. As pointed in [94], the KZ reduction is infeasible in practice due to its high complexity. Through the LLL algorithm, only the real-valued matrix can be processed which may lead to extra unnecessary complexity when the channel has large dimensions. In order to reduce the computational complexity further, the complex LLL (CLLL) algorithm was proposed in [95]. The overall complexity of CLLL algorithm is nearly half of the LLL algorithm without sacrificing any performance. Gram-Schmidt orthogonalization procedure and size reduction are the two core components of the LR algorithm. In order to simplify the system structure, the *Complex Lattice Reduction* (CLR) algorithm is employed in this report. A complex lattice is a set of points,

$$L(\boldsymbol{H}) = \{\boldsymbol{H}\boldsymbol{x} | x_l \in \mathbb{Z} + j\mathbb{Z}\}, \tag{2.90}$$

where $\boldsymbol{H} = \{\boldsymbol{h}_1, \boldsymbol{h}_2, \cdots, \boldsymbol{h}_{N_t}\}$ contains the bases of the lattice $L(\boldsymbol{H})$. Actually, any matrix $\tilde{\boldsymbol{H}}$ can generate the same lattice as $\boldsymbol{H}$ if and only if

$$\tilde{\boldsymbol{H}} = \boldsymbol{H}\boldsymbol{U}, \tag{2.91}$$

where $\boldsymbol{U}$ is a unimodular matrix ($|\det \boldsymbol{U}| = 1$) and all elements of $\boldsymbol{U}$ are complex integers, i.e. $u_{l,k} \in \mathbb{Z} + j\mathbb{Z}$. The aim of the CLR algorithm is to find a new basis $\tilde{\boldsymbol{H}}$ which is shorter and nearly orthogonal compared to the original matrix $\boldsymbol{H}$. By the QR decomposition, $\boldsymbol{H} = \boldsymbol{Q}\boldsymbol{R}$, where $\boldsymbol{Q}$ is an orthogonal matrix and the upper-triangular matrix $\boldsymbol{R}$ is a rotated and reflected representation of $\boldsymbol{H}$. Thus, each column vector $\boldsymbol{h}_k$ of $\boldsymbol{H}$ is given by [90]

$$\boldsymbol{h}_k = \sum_{l=1}^{k} r_{l,k}\boldsymbol{q}_l, \tag{2.92}$$

where $\boldsymbol{q}_l$ is the lth column of $\boldsymbol{Q}$. If $|r_{1,k}|, ..., |r_{k-1,k}|$ are close to zero, we can say that $\boldsymbol{h}_k$ is almost orthogonal to the space spanned by $\boldsymbol{h}_1, ..., \boldsymbol{h}_{k-1}$. Similarly, the QR decomposition of $\tilde{\boldsymbol{H}}$ is $\tilde{\boldsymbol{H}} = \tilde{\boldsymbol{Q}}\tilde{\boldsymbol{R}}$. Then, the basis for $L(\boldsymbol{H})$ is CLLL reduced if both of the following conditions are satisfied

$$|\tilde{r}_{l,k}| \leq \frac{1}{2}|\tilde{r}_{l,l}|, \ 1 \leq l < k \leq N_t, \tag{2.93}$$

$$\delta|\tilde{r}_{k-1,k-1}|^2 \leq |\tilde{r}_{k,k}|^2 + |\tilde{r}_{k-1,k}|^2,\ 2 \leq k \leq N_t, \tag{2.94}$$

where $\delta \in (\frac{1}{2}, 1]$ influences the quality of the reduced basis and the computational complexity. We usually set $\delta = \frac{3}{4}$ to achieve a trade-off between performance and complexity [92].

From the definition in (2.91), the lattice $L(\boldsymbol{H})$ can have infinitely many different bases other than $\tilde{\boldsymbol{H}}$. For any unimodular matrix $\boldsymbol{U}$ which satisfies $|\det\boldsymbol{U}| = 1$ and $u_{l,k} \in \mathbb{Z}+j\mathbb{Z}$, there will be a corresponding basis $\tilde{\boldsymbol{H}}$.

2.6.2 Lattice Reduction Aided Detection and Precoding

The CLR-reduced channel matrix $\tilde{\boldsymbol{H}}$ has a better channel quality compared to the original channel matrix $\boldsymbol{H}$. If the MIMO receivers were designed based on $\tilde{\boldsymbol{H}}$, a better detector performance can be achieved due to less noise enhancement by $\tilde{\boldsymbol{H}}$. The CLR aided MIMO detection structure is illustrated below,

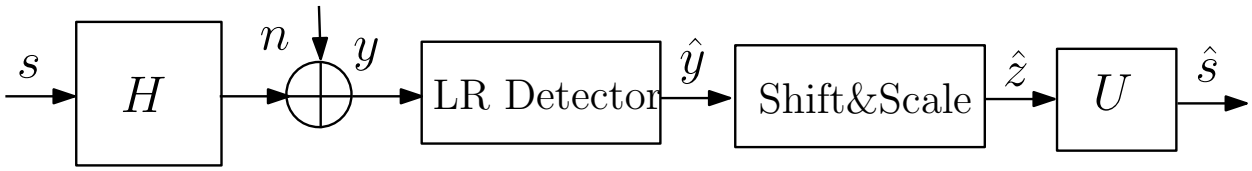

Figure 2.6: LR Aided MIMO Detection Structure.

In Fig. 2.6, the quantity $\boldsymbol{s}$ is the transmit M-QAM signal. The set of M-QAM constellation is given by $\mathbb{S} = \{\frac{1}{2}(1 \pm j)a, \frac{3}{2}(1 \pm j)a, ..., \frac{\sqrt{M}-1}{2}(1 \pm j)a\}$. The parameter $a = \sqrt{6/M-1}$ is used for normalizing the power of the transmit signals to 1. With $\tilde{\boldsymbol{H}} = \boldsymbol{HU}$, the received signal can be rewritten as

$$\boldsymbol{y} = \boldsymbol{Hs} + \boldsymbol{n} = \boldsymbol{HUU}^{-1}\boldsymbol{s} + \boldsymbol{n} = \tilde{\boldsymbol{H}}\boldsymbol{z} + \boldsymbol{n}, \tag{2.95}$$

where $\boldsymbol{z} = \boldsymbol{U}^{-1}\boldsymbol{s}$ is the equivalent transmit signal.

From (2.95), the receive filter of LR-aided ZF detection is designed based on the LR transformed channel matrix $\tilde{\boldsymbol{H}}$,

$$\boldsymbol{G_{LR-ZF}} = (\tilde{\boldsymbol{H}}^{\boldsymbol{H}}\tilde{\boldsymbol{H}})^{-1}\tilde{\boldsymbol{H}}^{\boldsymbol{H}}. \tag{2.96}$$

Then, the signal after LR detector is $\hat{\boldsymbol{z}} = \boldsymbol{z} + \boldsymbol{G_{LR-ZF}}\boldsymbol{n}$. Finally, the estimation of the original transmit signal $\boldsymbol{s}$ is given by

$$\hat{\boldsymbol{s}} = \boldsymbol{U}\hat{\boldsymbol{z}}. \tag{2.97}$$

Since $\boldsymbol{U}$ is a unimodular matix, the statistical properties of $\boldsymbol{Un}$ are identical to those of $\boldsymbol{n}$. Therefore, the estimation error covariance matrix of ZF detection is

$$\boldsymbol{\Phi}_{LR-ZF} = E\{(\hat{\boldsymbol{s}} - \boldsymbol{s})(\hat{\boldsymbol{s}} - \boldsymbol{s})^H\} = \sigma_n^2 \boldsymbol{G_{LR-ZF}} \boldsymbol{G_{LR-ZF}^H}, \tag{2.98}$$

From (2.98), the BER performance of the LR-aided ZF detector will be degraded by $\boldsymbol{G_{LR-ZF}}$. Therefore, the effect of noise enhancement will be moderated due to the fact that $\boldsymbol{G_{LR-ZF}}$ is better conditioned as compared to the conventional $\boldsymbol{G}_{ZF}$. The LR-aided MMSE detection can be implemented in a straightforward way on the extended channel matrix in (2.43).

For the LR-aided SIC detection, the QR decomposition is implemented on the lattice transformed channel matrix, $\tilde{\boldsymbol{H}} = \boldsymbol{QR}$, and then computes $\tilde{\boldsymbol{y}} = \boldsymbol{Q}^H \boldsymbol{y}$. The detection steps of LR-aided SIC are summarized bellow

$$\tilde{z}_{N_t} = \left\lceil \frac{\tilde{y}_{N_t}}{r_{N_t,N_t}} \right\rfloor, \tag{2.99}$$

$$\tilde{z}_i = \left\lceil \frac{\tilde{y}_i - \sum_{j=i+1}^{m} r_{i,j}\tilde{z}_j}{r_{i,i}} \right\rfloor, \tag{2.100}$$

where the quantity $r_{i,j}$ are the elements of $\boldsymbol{R}$ in row i and column j with $i = N_t - 1, ..., 1$. Finally, we have $\tilde{\boldsymbol{z}} = [\tilde{z}_1, ..., \tilde{z}_{N_t}]^T$.

After the receive filter, the estimated transmit signal $\hat{\boldsymbol{s}}$ can be obtained by $\hat{\boldsymbol{s}} = \boldsymbol{U}\tilde{\boldsymbol{z}}$. However, the elements of $\boldsymbol{U}\tilde{\boldsymbol{z}}$ are far from integers and a serious performance loss will be caused if $\boldsymbol{U}\tilde{\boldsymbol{z}}$ was quantized directly. In order to avoid the quantization error caused by rounding as much as possible, proper shifting and scaling work should be done before multiplying the received signal by $\boldsymbol{U}$. The estimation of $\boldsymbol{z}$ is,

$$\hat{\boldsymbol{z}} = a(\hat{\tilde{\boldsymbol{z}}} + \frac{1}{2}\boldsymbol{U}^{-1}\mathbf{1}_{N_t}), \tag{2.101}$$

where $\hat{\tilde{\boldsymbol{z}}} = \lceil \frac{1}{a}\tilde{\boldsymbol{z}} - \frac{1}{2}\boldsymbol{U}^{-1}\mathbf{1}_{N_t} \rfloor$. Finally the estimated transmit signal $\boldsymbol{s}$ can be easily obtained by $\hat{\boldsymbol{s}} = \boldsymbol{U}\hat{\boldsymbol{z}}$. Another promising application of lattice reduction in wireless

communications is efficient precoding. Instead of performing the CLLL reduction on $\boldsymbol{H}$, the CLLL reduction is implemented on $\boldsymbol{H}^T$ in the precoding scenario [91, 96], that is

$$\tilde{\boldsymbol{H}} = \boldsymbol{U}\boldsymbol{H}. \tag{2.102}$$

With $\boldsymbol{H} = \boldsymbol{U}^{-1}\tilde{\boldsymbol{H}}$, the received signal can be rewritten as

$$\boldsymbol{y} = \boldsymbol{H}\boldsymbol{P}\boldsymbol{s} + \boldsymbol{n} = \boldsymbol{U}^{-1}\tilde{\boldsymbol{H}}\boldsymbol{P}\boldsymbol{s} + \boldsymbol{n}. \tag{2.103}$$

Therefore, the design of the precoding filter $\boldsymbol{P}$ is based on the lattice reduced matrix $\tilde{\boldsymbol{H}}$.

2.6.3 Simulation Results

In this section, the BER performance of LR-aided MIMO detection and LR-aided precoding algorithms are illustrated, respectively. A $(2, 2, 2) \times 6$ MU-MIMO systems with un-coded QPSK modulation is considered. The channel matrix $\boldsymbol{H}$ is assumed to be a complex Gaussian matrix with zero mean and unit variance.

From Figure 2.7, we can find that the BER performance of LR-aided ZF detection algorithms is better than their conventional counterparts. In addition, the LR-aided SIC detectors show a similar diversity order with that of the SD. The best BER performance is achieved by SD, its computational complexity, however, is considerably higher than LR-aided SIC detections.

Figure 2.8 illustrates the BER performance of LR-aided precoding algorithms. It is clear that better BER performances are achieved by the LR-aided precoding compared to their corresponding conventional precoding algorithms at high E_b/N_0s. The improved gain comes from the LR transformation, which provides a better equivalent channel matrix. Actually, if the equivalent channel is strictly orthogonal between each other the maximum transmit diversity order could be got by the LR-aided linear precoding algorithms [91].

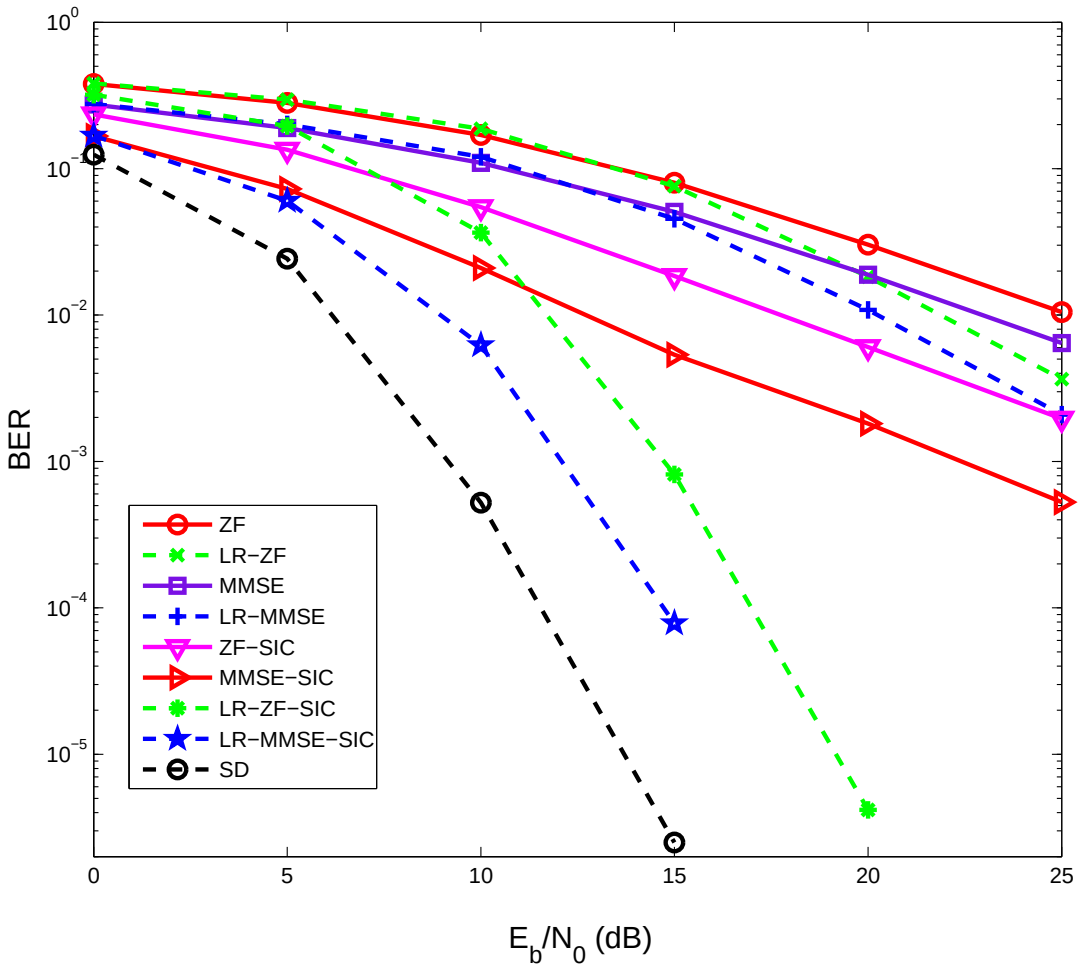

Figure 2.7: The BER performance of LR-aided MIMO Detection Algorithms.

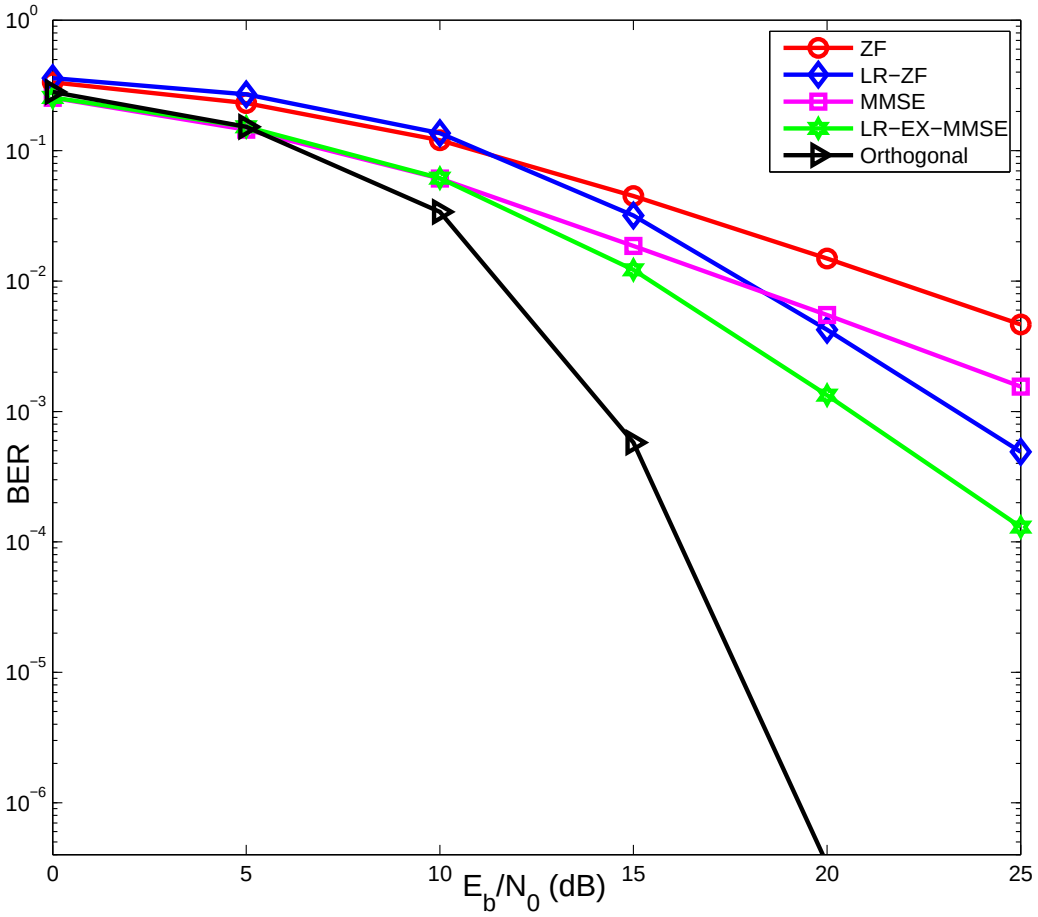

Figure 2.8: The BER performance of LR-aided MIMO Precoding Algorithms.

Chapter 3

Low-Complexity LR-Aided Regularized Block Diagonalization

Contents

Regularized Block Diagonalization (RBD) is a well-known precoding algorithm for MU-MIMO systems. By employing RBD precoding algorithm, the MU-MIMO broadcast channel is decomposed into multiple independent parallel SU-MIMO channels and achieves the maximum diversity order at high data rates. The computational complexity of the RBD precoding algorithm, however, is relatively high due to two singular SVD operations which hinder their applications for large MIMO systems. In this Chapter, a low-complexity lattice reduction-aided RBD algorithm (LC-RBD-LR) is proposed. The first SVD of RBD precoding algorithms is replaced by a QR decomposition, and the orthogonalization procedure provided by the second SVD is substituted by a lattice-reduction whose complexity is mainly contributed by a QR decomposition. Analytical and simulation results show that the proposed LC-RBD-LR algorithm can achieve almost the same

sum-rate performance as RBD, substantial BER performance gains and a simplified receiver structure, while requiring a lower complexity.

3.1 Introduction

Unlike the received signal in SU-MIMO systems, the received signals of different users in MU-MIMO systems not only suffer from the noise and inter-antenna interference but are also affected by the multiuser interference (MUI). Channel inversion based strategies such as ZF and MMSE precoding [64, 97, 98] can be still used to cancel the MUI, but they result in a reduced throughput or require a higher power at the transmitter [99]. BD precoding algorithm has been proposed in [29] to improve the sum-rate or reduce the transmitted power. However, BD precoding only takes the MUI into account and suffers a performance loss at low SNRs when the noise is the dominant factor. Therefore, the regularized block diagonalization (RBD) precoding which introduces a regularization to take the noise term into account has been proposed in [66].

The main steps for RBD are two SVD operations. The first SVD is implemented to transform the MU-MIMO channel into a set of parallel equivalent SU-MIMO channels, where each user channel has the same properties as a conventional SU-MIMO channel [30]. The second SVD is used to orthogonalize the equivalent SU-MIMO channels and obtain a power loading matrix. For the RBD algorithm we still need a unitary matrix for decoding, which is obtained by the second SVD, to orthogonalize each user's stream. The second SVD can be either computed at the transmit side or the receive side. If the second SVD is implemented at the transmit side, the corresponding decoding matrix needs to be informed to each distributed receiver, which requires an extra control overhead [100]. If the second SVD is implemented at the receive side, not only the complexity of the receiver will be increased but also the corresponding equivalent CSI after the first SVD precoding must be known or estimated by each receiver. In addition, due to these two SVD operations, the computational complexity of RBD is relatively high compared with the linear precoding algorithms.

In order to reduce the complexity of RBD, the first SVD of RBD is replaced with a less complex LQ decomposition in [101], which results in the same performance as the

original RBD precoding algorithm. We term the low-complexity implementation of RBD in [101] as QR/SVD RBD and adopt it to get the first precoding filters due to its lower computational complexity and equivalent performance to the original RBD in [66]. In order to reduce the complexity further and to obtain a better BER performance, the second SVD is replaced by a complex lattice reduction whose complexity is mainly due to a QR decomposition. The aim of the LR algorithm is to find a new basis which is nearly orthogonal as compared to the original matrix. Therefore, if the second precoding filters for the equivalent SU-MIMO channels after the first SVD were designed based on the lattice reduced channel matrix, a better BER performance can be achieved. Then, a low-complexity LR-aided RBD precoding algorithm is proposed, which not only has a lower complexity but also achieves a better BER performance than the RBD or QR/SVD RBD.

It is worth noting that the two SVDs are no longer required in the proposed algorithm which only needs the CSI at the transmitter and a quantization procedure at the receiver. Hence, the required computational effort for each user's receiver is reduced and a significant amount of transmit power can be saved which is very important considering the mobility of the users.

3.2 System Model

We consider an uncoded MU-MIMO broadcast channel, with N_t transmit antennas at the BS and N_k receive antennas at the kth user. With K users in the system, the total number of receive antennas is $N_r = \sum_{k=1}^{K} N_k$. We assume a flat fading MIMO channel and the received signal at the kth user is given by

$$\boldsymbol{y}_k = \beta^{-1}(\boldsymbol{H}_k \boldsymbol{P}_k \boldsymbol{s}_k + \boldsymbol{H}_k \sum_{j=1, j\neq k}^{K} \boldsymbol{P}_j \boldsymbol{s}_j + \boldsymbol{n}_k), \tag{3.1}$$

where $\boldsymbol{H}_k \in \mathbb{C}^{N_k \times N_t}$ is the kth user's channel matrix. The quantity $\boldsymbol{P}_k \in \mathbb{C}^{N_t \times N_k}$ is the precoding matrix, β is a scalar chosen to make sure the energy of the precoded signal is not greater than the average transmit power E_s. The quantity $\boldsymbol{s}_k \in \mathbb{C}^{N_k}$ is the kth user's transmit signal, and $\boldsymbol{n}_k \in \mathbb{C}^{N_k}$ is the kth user's Gaussian noise with independent and identically distributed (i.i.d.) entries of zero mean and variance σ_n^2.

3.3 Proposed LC-RBD-LR Algorithm

From the system model, the combined channel matrix is given by $\boldsymbol{H} = [\boldsymbol{H}_1^T \ \boldsymbol{H}_2^T \ \dots \ \boldsymbol{H}_K^T]^T$. We exclude the kth user's channel matrix and define $\overline{\boldsymbol{H}}_k = [\boldsymbol{H}_1^T \ \dots \ \boldsymbol{H}_{k-1}^T \ \boldsymbol{H}_{k+1}^T \ \dots \ \boldsymbol{H}_K^T]^T$, so that $\overline{\boldsymbol{H}}_k \in \mathbb{C}^{\overline{N}_k \times N_t}$, where $\overline{N}_k = N_r - N_k$. The proposed precoder design is performed in two steps. Correspondingly, the precoding matrix in (3.1) can be rewritten as $\boldsymbol{P}_k = \beta \boldsymbol{P}_k^a \boldsymbol{P}_k^b$.

Step 1: Obtain the first precoding matrix $\boldsymbol{P}_k^a$ in RBD by a LQ decomposition of an extension of the matrix $\overline{\boldsymbol{H}}_k$.

For user k, the channel extension of $\overline{\boldsymbol{H}}_k$ is defined as

$$\overline{\overline{\boldsymbol{H}}}_k = [\rho \boldsymbol{I}_{\overline{N}_k}, \overline{\boldsymbol{H}}_k], \tag{3.2}$$

where $\rho = \sqrt{\frac{N_r \sigma_n^2}{E_s}}$ and $\boldsymbol{I}_{\overline{N}_k}$ is a $\overline{N}_k \times \overline{N}_k$ identity matrix. The LQ decomposition of $\overline{\overline{\boldsymbol{H}}}_k^H$ is given by

$$\overline{\overline{\boldsymbol{H}}}_k = \boldsymbol{L}_k \boldsymbol{Q}_k, \tag{3.3}$$

where $\boldsymbol{Q}_k$ is an $(\overline{N}_k + N_t) \times (\overline{N}_k + N_t)$ unitary matrix and $\boldsymbol{L}_k$ is an $\overline{N}_k \times (\overline{N}_k + N_t)$ lower triangular matrix. The matrix $\boldsymbol{L}_k$ can be partitioned into two parts as

$$\boldsymbol{L}_k = \left[\boldsymbol{L}_k^1 \ \boldsymbol{L}_k^0 \right], \tag{3.4}$$

where $\boldsymbol{L}_k^1 \in \mathbb{C}^{\overline{N}_k \times \overline{N}_k}$ holds the lower triangular structure and $\boldsymbol{L}_k^0 \in \mathbb{C}^{\overline{N}_k \times \overline{N}_t}$ is a zero matrix. Multiplying both sides of (3.2) with $\boldsymbol{Q}_k^H$, we can obtain

$$\begin{aligned} \overline{\overline{\boldsymbol{H}}}_k \boldsymbol{Q}_k^H &= \left[\rho \boldsymbol{I}_{\overline{N}_k}, \overline{\boldsymbol{H}}_k \right] \begin{bmatrix} \boldsymbol{Q}_{k,1} & \boldsymbol{Q}_{k,2} \\ \boldsymbol{Q}_{k,3} & \boldsymbol{Q}_{k,4} \end{bmatrix} \\ &= \left[\boldsymbol{L}_k^1 \ \boldsymbol{L}_k^0 \right], \end{aligned} \tag{3.5}$$

where $\boldsymbol{Q}_{k,1} \in \mathbb{C}^{\overline{N}_k \times \overline{N}_k}$, $\boldsymbol{Q}_{k,2} \in \mathbb{C}^{\overline{N}_k \times N_t}$, $\boldsymbol{Q}_{k,3} \in \mathbb{C}^{N_t \times \overline{N}_k}$ and $\boldsymbol{Q}_{k,4} \in \mathbb{C}^{N_t \times N_t}$. Because L_k^0 is a zero matrix, we can obtain

$$\overline{\boldsymbol{H}}_k \boldsymbol{Q}_{k,4} = -\rho \boldsymbol{I}_{\overline{N}_k} \boldsymbol{Q}_{k,2}, \tag{3.6}$$

$$\boldsymbol{Q}_{k,4}^H \overline{\boldsymbol{H}}_k^H = -\rho \boldsymbol{Q}_{k,2}^H \boldsymbol{I}_{\overline{N}_k}. \tag{3.7}$$

Multiplying both sides of (3.6) with $\boldsymbol{Q}_{k,4}^H \overline{\boldsymbol{H}}_k^H$ we have,

$$\boldsymbol{Q}_{k,4}^H \overline{\boldsymbol{H}}_k^H \overline{\boldsymbol{H}}_k \boldsymbol{Q}_{k,4} - \rho^2 \boldsymbol{Q}_{k,2}^H \boldsymbol{Q}_{k,2} = \boldsymbol{0}. \tag{3.8}$$

Due to the fact that $\boldsymbol{Q}_{k,2}^H \boldsymbol{Q}_{k,2} + \boldsymbol{Q}_{k,4}^H \boldsymbol{Q}_{k,4} = \boldsymbol{I}_{\overline{N}_k}$, we can obtain

$$\boldsymbol{Q}_{k,4}^H (\overline{\boldsymbol{H}}_k^H \overline{\boldsymbol{H}}_k + \rho^2 \boldsymbol{I}) \boldsymbol{Q}_{k,4} = \rho^2 \boldsymbol{I}_{\overline{N}_k}. \tag{3.9}$$

Considering the SVD decomposition of $\overline{\boldsymbol{H}}_k = \overline{\boldsymbol{U}}_k \overline{\boldsymbol{\Sigma}}_k \overline{\boldsymbol{V}}_k^H$, we have

$$\boldsymbol{Q}_{k,4}^H \overline{\boldsymbol{V}}_k (\overline{\boldsymbol{\Sigma}}_k^T \overline{\boldsymbol{\Sigma}}_k + \rho^2 \boldsymbol{I}_{\overline{N}_k}) \overline{\boldsymbol{V}}_k^H \boldsymbol{Q}_{k,4} = \rho^2 \boldsymbol{I}_{\overline{N}_k}. \tag{3.10}$$

Thus, we can obtain

$$\boldsymbol{Q}_{k,4} = \rho \overline{\boldsymbol{V}}_k (\overline{\boldsymbol{\Sigma}}_k^T \overline{\boldsymbol{\Sigma}}_k + \rho^2 \boldsymbol{I}_{\overline{N}_k})^{-1/2}. \tag{3.11}$$

Mathematically, the $\boldsymbol{Q}_{k,4}$ in (3.11) is equivalent to the first precoding matrix $\boldsymbol{P}_i^a$ of RBD in (2.61) and satisfies the RBD constraint defined in (2.58). Compared to the conventional RBD precoding, the first precoding filter $\boldsymbol{P}_i^a$ for the proposed LC-RBD-LR algorithm is obtained by an LQ decomposition. Because the first SVD operation is avoided, a considerable computational complexity can be reduced. Then, the first precoding matrix $\boldsymbol{P}_k^a$ for the kth user is obtained as

$$\boldsymbol{P}_k^a = \boldsymbol{Q}_k(\overline{N}_k + 1 : \overline{N}_k + N_t,\ \overline{N}_k + 1 : \overline{N}_k + N_t), \tag{3.12}$$

and the first combined precoding matrix for all users is

$$\boldsymbol{P}^a = [\boldsymbol{P}_1^a,\ \boldsymbol{P}_2^a,\ \ldots,\ \boldsymbol{P}_K^a]. \tag{3.13}$$

Step 2: Employ the CLR algorithm instead of the second SVD to implement the size-reduction, and obtain the second precoding matrix $\boldsymbol{P}^b$ by implementing channel inversion.

The aim of the CLR transformation is to find a new basis $\tilde{\boldsymbol{H}}$ which is nearly orthogonal compared to the original matrix $\boldsymbol{H}$ for a given lattice $L(\boldsymbol{H})$. After the first precoding, the effective channel matrix for the kth user is

$$\boldsymbol{H}_{\text{eff}_k} = \boldsymbol{H}_k \boldsymbol{P}_k^a. \tag{3.14}$$

We perform the CLR transformation on $\boldsymbol{H}_{\mathrm{eff}_k}^T$ in the precoding scenario [91], that is

$$\tilde{\boldsymbol{H}}_{\mathrm{eff}_k} = \boldsymbol{U}_k \boldsymbol{H}_{\mathrm{eff}_k}, \tag{3.15}$$

where $\boldsymbol{U}_k$ is a unimodular matrix ($\det|\boldsymbol{U}_{\mathrm{k}}| = 1$) and all elements of $\boldsymbol{U}_k$ are complex integers, i.e. $u_{i,j} \in \mathbb{Z} + j\mathbb{Z}$.

By using the ZF precoding approach, the second precoding matrix for user k is given as

$$\tilde{\boldsymbol{P}}_{\mathrm{ZF}_k}^b = \tilde{\boldsymbol{H}}_{\mathrm{eff}_k}^H (\tilde{\boldsymbol{H}}_{\mathrm{eff}_k} \tilde{\boldsymbol{H}}_{\mathrm{eff}_k}^H)^{-1}. \tag{3.16}$$

The MMSE precoding is equivalent to ZF with respect to an extended system model [90, 102]. The extended channel matrix $\underline{\boldsymbol{H}}$ for the precoding scheme is defined as

$$\underline{\boldsymbol{H}} = [\boldsymbol{H},\ \sigma_n \boldsymbol{I}_{N_r}]. \tag{3.17}$$

The MMSE precoding filter can be rewritten as $\boldsymbol{P}_{\mathrm{MMSE}} = \boldsymbol{A}\underline{\boldsymbol{H}}^H (\underline{\boldsymbol{H}}\underline{\boldsymbol{H}}^H)^{-1}$, where $\boldsymbol{A} = [\boldsymbol{I}_{N_t},\ \boldsymbol{0}_{N_t,N_r}]$. The rows of $\underline{\boldsymbol{H}}$ determine the effective transmit power amplification. Correspondingly, the CLR transformation should be applied to the transpose of the extended channel matrix $\underline{\boldsymbol{H}}_{\mathrm{eff}_k}^T = [\boldsymbol{H}_{\mathrm{eff}_k},\ \sigma_n \boldsymbol{I}_{N_k}]^T$ for the MMSE precoding, and thus the CLR transformed channel matrix $\underline{\tilde{\boldsymbol{H}}}_{\mathrm{eff}_k}$ is obtained. Then, the CLR-aided MMSE precoding filter is given by

$$\tilde{\boldsymbol{P}}_{\mathrm{MMSE}_k}^b = \boldsymbol{A}\underline{\tilde{\boldsymbol{H}}}_{\mathrm{eff}_k}^H (\underline{\tilde{\boldsymbol{H}}}_{\mathrm{eff}_k} \underline{\tilde{\boldsymbol{H}}}_{\mathrm{eff}_k}^H)^{-1}. \tag{3.18}$$

Finally, the second precoding matrix $\tilde{\boldsymbol{P}}^b$ for all users is

$$\tilde{\boldsymbol{P}}^b = \begin{bmatrix} \tilde{\boldsymbol{P}}_1^b & 0 & \dots & 0 \\ 0 & \tilde{\boldsymbol{P}}_2^b & \dots & 0 \\ \vdots & \vdots & \ddots & \vdots \\ 0 & 0 & 0 & \tilde{\boldsymbol{P}}_K^b \end{bmatrix}. \tag{3.19}$$

The resulting precoding matrix is $\tilde{\boldsymbol{P}} = \beta \boldsymbol{P}^a \tilde{\boldsymbol{P}}^b$, where the gain factor $\beta = \sqrt{E_s/(\|\boldsymbol{P}^a \tilde{\boldsymbol{P}}^b\|^2)}$. Since the lattice reduced precoding matrix $\tilde{\boldsymbol{P}}^b$ has near-orthogonal columns, it is able to reduce the interference to a lower level than the precoder $\boldsymbol{P}^b$ obtained from the linear or BD designs. The required transmit power will be reduced and a better BER performance can be achieved by the proposed LC-RBD-LR algorithm.

The received signal is finally obtained as

$$\boldsymbol{y} = \beta^{-1}(\boldsymbol{H}\tilde{\boldsymbol{P}}\boldsymbol{s} + \boldsymbol{n}). \tag{3.20}$$

The main processing work left for the receiver is to quantize the received signal $\boldsymbol{y}$ to the nearest transmitted symbols and the decoding matrix $\boldsymbol{G}_k$ in the conventional RBD precoding is not needed anymore.

3.4 Computational Complexity Analysis

In this section we use the total number of FLOPs to measure the computational complexity of the proposed and existing algorithms. According to [95], the average complexity of the CLR algorithm is almost 1.6 times of the QR decomposition. FLOPs for real QR, SVD and complex QR decomposition are given in [103]. In real arithmetic, a multiply followed by an addition needs 2 FLOPs. With complex-valued quantities, a multiplication followed by an addition needs 8 FLOPs. Thus, the complexity of a complex matrix multiplication is nearly 4 times its real counterpart. For a complex $m \times n$ matrix $\boldsymbol{A}$, its SVD is given by $\boldsymbol{A} = \boldsymbol{U}\boldsymbol{\Sigma}\boldsymbol{V}^H$, where $\boldsymbol{U}$ and $\boldsymbol{V}$ are unitary matrices and $\boldsymbol{\Sigma}$ is a diagonal matrix containing the singular values of matrix $\boldsymbol{A}$. Rewriting this formulation, we have

$$\begin{bmatrix} \boldsymbol{A}_r & \boldsymbol{A}_i \\ -\boldsymbol{A}_i & \boldsymbol{A}_r \end{bmatrix} = \begin{bmatrix} \boldsymbol{U}_r & \boldsymbol{U}_i \\ \boldsymbol{U}_i & -\boldsymbol{U}_r \end{bmatrix} \begin{bmatrix} \boldsymbol{\Sigma} & 0 \\ 0 & \boldsymbol{\Sigma} \end{bmatrix} \begin{bmatrix} \boldsymbol{V}_r^T & \boldsymbol{V}_i^T \\ \boldsymbol{V}_i^T & -\boldsymbol{V}_r^T \end{bmatrix}. \tag{3.21}$$

From (3.21), the number of FLOPs required by a $m \times n$ complex SVD is equivalent to the complexity required by its extended $2m \times 2n$ real matrix. We summarize the total FLOPs needed for the matrix operations below:

- Multiplication of $m \times n$ and $n \times p$ complex matrices: $8mnp - 2mp$;
- QR decomposition of an $m \times n$ $(m \leq n)$ complex matrix: $16(n^2m - nm^2 + \frac{1}{3}m^3)$;
- SVD of an $m \times n$ $(m \leq n)$ complex matrix where only $\boldsymbol{\Sigma}$ and $\boldsymbol{V}$ are obtained: $32(nm^2 + 2m^3)$;
- SVD of an $m \times n$ $(m \leq n)$ complex matrix where $\boldsymbol{U}$, $\boldsymbol{\Sigma}$ and $\boldsymbol{V}$ are obtained: $8(4n^2m + 8nm^2 + 9m^3)$;

Table 3.1: Computational complexity of LC-RBD-LR algorithm

Steps	Operations	Flops	Case $(2,2,2)\times 6$
1	$\mathrm{QR}(\overline{\overline{\boldsymbol{H}}}_k^H)$	$16K(N_t^2\overline{N}_k+$ $N_t\overline{N}_k^2+\frac{1}{3}\overline{N}_k^3)$	12544
2	$\boldsymbol{H}_k\boldsymbol{P}_k^a$	$K(8N_k^2N_t-2N_k^2)$	552
3_{ZF}	$\mathrm{CLR}(\boldsymbol{H}_{\mathrm{eff}_k}^T)^T$	$25.6K(N_t^2N_k-$ $N_tN_k^2+\frac{1}{3}N_k^3)$	3891
3_{MMSE}	$\mathrm{CLR}(\underline{\boldsymbol{H}}_{\mathrm{eff}_k}^T)^T$	$25.6K(N_t^2N_k+$ $N_tN_k^2+\frac{1}{3}N_k^3)$	7578
4_{ZF}	$\tilde{\boldsymbol{H}}_{\mathrm{eff}_k}^H(\tilde{\boldsymbol{H}}_{\mathrm{eff}_k}\tilde{\boldsymbol{H}}_{\mathrm{eff}_k}^H)^{-1}$	$K(\frac{4}{3}N_k^3+12N_k^2N_t$ $-2N_k^2-2N_kN_t)$	800 Total 17787
4_{MMSE}	$\underline{\tilde{\boldsymbol{H}}}_{\mathrm{eff}_k}^H(\underline{\tilde{\boldsymbol{H}}}_{\mathrm{eff}_k}\underline{\tilde{\boldsymbol{H}}}_{\mathrm{eff}_k}^H)^{-1}$	$K(\frac{4}{3}N_k^3+12N_k^2N_t$ $-2N_kN_t)$	824 Total 21498

- Inversion of an $m\times m$ real matrix: $2m^3-2m^2+m$.

For the case shown in Table 3.1, Table 3.2 and Table 3.3, the complexity of the proposed LC-RBD-LR-ZF is about 43.6% of RBD and 67.5% of the QR/SVD RBD, while the complexity of the proposed LC-RBD-LR-MMSE is about 52.7% of RBD and 81.6% of the QR/SVD RBD. Clearly, the proposed algorithm requires the lowest complexity.

The required number of FLOPs of the proposed and existing algorithms are simulated for different system dimensions and the results are displayed in Figure 3.1. The simulations are implemented in Matlab and we average the curves over 100 independent trials. Moreover, we assume that each user is equipped with $N_k=2$ antennas and the number of users K is set to make the total number of receive antennas N_r equal to the number of transmit

Table 3.2: Computational complexity of Conventional RBD

Steps	Operations	Flops	Case $(2,2,2)\times 6$
1	$\boldsymbol{U}_k^a\boldsymbol{\Sigma}_k^a\boldsymbol{V}_k^{aH}$	$32K(N_t\overline{N}_k^2+2\overline{N}_k^3)$	21504
2	$(\boldsymbol{\Sigma}_k^{aT}\boldsymbol{\Sigma}_k^a+\rho^2\boldsymbol{I}_b)^{-\frac{1}{2}}$	$K(18N_t+\overline{N}_k)$	336
3	$\boldsymbol{V}_k^a\boldsymbol{D}_k^a,(\boldsymbol{D}_k^a\leftarrow 2)$	$8KN_t^3$	5184
4	$\boldsymbol{H}_k\boldsymbol{P}_k^a$	$K(8N_k^2N_t-2N_k^2)$	552
5	$\boldsymbol{U}_k^b\boldsymbol{\Sigma}_k^b\boldsymbol{V}_k^{bH}$	$64K(\frac{9}{8}N_k^3+$ $N_tN_k^2+\frac{1}{2}N_t^2N_k)$	13248 Total 40824

Table 3.3: Computational complexity of QR/SVD RBD

Steps	Operations	Flops	Case $(2,2,2)\times 6$
1	$\overline{\overline{\boldsymbol{H}}}_k^H=\boldsymbol{Q}_k\boldsymbol{R}_k$	$16K(N_t^2\overline{N}_k+$ $N_t\overline{N}_k^2+\frac{1}{3}\overline{N}_k^3)$	12544
2	$\boldsymbol{H}_{\mathrm{eff}_k}=\boldsymbol{H}_k\boldsymbol{P}_k^a$	$K(8N_k^2N_t-2N_k^2)$	552
3	$\boldsymbol{H}_{\mathrm{eff}_k}=\boldsymbol{U}_k^b\boldsymbol{\Sigma}_k^b\boldsymbol{V}_k^{bH}$	$64K(\frac{9}{8}N_k^3+$ $N_tN_k^2+\frac{1}{2}N_t^2N_k)$	13248 Total 26344

antennas N_t. From Figure 3.1, it is clear that the proposed LC-RBD-LR algorithms show a lower computational complexity than that of the RBD and QR/SVD RBD algorithms. It is worth noting that with the increase of the system dimension, the complexity reduction becomes more considerable.

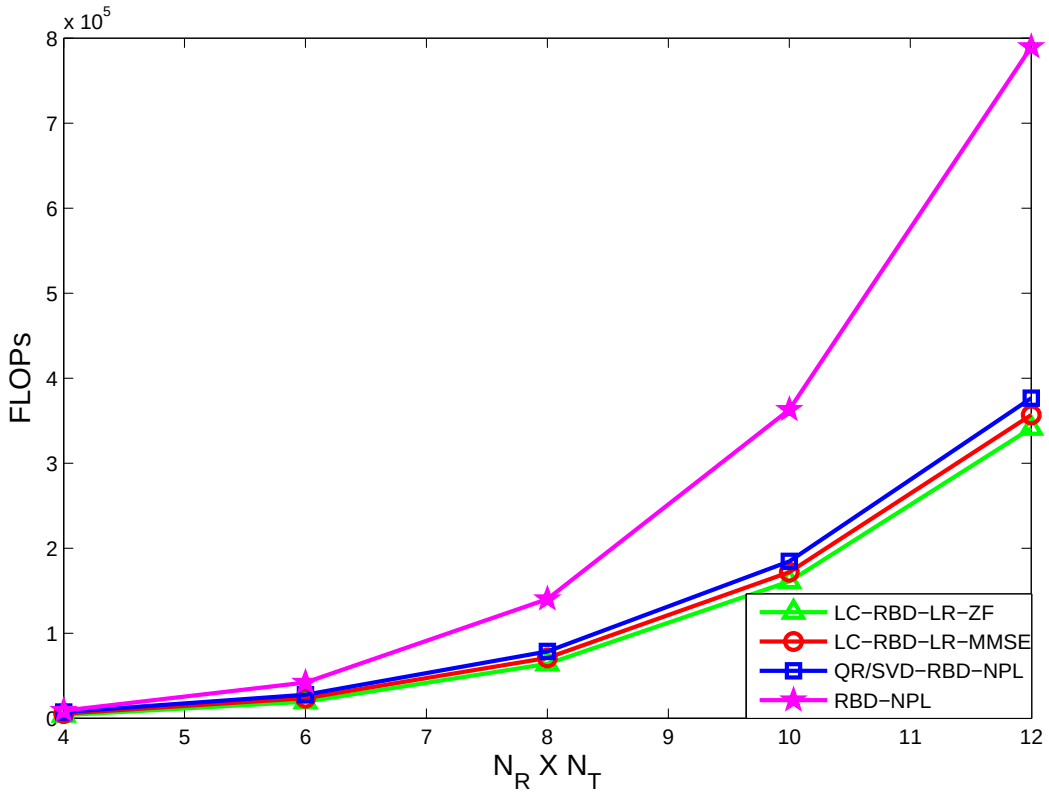

Figure 3.1: Computational Complexity in FLOPs for MU-MIMO Systems

3.5 Connection with BD precoding

The connection of LC-RBD-LR from the RBD precoding to the BD precoding is straightforward by defining the channel extension of $\overline{\boldsymbol{H}}_k$ as

$$\overline{\overline{\boldsymbol{H}}}_k = \left[\mathbf{0}, \overline{\boldsymbol{H}}_k\right], \tag{3.22}$$

where $\mathbf{0} \in \mathbb{C}^{\overline{N}_k \times \overline{N}_k}$ is a zero matrix. The LQ decomposition of $\overline{\overline{\boldsymbol{H}}}_k$ is given by

$$\overline{\overline{\boldsymbol{H}}}_k = \boldsymbol{L}_k \boldsymbol{Q}_k, \tag{3.23}$$

where $\boldsymbol{L}_k \in \mathbb{C}^{\overline{N}_k \times (\overline{N}_k + N_t)}$ is a lower triangular matrix and $\boldsymbol{Q}_k \in \mathbb{C}^{(\overline{N}_k + N_t) \times (\overline{N}_k + N_t)}$ is a unitary matrix. Since $\overline{\overline{\boldsymbol{H}}}_k$ is a rectangular matrix, we can express or partition the $\boldsymbol{L}_k$ matrix into two factors as

$$\boldsymbol{L}_k = \left[\boldsymbol{L}_k^1 \, \boldsymbol{L}_k^0\right], \tag{3.24}$$

where $\boldsymbol{L}_k^1 \in \mathbb{C}^{\overline{N}_k \times \overline{N}_k}$ holds the lower triangular structure and $\boldsymbol{L}_k^0 \in \mathbb{C}^{\overline{N}_k \times \overline{N}_t}$ is a zero matrix. Multiplying both sides of (3.22) with $\boldsymbol{Q}_k^H$, we can obtain

$$\overline{\overline{\boldsymbol{H}}}_k \boldsymbol{Q}_k^H = \left[\mathbf{0}, \overline{\boldsymbol{H}}_k\right] \begin{bmatrix} \boldsymbol{Q}_{k,1} & \boldsymbol{Q}_{k,2} \\ \boldsymbol{Q}_{k,3} & \boldsymbol{Q}_{k,4} \end{bmatrix}, \tag{3.25}$$

where $\boldsymbol{Q}_{k,1} \in \mathbb{C}^{\overline{N}_k \times \overline{N}_k}$, $\boldsymbol{Q}_{k,2} \in \mathbb{C}^{\overline{N}_k \times N_t}$, $\boldsymbol{Q}_{k,3} \in \mathbb{C}^{N_t \times \overline{N}_k}$ and $\boldsymbol{Q}_{k,4} \in \mathbb{C}^{N_t \times N_t}$. Since $\boldsymbol{L}_k^0$ is a zero matrix, we can get the fact that

$$\overline{\boldsymbol{H}}_k \boldsymbol{Q}_{k,4} = \boldsymbol{L}_k^0 = \mathbf{0}, \tag{3.26}$$

the matrix $\boldsymbol{Q}_{k,4}$ forms an orthogonal basis for the null space $\overline{\boldsymbol{H}}_k$ and satisfies the BD constraint in (2.57). Therefore, the first BD precoding filter for the kth user is alternatively obtained as

$$\boldsymbol{P}_k^a = \boldsymbol{Q}_{k,4}. \tag{3.27}$$

After the first precoding, we transform the MU-MIMO channel into equivalent parallel SU-MIMO channels. The second precoding filter $\boldsymbol{P}_k^b$ can be obtained by implementing the LR-aided linear precoding process in Step 2. Note that the dimension constraint of the conventional BD-type precoding in (2.67) is overcame by the proposed LC-BD-LR type precoding algorithm since the columns of $\overline{\boldsymbol{H}}$ are increased from the matrix extension in (3.6) and (3.22).

3.6 The Influence of Imperfect Channels

It is well-known in the literature that perfect CSI is impractical due to the often inaccurate channel estimation and the CSI feedback errors [20, 104]. The estimation errors or feedback errors can be modeled as a complex random Gaussian noise $\boldsymbol{E}$ with i.i.d. entries of zero mean and variance σ_e^2. The imperfect channel matrix $\boldsymbol{H}_e$ is defined as

$$\boldsymbol{H}_e = \boldsymbol{H} + \boldsymbol{E}, \tag{3.28}$$

where the precoding matrix $\boldsymbol{P}$ has to be designed based on the feedback channel $\boldsymbol{H}_e$ while the physical channel is $\boldsymbol{H}$ during each transmission. Correspondingly, the precoding matrix $\boldsymbol{P}$ has to be designed based on the feedback channel $\boldsymbol{H}_e$ while the physical channel is $\boldsymbol{H}$ during each transmission. Therefore, the BER performance will be degraded by the distortion term $\boldsymbol{E}$. Assuming that the precoding matrix $\boldsymbol{P}$ is designed according to the LC-RBD-LR-ZF precoding algorithm, the received signal is given by

$$\boldsymbol{y} = (\boldsymbol{H}_e - \boldsymbol{E})\boldsymbol{P}\boldsymbol{s} + \beta^{-1}\boldsymbol{n} = \boldsymbol{s} - \boldsymbol{E}\boldsymbol{P}\boldsymbol{s} + \beta^{-1}\boldsymbol{n}, \tag{3.29}$$

where $\boldsymbol{E}\boldsymbol{P}\boldsymbol{s}$ is the interference term caused by the imperfect CSI. The error covariance matrix is obtained as

$$\boldsymbol{\Phi}_{ee} = E[(\boldsymbol{y} - \boldsymbol{s})(\boldsymbol{y} - \boldsymbol{s})^H] = \sigma_e^2 E[\boldsymbol{P}\boldsymbol{P}^H] + \beta^{-2}\sigma_n^2. \tag{3.30}$$

With perfect CSI, σ_e^2 is zero in $\boldsymbol{\Phi}_{ee}$ and the total error is only determined by the noise term $\boldsymbol{n}$; if there exists estimation errors or feedback errors, however, the total error $\boldsymbol{\Phi}_{ee}$ is not only affected by the noise $\boldsymbol{n}$ but also influenced by the distortion term $\boldsymbol{E}$. Thus the BER performance would become worse with the increase of the distortion power σ_e^2.

Another factor that we should take into account is the spatial correlation caused by sparse scattering and insufficient spacing between adjacent antennas [104]. The correlated channel model given in Section 2.3.1 is applied and we examine the performance of the above precoding algorithms with correlation coefficient $|r| = 0.2, 0.5$ and 0.7 in the following.

3.7 Simulation Results

A system with $N_t = 6$ transmit antennas and $K = 3$ users each equipped with $N_k = 2$ receive antennas is considered; this scenario is denoted as $(2, 2, 2) \times 6$ case.

3.7.1 Perfect Channel Scenario

The transmitted signal $\boldsymbol{s}_k$ of the kth user employs 4-QAM modulation. The channel matrix $\boldsymbol{H}_k$ of the kth user is modeled as a complex Gaussian channel matrix with zero mean and unit variance. We assume an uncorrelated block fading channel, that is, the channel is static during each transmit packet and there is no correlation between the antennas. We also assume that the channel estimation is perfect at the receive side and the feedback channel is error free. For simplicity we do not consider the power loading between users and streams and we term this strategy as no power loading (NPL). The number of simulation trials is 10^6 and the packet length is 10^2 symbols. The E_b/N_0 is defined as $E_b/N_0 = \frac{N_r E_s}{N_t M N_0}$ with M being the number of transmitted information bits per channel symbol.

Figure 3.2 shows the BER performance of the proposed and existing algorithms. It is clear that the proposed algorithm has a better performance compared to the BD, RBD and QR/SVD RBD algorithms. The QR/SVD RBD has the same BER performance as the RBD. At the BER of 10^{-2}, LC-RBD-LR-ZF has a gain of more than 6 dB compared to the RBD, whereas LC-RBD-LR-MMSE has a gain of more than 7 dB over RBD. It is worth noting that the BER performance of RBD is outperformed by the proposed LC-RBD-LR-MMSE in the whole E_b/N_0 range and the improved BER gains become more significant with the increase of E_b/N_0. The BER performance of RBD is actually dependent on the power loading algorithm being used, an *improved diversity* (impD) power loading algorithm is proposed in [66] to achieve a better BER performance for RBD. For a fair comparison, the RBD with impD power loading is simulated and the comparison with the proposed algorithm is shown as well in Figure 3.2. As we can see, RBD-impD shows a 5 dB gains over RBD-NPL at BER around 2.8×10^{-3}; however, it still gets 5 dB loss compared to the proposed LC-RBD-LR-MMSE algorithm.

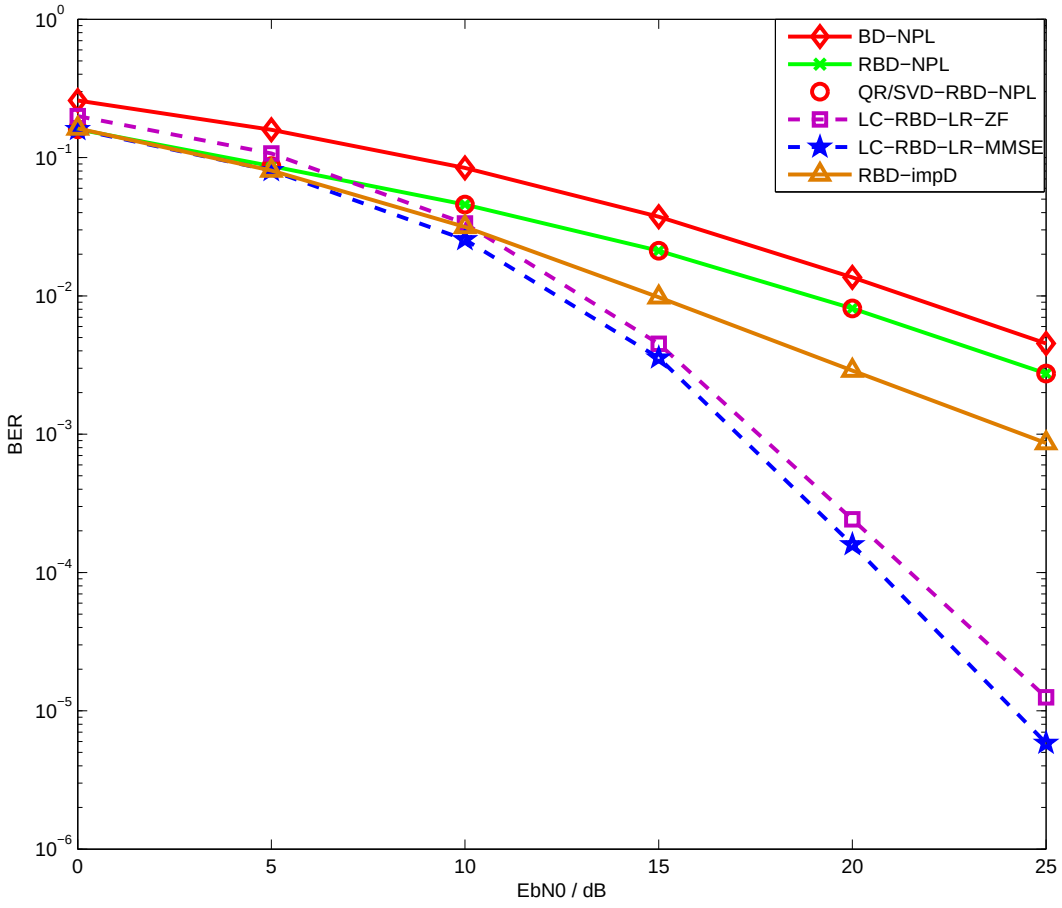

Figure 3.2: BER performance, $(2, 2, 2) \times 6$ *MU-MIMO*

Figure 3.3 illustrates the sum-rate of the proposed and existing algorithms. The sum-rate is calculated using [105]:

$$C = \log(\det(\boldsymbol{I} + \sigma_n^{-2}\boldsymbol{H}\boldsymbol{P}\boldsymbol{P}^H\boldsymbol{H}^H)) \ \text{(bits/Hz)}. \tag{3.31}$$

From Figure 3.3, the proposed LC-RBD-LR-MMSE has the same sum-rate as RBD at low E_b/N_0s. At high E_b/N_0s, it is slightly inferior to the performance of RBD but requires a lower computational complexity.

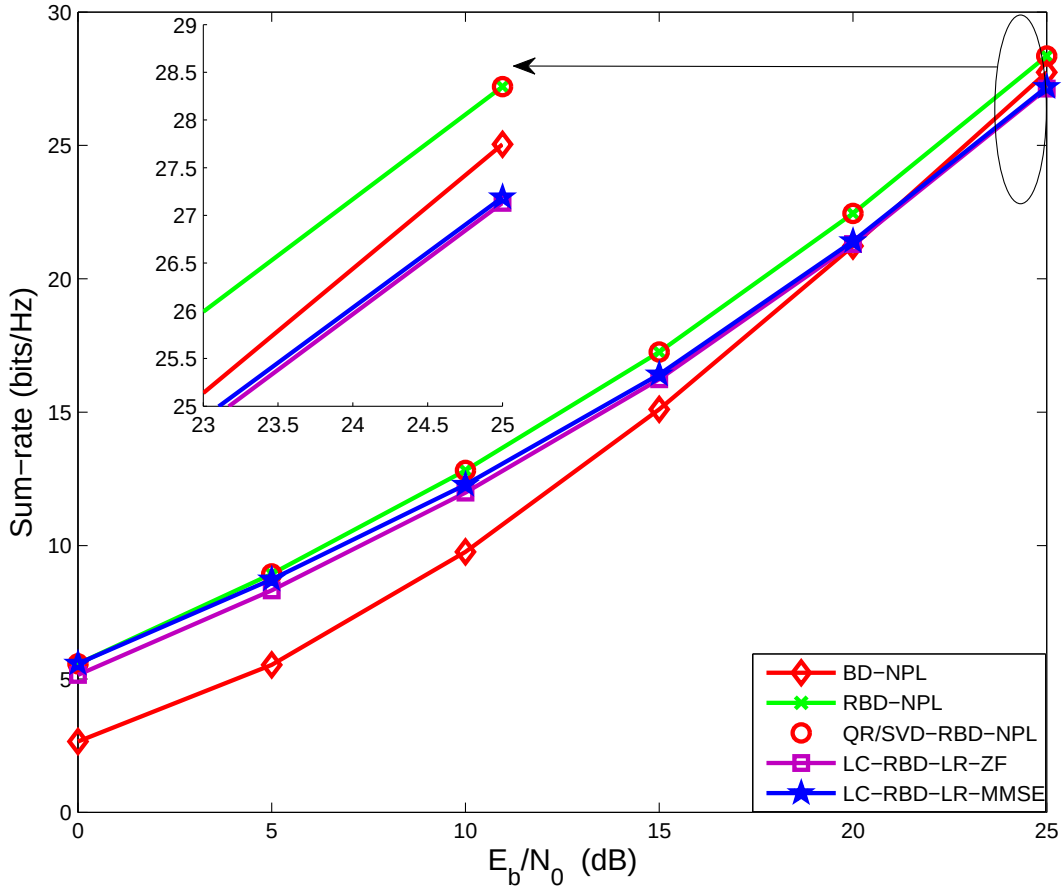

Figure 3.3: Sum-rate performance, $(2, 2, 2) \times 6$ *MU-MIMO*

3.7.2 Imperfect Channel Scenario

In order to measure the robustness of the proposed LC-RBD-LR precoding algorithms, we need to consider the scenarios of imperfect CSI at the transmit side and channels with spatial correlation as well.

Figure 3.4 gives the BER performance of the above algorithms with imperfect CSI of a fixed $E_b/N_0 = 10$ dB. It is clear that by increasing the distortion noise power σ_e^2, the BER gets worse for all the above algorithms. The proposed LC-RBD-LR-MMSE outperforms RBD when σ_e^2 is below 10^{-1}, however, for severe distortions, RBD is more robust and reliable than the other algorithms.

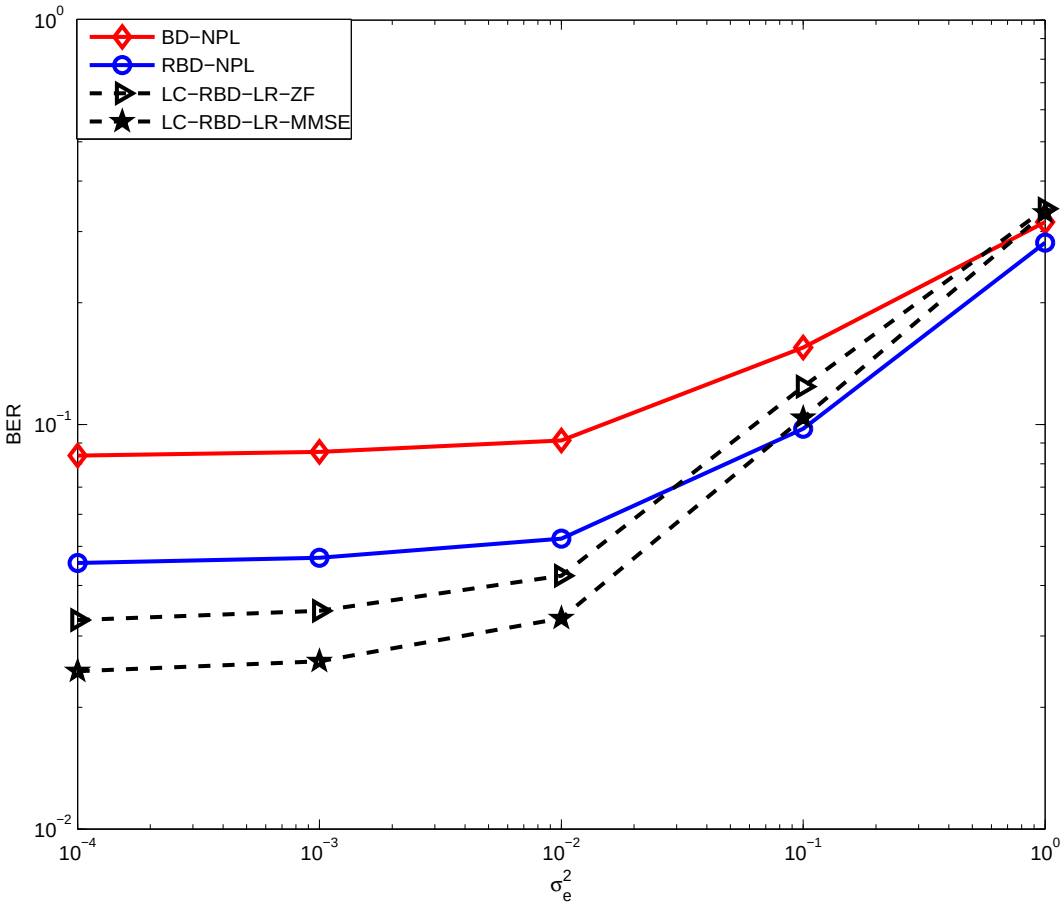

Figure 3.4: Sum-rate performance, $(2, 2, 2) \times 6$ *MU-MIMO*

Figure 3.5 and Figure 3.6 display the BER and sum-rate performances of the above algorithms with spatial correlation. It is obvious that both BER and sum-rate performance deteriorate with the increase of the correlation coefficient r. From Figure 3.5, the proposed LC-RBD-LR-ZF and LC-RBD-LR-MMSE outperform the BD and RBD algorithms from slight to severe spatial correlations. Due to the second step being based on the channel inversion strategy, the proposed algorithms still suffer a little sum-rate loss at high SNRs. At low SNRs, however, the sum-rate of the proposed LC-RBD-LR-MMSE gradually becomes better compared to the RBD. For example, with the highly correlated scenario $|r| = 0.7$, the sum-rate of LC-RBD-LR-MMSE is better than RBD from 0 dB to 10 dB, which illustrates the robustness when the proposed algorithms encounter spatial correlation.

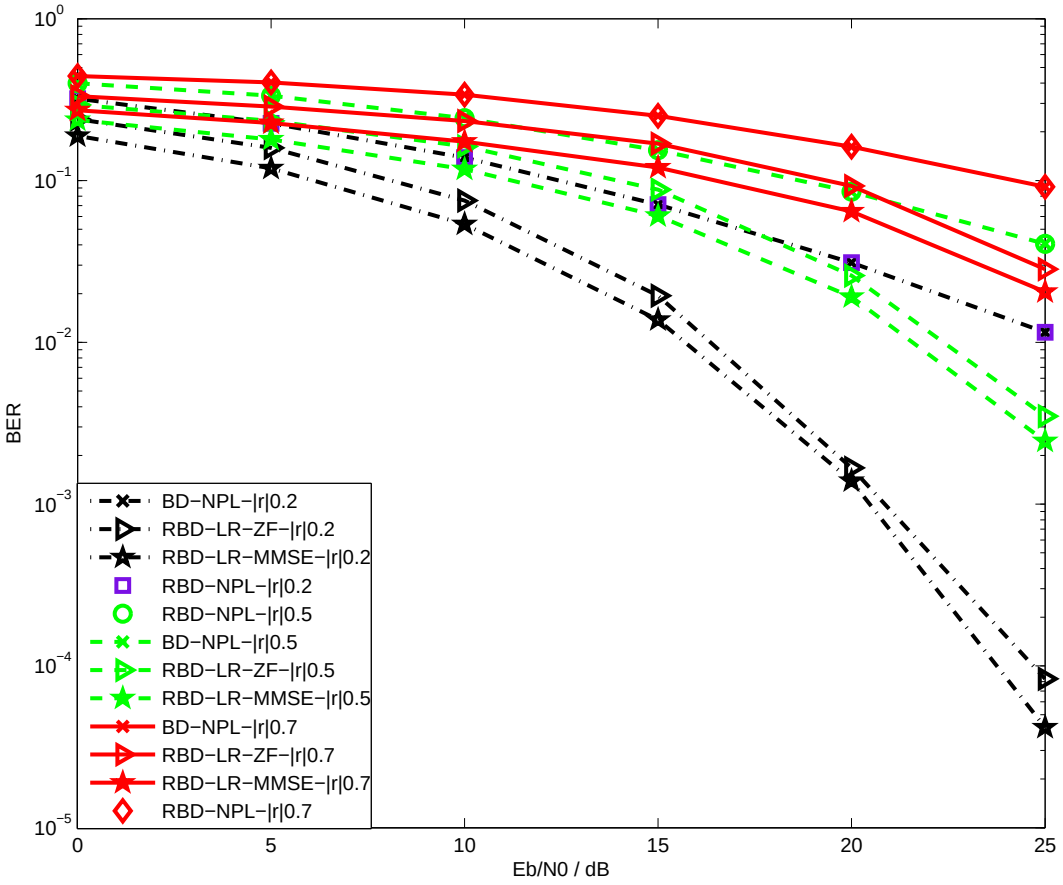

Figure 3.5: Sum-rate performance, $(2, 2, 2) \times 6$ *MU-MIMO*

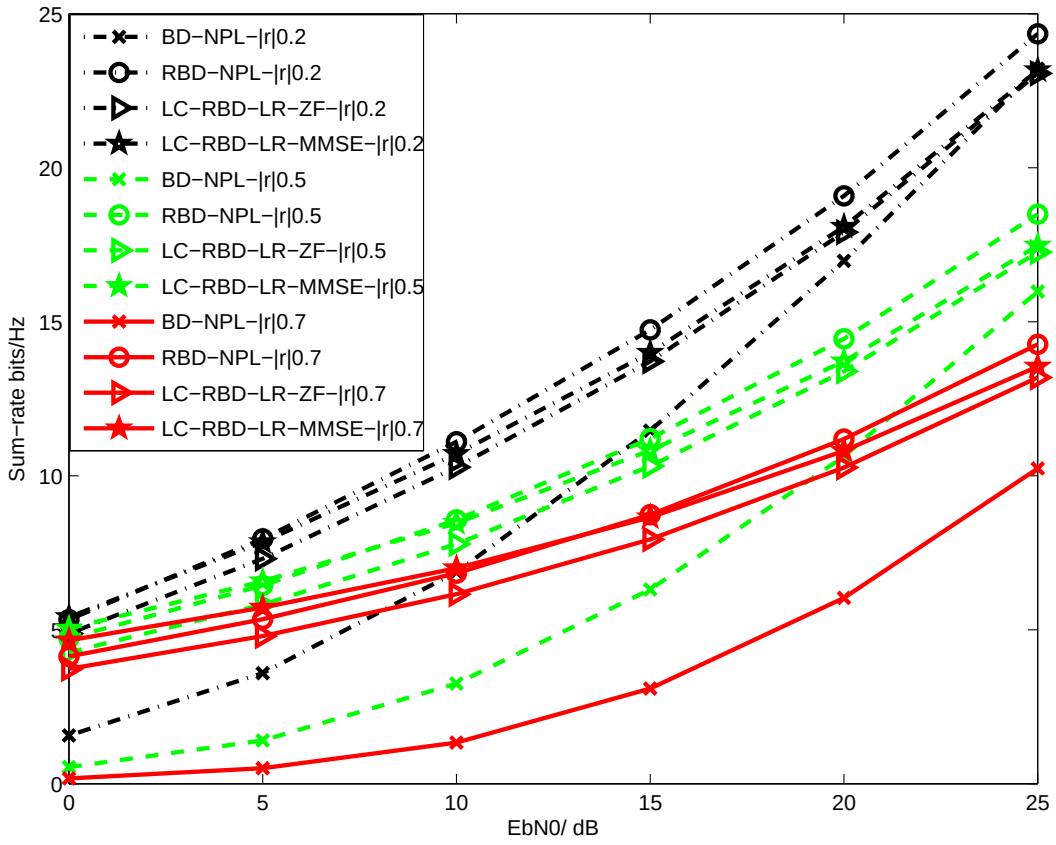

Figure 3.6: Sum-rate performance, $(2, 2, 2) \times 6$ *MU-MIMO*

3.8 Summary

In this Chapter, a low-complexity precoding algorithm for MU-MIMO systems has been proposed. The complexity of the precoding process is reduced and a considerable BER gain is achieved by the proposed LC-RBD-LR algorithm at a cost of a slight sum-rate loss at high SNRs. The computational complexity of the proposed LC-RBD-LR algorithm is analyzed and compared to existing algorithms. The proposed algorithm shows a robust performance in the presence of imperfect CSI and spatial correlation. It is worth noting that the receiver is simplified by employing the proposed LC-RBD-LR algorithm at the transmit side as there is no need for an SVD at the receiver.

Chapter 4

Low-Complexity Block Diagonalization Type Precoding Algorithms

Contents

Based on multiple QR decompositions and lattice reductions, the LC-RBD-LR precoding algorithm has been proposed for the improvement of RBD in Chapter 3. The main computational complexity of BD-type precoding algorithms comes from two singular value decomposition (SVD) operations, which depends on the number of users and the dimensions of each user's channel matrix. Then, if the dimensions of a wireless system are high, the implementation of the BD-type precoding algorithms could be an issue. In this Chapter, another class of low-complexity BD-type precoding algorithms, which can offer further reduction in computational complexity compared to the LC-RBD-LR while main-

taining almost the same performance, are developed and proposed. Based on a channel inversion technique, QR decompositions, and lattice reductions, the proposed precoding algorithms decouple the MU-MIMO channel into equivalent SU-MIMO channels. Analytical and simulation results show that the proposed precoding algorithms can achieve a comparable sum-rate performance as BD-type precoding algorithms, substantial BER performance gains, and a simplified receiver structure, while requiring a much lower complexity.

4.1 Introduction

In order to meet the continuous growing data traffic, a downlink peak spectrum efficiency of 30 bps/Hz and an uplink peak spectrum efficiency of 15 bps/Hz is proposed in LTE-Advanced [14], and a configuration of up to 8 transmit antennas for the downlink is suggested. A new amendment for the WLAN standard IEEE 802.11ac [13] also recommends up to 8 MIMO spatial streams. Configurations with dozens of antennas are now being considered [23]. High-dimensional MIMO systems or large MIMO systems are very promising for the next generation of wireless communication systems due to their potential to improve rate and reliability dramatically [24]. However, it is a challenge to design a suitable precoding algorithm with good overall performance and low computational complexity at the same time for high-dimensional MIMO systems.

As we discussed in the previous Section, the main steps of the BD-type precoding algorithms are two SVD operations. And another distinctive aspect of the BD-type precoding algorithms is that they need a decoding matrix which can be obtained by the second SVD operation to orthogonalize each user's streams. This requirement brings extra control overhead or computational complexity. In addition, as revealed in Chapter 3, the computational complexity of the BD-type precoding algorithms depends on the number of users and the dimensions of each user's channel matrix which could result in a considerable computational cost for MU-MIMO systems with a large number of users each with multiple receive antennas.

Recent work on the BD-type precoding algorithms has focused on the reduction of their computational complexity. A low complexity *Generalized ZF* (GZI) channel inversion

method has been proposed in [106] to equivalently implement the first SVD operation of the original BD precoding which is proposed in [29], and a *Generalized MMSE* (GMI) channel inversion method is also developed in [106] for the original RBD precoding which is proposed in [66]. In [101] the first SVD operation of the RBD precoding is replaced with a less complex QR decomposition [103]. We term the work in [106] as GMI-type BD precoding and the work in [101] as QR/SVD-type BD precoding. For the second SVD operation, however, both the GMI-type and QR/SVD-type BD precoding schemes still employ it in a similar way as the conventional BD-type precoding algorithms. Therefore, the decoding matrix for the effective channel needs to be known or estimated at the receiver of each user for the GMI-type or QR/SVD-type BD precoding algorithms.

In this Chapter, we first develop a *Simplified GMI* (S-GMI) precoding scheme which employs a channel inversion and less complex QR decompositions computed with a lower matrix dimension instead of the first SVD operation, to obtain the equivalent parallel SU-MIMO channels. In order to reduce the computational complexity further and also to achieve a better BER performance, we transform the equivalent SU-MIMO channels into the lattice space by utilizing the LR technique [95, 107] whose complexity is mainly due to a QR decomposition. Then, a linear precoding strategy is employed as an alternative to the second SVD operation to parallelize each user's streams. Finally, the proposed LR-S-GMI precoding algorithms are obtained. According to the specific precoding constraint, the proposed LR-S-GMI precoding algorithms are categorized as LR-S-GMI-ZF and LR-S-GMI-MMSE precoding, respectively.

The assumption that full CSI is available at the transmit side is valid in time-division duplex (TDD) systems because the uplink and downlink share the same frequency band. For frequency-division duplex (FDD) systems, however, the CSI needs to be estimated at the receiver and to be fed back to the transmitter. For the proposed LR-S-GMI precoding algorithms, it is worth noting that the two SVDs and the decoding matrix are no longer required. Only the CSI needs to be known at the transmitter and a quantization procedure must be performed at the receiver. Hence, the required computational effort for each user's receiver can be reduced and a significant amount of transmit power can be saved which is very important considering the mobility of the distributed users. From the simulation results, we will show that a better BER performance is achieved by the

proposed LR-S-GMI precoding algorithms. For the sum-rate performance, the proposed LR-S-GMI precoding algorithms are comparable to their corresponding conventional BD-type precoding algorithms. We will also illustrate that the proposed LR-S-GMI precoding algorithms have a lower computational complexity than the other precoding algorithms reported in the literature so far.

4.2 System Model

We consider an uncoded MU-MIMO downlink channel, with N_t transmit antennas at the BS and N_i receive antennas at the ith user equipment (UE). With K users in the system, the total number of receive antennas is $N_r = \sum_{i=1}^{K} N_i$. A block diagram of such a system is illustrated in Figure 4.1

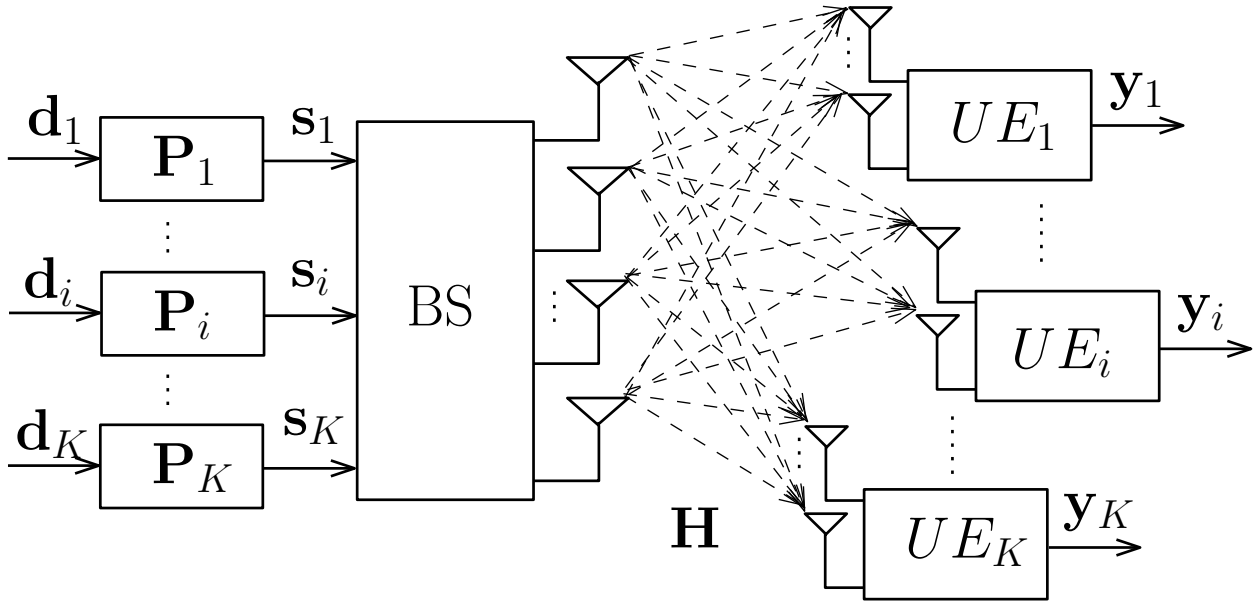

Figure 4.1: MU-MIMO System Model

From the system model, the combined channel matrix $\boldsymbol{H}$ and the joint precoding matrix $\boldsymbol{P}$ are given by

$$\boldsymbol{H} = [\boldsymbol{H}_1^T \; \boldsymbol{H}_2^T \; \ldots \; \boldsymbol{H}_K^T]^T \in \mathbb{C}^{N_r \times N_t}, \tag{4.1}$$

$$\boldsymbol{P} = [\boldsymbol{P}_1 \; \boldsymbol{P}_2 \; \ldots \; \boldsymbol{P}_K] \in \mathbb{C}^{N_t \times N_r}, \tag{4.2}$$

where $\boldsymbol{H}_i \in \mathbb{C}^{N_i \times N_t}$ is the ith user's channel matrix. The quantity $\boldsymbol{P}_i \in \mathbb{C}^{N_t \times N_i}$ is the ith user's precoding matrix. We assume a flat fading MIMO channel and the received signal $\boldsymbol{y}_i \in \mathbb{C}^{N_i}$ at the ith user is given by

$$\boldsymbol{y}_i = \boldsymbol{H}_i \boldsymbol{x}_i + \boldsymbol{H}_i \sum_{j=1, j \neq i}^{K} \boldsymbol{x}_j + \boldsymbol{n}_i, \tag{4.3}$$

where the quantity $\boldsymbol{x}_i \in \mathbb{C}^{N_i}$ is the ith user's transmitted signal, and $\boldsymbol{n}_i \in \mathbb{C}^{N_i}$ is the ith user's Gaussian noise with independent and identically distributed (i.i.d.) entries of zero mean and variance σ_n^2. Assuming that the average transmit power for each user is ξ_i, then, the power constraint $\mathrm{E}\|\boldsymbol{x}_i\|^2 = \xi_i$ is imposed. We construct an unnormalized signal $\boldsymbol{s}_i$ such that

$$\boldsymbol{x}_i = \frac{\boldsymbol{s}_i}{\sqrt{\mathrm{E}_{\gamma_i}}}, \tag{4.4}$$

where $\boldsymbol{s}_i = \boldsymbol{P}_i \boldsymbol{d}_i$ with $\boldsymbol{d}_i$ is the transmit data vector and E_{γ_i} is the average energy of γ_i with $\gamma_i = \|\boldsymbol{s}_i\|^2/\xi_i$. The physical meaning of dividing $\boldsymbol{s}_i$ by the scalar $\sqrt{\mathrm{E}_{\gamma_i}}$ is to make sure the average transmit power ξ_i is still the same after the precoding process. With this normalization, $\boldsymbol{x}_i$ obeys $\mathrm{E}\|\boldsymbol{x}_i\|^2 = \xi_i$.

The received signal $\boldsymbol{y}_i$ is weighted by the scalar $\sqrt{\mathrm{E}_{\gamma_i}}$ to form the estimate

$$\hat{\boldsymbol{d}}_i = \sqrt{\mathrm{E}_{\gamma_i}} \boldsymbol{y}_i. \tag{4.5}$$

Note that it is necessary to cancel $\sqrt{\mathrm{E}_{\gamma_i}}$ out at the receiver to get the correct amplitude of the desired signal part. The average energy E_{γ_i} is independent from the channel and the data, which means the receivers do not need to know the instantaneous CSI for the precoding techniques to work [65]. As analyzed and illustrated in [26], however, the performance difference between the average E_{γ_i} and the instantaneous γ_i is very small. Therefore, we follow the strategy developed in [65] and [26] to assume the receivers need to know only $\sqrt{\mathrm{E}_{\gamma_i}}$ but use γ_i instead of E_{γ_i} for simulation convenience as γ_i is simpler to compute. The simulation results represent the performance of either normalization method. In this case, we can replace (4.4) and (4.5) with the instantaneous γ_i in the simulations and employ

$$\boldsymbol{x}_i = \frac{\boldsymbol{s}_i}{\sqrt{\gamma_i}} \text{ and } \hat{\boldsymbol{d}}_i = \sqrt{\gamma}_i \boldsymbol{y}_i. \tag{4.6}$$

4.3 Proposed LR-S-GMI Precoding Algorithms

In this section, we describe the proposed low-complexity LR-S-GMI precoding algorithms based on a strategy that employs a channel inversion method [106], QR decompositions, and lattice reductions. Similar to the BD-type precoding algorithms, the design of the proposed LR-S-GMI precoding algorithms is computed in two steps.

First, we obtain the first precoding filter $\boldsymbol{P}_i^a$ in the conventional BD-type precoding algorithms for LR-S-GMI precoding algorithms by using one channel inversion and K QR decompositions. By applying the MMSE channel inversion, we have

$$\begin{aligned} \boldsymbol{H}_{\text{mse}}^{\dagger} &= \boldsymbol{H}^H(\boldsymbol{H}\boldsymbol{H}^H + \alpha \boldsymbol{I}_{N_r})^{-1} \\ &= [\boldsymbol{H}_{1,\text{mse}}, \boldsymbol{H}_{2,\text{mse}}, \ldots, \boldsymbol{H}_{K,\text{mse}}]. \end{aligned} \tag{4.7}$$

where the sub-matrix $\boldsymbol{H}_{i,\text{mse}} \in \mathbb{C}^{N_t \times N_i}$. Considering a high SNR case, it can be shown that $\boldsymbol{H}\boldsymbol{H}_{\text{mse}}^{\dagger} \approx \boldsymbol{I}_{N_t}$ [64]. This means that the off-diagonal block matrices of $\boldsymbol{H}\boldsymbol{H}_{\text{mse}}^{\dagger}$ converge to zeros with increasing the SNR. Hence, the matrix $\boldsymbol{H}_{i,\text{mse}}$ is approximately in the null space of $\overline{\boldsymbol{H}}_i$ which is defined in (2.56)

$$\overline{\boldsymbol{H}}_i \boldsymbol{H}_{i,\text{mse}} \approx \boldsymbol{0}. \tag{4.8}$$

Considering the QR decomposition of $\boldsymbol{H}_{i,\text{mse}} = \boldsymbol{Q}_{i,\text{mse}}\boldsymbol{R}_{i,\text{mse}}$, we have

$$\overline{\boldsymbol{H}}_i \boldsymbol{H}_{i,\text{mse}} = \overline{\boldsymbol{H}}_i \boldsymbol{Q}_{i,\text{mse}}\boldsymbol{R}_{i,\text{mse}} \approx \boldsymbol{0} \text{ for } i = 1, \ldots, K, \tag{4.9}$$

where $\boldsymbol{Q}_{i,\text{mse}} \in \mathbb{C}^{N_t \times N_i}$ is an orthogonal matrix and $\boldsymbol{R}_{i,\text{mse}} \in \mathbb{C}^{N_i \times N_i}$ is an upper triangular matrix. Since $\boldsymbol{R}_{i,\text{mse}}$ is invertible, we have

$$\overline{\boldsymbol{H}}_i \boldsymbol{Q}_{i,\text{mse}} \approx \boldsymbol{0}. \tag{4.10}$$

Thus, $\boldsymbol{Q}_{i,\text{mse}}$ satisfies the RBD constraint defined in (2.58) to balance the MUI and the noise.

We have simplified the design of the first precoding filter $\boldsymbol{P}_i^a$ for the RBD precoding here as compared to [106] where a residual interference suppression filter $\boldsymbol{T}_i$ is applied after the first precoding process $\boldsymbol{P}_i^a$. The filter $\boldsymbol{T}_i$ increases the complexity and cannot completely cancel the MUI. Therefore, we omit the residual interference suppression part

since it is not necessary for the RBD precoding. We term the simplified GMI as S-GMI precoding in this work. Then, the first precoding filter for the RBD precoding can be equivalently obtained as

$$\boldsymbol{P}_i^a = \boldsymbol{Q}_{i,\mathrm{mse}}, \tag{4.11}$$

where $\boldsymbol{P}_i^a \in \mathbb{C}^{N_t \times N_i}$ and the first combined precoding matrix is

$$\boldsymbol{P}^a = [\boldsymbol{P}_1^a,\ \boldsymbol{P}_2^a,\ \ldots,\ \boldsymbol{P}_K^a]. \tag{4.12}$$

Similarly, the extension of the channel inversion method from the RBD precoding to the BD precoding is straightforward on

$$\boldsymbol{H}_{\mathrm{zf}}^{\dagger} = \boldsymbol{H}^H(\boldsymbol{H}\boldsymbol{H}^H)^{-1} = [\boldsymbol{H}_{1,\mathrm{zf}}, \boldsymbol{H}_{2,\mathrm{zf}}, \ldots, \boldsymbol{H}_{K,\mathrm{zf}}]. \tag{4.13}$$

Moreover, the obtained MUI is strictly zero as $\overline{\boldsymbol{H}}_i\boldsymbol{H}_{i,\mathrm{zf}} = \boldsymbol{0}$. Assuming the QR decomposition of $\boldsymbol{H}_{i,\mathrm{zf}}$ is $\boldsymbol{H}_{i,\mathrm{zf}} = \boldsymbol{Q}_{i,\mathrm{zf}}\boldsymbol{R}_{i,\mathrm{zf}}$, then, we have

$$\overline{\boldsymbol{H}}_i\boldsymbol{Q}_{i,\mathrm{zf}} = \boldsymbol{0}. \tag{4.14}$$

Thus, $\boldsymbol{Q}_{i,\mathrm{zf}}$ satisfies the BD constraint defined in (2.57). Then, the first precoding matrix for the BD precoding can be equivalently obtained as

$$\boldsymbol{P}_i^a = \boldsymbol{Q}_{i,\mathrm{zf}}. \tag{4.15}$$

This channel inversion method for the BD precoding is termed as GZI in [106].

Next, we employ the LR-aided linear precoding algorithm instead of the second SVD operation to obtain the second precoding filter $\boldsymbol{P}_i^b$. The aim of the LR transformation is to find a new basis $\tilde{\boldsymbol{H}}$ which is nearly orthogonal compared to the original matrix $\boldsymbol{H}$ for a given lattice $L(\boldsymbol{H})$. The most commonly used LR algorithm has been first proposed by Lenstra, Lenstra and L. Lovász (LLL) in [92] with polynomial time complexity. In order to reduce the computational complexity, a complex LLL (CLLL) algorithm was proposed in [95], which reduces the overall complexity of the LLL algorithm by nearly half without sacrificing any performance. We employ the CLLL algorithm to implement the LR transformation in this work.

After the first precoding, we transform the MU-MIMO channel into parallel or approximately parallel SU-MIMO channels and the effective channel matrix for the ith user is

$$\boldsymbol{H}_{\mathrm{eff}_i} = \boldsymbol{H}_i \boldsymbol{P}_i^a. \tag{4.16}$$

We perform the LR transformation on $\boldsymbol{H}_{\mathrm{eff}_i}^T$ in the precoding scenario [91], that is

$$\tilde{\boldsymbol{H}}_{\mathrm{eff}_i} = \boldsymbol{T}_i \boldsymbol{H}_{\mathrm{eff}_i} \text{ and } \boldsymbol{H}_{\mathrm{eff}_i} = \boldsymbol{T}_i^{-1} \tilde{\boldsymbol{H}}_{\mathrm{eff}_i}, \tag{4.17}$$

where $\boldsymbol{T}_i$ is a unimodular matrix with $\det|\boldsymbol{T}_{\mathrm{i}}| = 1$ and all elements of $\boldsymbol{T}_i$ are complex integers, i.e. $t_{l,k} \in \mathbb{Z} + j\mathbb{Z}$. The physical meaning of the constraint $\det|\boldsymbol{T}_{\mathrm{i}}| = 1$ is that the channel energy is unchanged after the LR transformation.

Following the LR transformation, we employ the linear precoding constraint to get the second precoding filter to parallelize each user's streams instead of the second SVD operation in Equation (2.63). The ZF precoding constraint is implemented for user i as

$$\tilde{\boldsymbol{P}}_{\mathrm{ZF}_i}^b = \tilde{\boldsymbol{H}}_{\mathrm{eff}_i}^H (\tilde{\boldsymbol{H}}_{\mathrm{eff}_i} \tilde{\boldsymbol{H}}_{\mathrm{eff}_i}^H)^{-1}. \tag{4.18}$$

It is well-known that the performance of MMSE precoding is always better than that of ZF precoding. We can get the second precoding filter by employing an MMSE precoding constraint. The MMSE precoding is actually equivalent to the ZF precoding with respect to an extended system model [90, 108]. The extended channel matrix $\underline{\boldsymbol{H}}$ for the MMSE precoding scheme is defined as

$$\underline{\boldsymbol{H}} = \left[\boldsymbol{H}, \sqrt{\alpha} \boldsymbol{I}_{N_r} \right]. \tag{4.19}$$

By introducing the regularization factor α, a trade-off between the level of MUI and noise is introduced [64]. Then, the MMSE precoding filter is obtained as

$$\boldsymbol{P}_{\mathrm{MMSE}} = \boldsymbol{A} \underline{\boldsymbol{H}}^H (\underline{\boldsymbol{H}} \underline{\boldsymbol{H}}^H)^{-1}, \tag{4.20}$$

where $\boldsymbol{A} = \left[\boldsymbol{I}_{N_t}, \boldsymbol{0}_{N_t \times N_r} \right]$, and the multiplication by $\boldsymbol{A}$ will not result in transmit power amplification since $\boldsymbol{A}\boldsymbol{A}^H = \boldsymbol{I}_{N_t}$. From the mathematical expression in Equation (4.20), the rows of $\underline{\boldsymbol{H}}$ determine the effective transmit power amplification of the MMSE precoding. Correspondingly, the LR transformation for the MMSE precoding should be applied to the transpose of the extended channel matrix $\underline{\boldsymbol{H}}_{\mathrm{eff}_i}^T = \left[\boldsymbol{H}_{\mathrm{eff}_i}, \sqrt{\alpha} \boldsymbol{I}_{N_i} \right]^T$, and the LR transformed channel matrix $\underline{\tilde{\boldsymbol{H}}}_{\mathrm{eff}_i}$ is obtained as

$$\underline{\tilde{\boldsymbol{H}}}_{\mathrm{eff}_i} = \underline{\boldsymbol{T}}_i \underline{\boldsymbol{H}}_{\mathrm{eff}_i}, \tag{4.21}$$

where $\underline{\boldsymbol{T}}_i$ is the unimodular matrix for $\underline{\boldsymbol{H}}_{\mathrm{eff}_i}$. Then, the LR-aided MMSE precoding filter is given by

$$\tilde{\boldsymbol{P}}^b_{\mathrm{MMSE}_i} = \boldsymbol{A}_i \tilde{\underline{\boldsymbol{H}}}^H_{\mathrm{eff}_i} (\tilde{\underline{\boldsymbol{H}}}_{\mathrm{eff}_i} \tilde{\underline{\boldsymbol{H}}}^H_{\mathrm{eff}_i})^{-1}, \tag{4.22}$$

where the matrix $\boldsymbol{A}_i = \left[\boldsymbol{I}_{N_i}, \boldsymbol{0}_{N_i \times N_i}\right]$. Finally, the combined second precoding matrix $\tilde{\boldsymbol{P}}^b$ for all users is

$$\tilde{\boldsymbol{P}}^b = \mathrm{diag}\{\tilde{\boldsymbol{P}}^b_1, \tilde{\boldsymbol{P}}^b_2, \ldots, \tilde{\boldsymbol{P}}^b_K\}. \tag{4.23}$$

The overall precoding matrix is $\tilde{\boldsymbol{P}} = \boldsymbol{P}^a \tilde{\boldsymbol{P}}^b$. Since the lattice reduced precoding matrix $\tilde{\boldsymbol{P}}^b$ has near orthogonal columns, the required transmit power will be reduced compared to the linear or BD-type precoding algorithms. Thus, a better BER performance than that of the BD-type precoding algorithms can be achieved by the proposed LR-S-GMI precoding algorithms.

The received signal is finally obtained as

$$\boldsymbol{y} = \boldsymbol{H} \tilde{\boldsymbol{P}} \boldsymbol{d} + \sqrt{\gamma} \boldsymbol{n}, \tag{4.24}$$

where $\gamma = \|\tilde{\boldsymbol{P}} \boldsymbol{d}\|^2$. The main processing work left for the receiver is to quantize the received signal $\boldsymbol{y}$ to the nearest data vector and the decoding matrix $\boldsymbol{G}$ described in the BD-type, QR/SVD RBD, GZI, and GMI precoding algorithms is not needed anymore.

The proposed precoding algorithms are called LR-S-GMI-ZF and LR-S-GMI-MMSE depending on the choice of the second precoding filter as given in Equation (4.18) and (4.22), respectively. We will focus on the LR-S-GMI-MMSE precoding since a better performance is achieved. The implementing steps of the LR-S-GMI-MMSE precoding algorithm are summarized in Table 4.1. By replacing the steps 8 and 9 in Table 4.1 with the formulation in (4.18), the LR-S-GMI-ZF precoding algorithm can be obtained. Similarly, the first precoding matrix can also be computed according to the GZI method in Equation (4.15), and combined with Equation (4.18) or (4.22) to get the second precoding matrix. Then, the LR-GZI-ZF and LR-GZI-MMSE precoding algorithms can be obtained, respectively.

Table 4.1: The LR-S-GMI-MMSE Precoding Algorithm

Steps	Operations
	Applying the MMSE Channel Inversion
(1)	$\boldsymbol{H}_{\mathrm{mse}}^{\dagger} = \boldsymbol{H}^{H}(\boldsymbol{H}\boldsymbol{H}^{H} + \alpha\boldsymbol{I})^{-1}$
(2)	for i = 1 : K
(3)	$[\boldsymbol{Q}_{i,\mathrm{mse}}^{\dagger}\ \boldsymbol{R}_{i,\mathrm{mse}}^{\dagger}] = \mathrm{QR}(\boldsymbol{H}_{i,\mathrm{mse}}^{\dagger},\ 0)$
(4)	$\boldsymbol{P}_{i}^{a} = \boldsymbol{Q}_{i,\mathrm{mse}}^{\dagger}$
(5)	$\boldsymbol{H}_{\mathrm{eff}_i} = \boldsymbol{H}_{i}\boldsymbol{P}_{i}^{a}$
(6)	$\underline{\boldsymbol{H}}_{\mathrm{eff}_i} = \left[\boldsymbol{H}_{\mathrm{eff}_i}\ \sqrt{\alpha}\boldsymbol{I}_{N_i}\right]$
(7)	$[\underline{\boldsymbol{T}}_{i}^{T}\ \underline{\boldsymbol{H}}_{\mathrm{eff}_i}^{T}] = \mathrm{CLLL}(\tilde{\underline{\boldsymbol{H}}}_{\mathrm{eff}_i}^{T})$
(8)	$\boldsymbol{A}_{i} = [\boldsymbol{I}_{M_i}\ \boldsymbol{0}_{M_i \times N_i}]$
(9)	$\tilde{\boldsymbol{P}}_{\mathrm{MMSE}_i}^{b} = \boldsymbol{A}_{i}\tilde{\underline{\boldsymbol{H}}}_{\mathrm{eff}_i}^{H}(\tilde{\underline{\boldsymbol{H}}}_{\mathrm{eff}_i}\tilde{\underline{\boldsymbol{H}}}_{\mathrm{eff}_i}^{H})^{-1}$
(10)	end
	Compute the overall precoding matrix
(11)	$\boldsymbol{P}^{a} = [\boldsymbol{P}_{1}^{a},\ \boldsymbol{P}_{2}^{a},\ \ldots,\ \boldsymbol{P}_{K}^{a}]$
(12)	$\tilde{\boldsymbol{P}}^{b} = \mathrm{diag}\{\tilde{\boldsymbol{P}}_{1}^{b}, \tilde{\boldsymbol{P}}_{2}^{b}, \ldots, \tilde{\boldsymbol{P}}_{K}^{b}\}$
(13)	$\tilde{\boldsymbol{P}} = \boldsymbol{P}^{a}\tilde{\boldsymbol{P}}^{b}$
	Calculate the scaling factor γ
(14)	$\gamma = (\|\tilde{\boldsymbol{P}}\boldsymbol{d}\|_{F}^{2}/E_{s})$
	Get the received signal
(15)	$\boldsymbol{y} = \boldsymbol{H}\tilde{\boldsymbol{P}}\boldsymbol{d} + \sqrt{\gamma}\boldsymbol{n}$
	Transform back from lattice space
(16)	$\hat{\boldsymbol{d}} = \underline{\boldsymbol{T}}\lceil\boldsymbol{y}\rfloor$

4.4 Performance Analysis

In this section, we carry out an analysis of the performance of the proposed LR-S-GMI precoding algorithms. We consider a performance analysis in terms of BER, sum-rate and computational complexity.

4.4.1 BER Performance Analysis

For the BD precoding, the effective SU-MIMO channels are strictly parallel between each other after the first precoding filtering. For the RBD precoding, however, the residual interference $\overline{\boldsymbol{H}}_i \boldsymbol{P}_i^{a(\mathrm{RBD})}$ is not zero between the users. We use $\boldsymbol{J}_f$ to denote $\overline{\boldsymbol{H}}_i \boldsymbol{P}_i^{a(\mathrm{RBD})}$ for convenience. From Equation (2.61), the following formula is obtained

$$\boldsymbol{J}_f \boldsymbol{J}_f^H = \overline{\boldsymbol{H}}_i \overline{\boldsymbol{V}}_i (\overline{\boldsymbol{\Sigma}}_i^T \overline{\boldsymbol{\Sigma}}_i + \alpha \boldsymbol{I}_{N_t})^{-1} \overline{\boldsymbol{V}}_i^H \overline{\boldsymbol{H}}_i{}^H. \tag{4.25}$$

Mathematically, the quantity $\overline{\boldsymbol{V}}_i (\overline{\boldsymbol{\Sigma}}_i^T \overline{\boldsymbol{\Sigma}}_i + \alpha \boldsymbol{I}_{N_t})^{-1} \overline{\boldsymbol{V}}_i^H$ can be expressed as $(\overline{\boldsymbol{H}}_i^H \overline{\boldsymbol{H}}_i + \alpha \boldsymbol{I}_{N_t})^{-1}$ by utilizing the SVD decomposition. Substituting this into Equation (4.25), the formula can be rewritten as

$$\boldsymbol{J}_f \boldsymbol{J}_f^H = \overline{\boldsymbol{H}}_i (\overline{\boldsymbol{H}}_i^H \overline{\boldsymbol{H}}_i + \alpha \boldsymbol{I}_{N_t})^{-1} \overline{\boldsymbol{H}}_i{}^H. \tag{4.26}$$

With the increase of the SNR, α approaches zero and then we have

$$\boldsymbol{J}_f \boldsymbol{J}_f^H \approx \overline{\boldsymbol{H}}_i (\overline{\boldsymbol{H}}_i^H \overline{\boldsymbol{H}}_i)^{-1} \overline{\boldsymbol{H}}_i{}^H. \tag{4.27}$$

By further manipulating the expression in Equation (4.27), we obtain

$$\begin{aligned} &\boldsymbol{J}_f \boldsymbol{J}_f^H \overline{\boldsymbol{H}}_i \approx \overline{\boldsymbol{H}}_i (\overline{\boldsymbol{H}}_i^H \overline{\boldsymbol{H}}_i)^{-1} \overline{\boldsymbol{H}}_i{}^H \overline{\boldsymbol{H}}_i = \overline{\boldsymbol{H}}_i \\ &\text{Thus } \boldsymbol{J}_f \boldsymbol{J}_f^H \approx \boldsymbol{I}_{N_t}, \end{aligned} \tag{4.28}$$

that is, the residual interference matrix $\boldsymbol{J}_f$ of the RBD precoding converges to an identity matrix at high SNRs. For the S-GMI precoding algorithm developed in Section IV with the SNR increase we have

$$\overline{\boldsymbol{H}}_i \boldsymbol{P}_i^a = \overline{\boldsymbol{H}}_i \boldsymbol{Q}_{i,\mathrm{mse}}^{\dagger} \approx \boldsymbol{0}. \tag{4.29}$$

By comparing (4.28) and (4.29), the impact of the residual interference of S-GMI precoding would be smaller than that of the conventional RBD precoding algorithm. Thus, we expect that a better BER performance is achieved by the S-GMI precoding algorithm over the conventional RBD precoding algorithm.

As pointed out in [65], the BER performance for a MIMO precoding system is actually determined by the energy of the transmitted signal γ_i. In order to reduce γ_i and improve the BER performance further, we transform the effective channel $\boldsymbol{H}_{\mathrm{eff}}$ into the lattice

space. By doing this, an improved basis $\tilde{\boldsymbol{H}}_{\text{eff}}$ is computed. Actually, the LR transformed channel matrix $\tilde{\boldsymbol{H}}_{\text{eff}}$ is quasi-orthogonal rather than strictly orthogonal. We can employ the condition number which is defined as [103]

$$\text{cond}(\boldsymbol{H}) = \|\boldsymbol{H}\|_F \|\boldsymbol{H}^{-1}\|_F \tag{4.30}$$

to measure the orthogonality of the channel matrix. From the above definition of the condition number in Equation (4.30), we get that $\text{cond}(\boldsymbol{H}) = 1$ with equality for an orthogonal basis while matrices which are nearly singular have large condition numbers. In Figure 4.2, the probability density functions (PDFs) of the condition numbers for the effective channel matrices are illustrated. For the effective channel matrix of the proposed LR-S-GMI-MMSE precoding algorithm, not only the spread in the condition numbers but also their average value is much smaller compared to the effective channel matrices achieved by the existing precoding algorithms. Therefore, a significant reduction in the required transmit power γ_i is achieved and a better BER performance can be obtained by the proposed LR-S-GMI-MMSE precoding algorithm.

4.4.2 Achievable Sum-Rate Analysis

Recall that at high SNRs, the MU-MIMO channel is approximately decoupled into equivalent SU-MIMO channels by applying the first precoding filtering in Equation (4.10). Then, we can transform the MU-MIMO sum-rate analysis [105] to a set of SU-MIMO sum-rate analysis tasks. For the second precoding filter, the LR-aided MMSE precoding is actually equal to the LR-aided ZF precoding under the high SNR scenario. Therefore, the ith user's received signal is

$$\boldsymbol{y}_i = \boldsymbol{z}_i + \sqrt{\gamma}_i \boldsymbol{n}_i, \tag{4.31}$$

where $\boldsymbol{z}_i = \boldsymbol{T}_i^{-1}\boldsymbol{d}_i$. By assuming that the average transmit power is $\xi_i = 1$, and because of the fact that $\boldsymbol{H}_{\text{eff}_i} = \boldsymbol{U}_i \boldsymbol{\Sigma}_i {\boldsymbol{V}_i}^H$, we get the normalization factor γ_i as

$$\begin{aligned} \gamma_i &= \|\boldsymbol{H}_{\text{eff}_i}^{-1}\boldsymbol{z}_i\|_{\text{F}}^2 = Tr(\boldsymbol{\Sigma}_i^{-2}\boldsymbol{z}_i\boldsymbol{z}_i^H) \\ &= \sum_{l=1}^{L_{\text{eff}}} \frac{\xi_l^2}{\lambda_l^2}, \end{aligned} \tag{4.32}$$

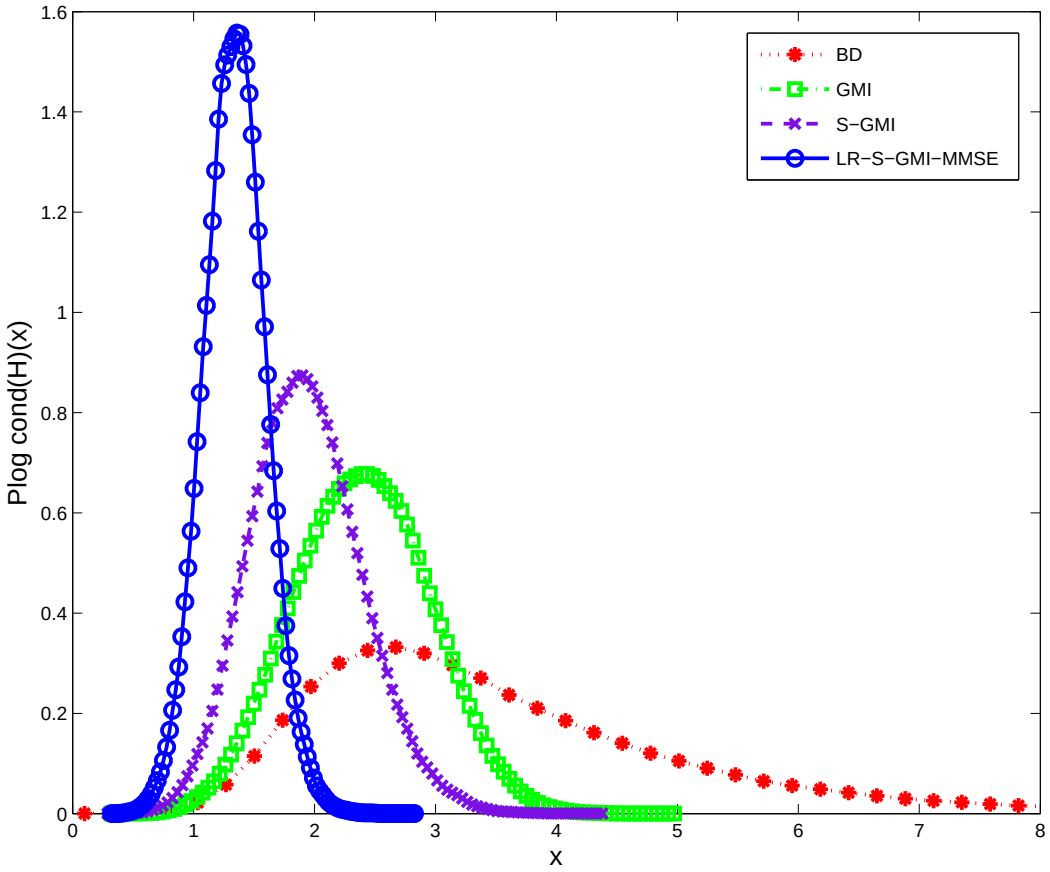

Figure 4.2: PDFs of the natural logarithm of $\mathrm{cond}(\boldsymbol{H})$ *for* 6×6 *matrices*

where the quantity λ_l is the lth singular value of $\mathbf{\Sigma}_i$ and ξ_l denotes the energy of the lth stream of $\boldsymbol{z}_i$.

From (4.32), the received SNR for the lth stream of user i is obtained as

$$\mathrm{SNR}_l = \frac{\xi_l^2}{\sigma_n^2 \sum_{m=1}^{L_{\mathrm{eff}}} \frac{\xi_m^2}{\lambda_m^2}}. \tag{4.33}$$

Then, the achievable sum-rate for user i is given by

$$C_i = \sum_{l=1}^{L_{\mathrm{eff}}} \log\left(1 + \frac{\xi_l^2}{\sigma_n^2 \sum_{m=1}^{L_{\mathrm{eff}}} \frac{\xi_m^2}{\lambda_m^2}}\right) = \sum_{l=1}^{L_{\mathrm{eff}}} \log\left(1 + \frac{\xi_l^2}{\sigma_n^2 \gamma_i}\right). \tag{4.34}$$

Note that the achievable sum-rate C_i is degraded by the normalization factor γ_i. The value of C_i approaches its maximum when $\frac{\xi_1^2}{\lambda_1^2} = \frac{\xi_2^2}{\lambda_2^2} = \ldots = \frac{\xi_{L_{\mathrm{eff}}}^2}{\lambda_{L_{\mathrm{eff}}}^2}$, thus we have

$$C_i \leq \sum_{l=1}^{L_{\mathrm{eff}}} \log\left(1 + \frac{\lambda_l^2}{\sigma_n^2 L_{\mathrm{eff}}}\right). \tag{4.35}$$

Finally, the maximum achievable sum-rate of the proposed LR-S-GMI precoding algorithms at high SNRs can be expressed as

$$C = \sum_{i=1}^{K} \sum_{l=1}^{L_{\mathrm{eff}}} \log_2\left(1 + \frac{\lambda_l^2}{\sigma_n^2 L_{\mathrm{eff}}}\right). \tag{4.36}$$

For the BD precoding, we multiply the decoding matrix $\boldsymbol{G}_i = \boldsymbol{U}_i^H$ at the ith user's receiver and the received signal is given by

$$\boldsymbol{y}_i = \mathbf{\Sigma}_i \boldsymbol{d}_i + \boldsymbol{U}_i^H \boldsymbol{n}_i. \tag{4.37}$$

Due to the fact that $\overline{\boldsymbol{V}}_i^{(0)}$ and $\boldsymbol{V}_i^{(1)}$ are semi-unitary matrices, we get ${\overline{\boldsymbol{V}}_i^{(0)}}^H \overline{\boldsymbol{V}}_i^{(0)} = \boldsymbol{I}$ and ${\boldsymbol{V}_i^{(1)}}^H \boldsymbol{V}_i^{(1)} = \boldsymbol{I}$. Then, by applying the equivalence $Tr(\boldsymbol{ABC}) = Tr(\boldsymbol{CAB})$, the normalization factor γ_i^{BD} for BD can be expressed as

$$\gamma_i^{\mathrm{BD}} = \|\overline{\boldsymbol{V}}_i^{(0)} \boldsymbol{V}_i^{(1)} \boldsymbol{d}_i\|^2 = \|\boldsymbol{d}_i\|^2. \tag{4.38}$$

Since the statistical property of $\boldsymbol{n}_i$ is not changed by the multiplication with the unitary matrix $\boldsymbol{U}_i^H$, we get the lth received SNR as

$$\mathrm{SNR}_l = \frac{\lambda_l^2}{\sigma_n^2}. \tag{4.39}$$

For simplicity, we do not consider the power loading between users and streams in the following derivation and term this strategy as no power loading (NPL). Then, the achievable sum-rate for the BD precoding algorithm is given by

$$C^{(\mathrm{BD})} = \sum_{i=1}^{K} \sum_{l=1}^{L_{\mathrm{eff}}} \log_2 \left(1 + \frac{\lambda_l^2}{\sigma_n^2} \right). \tag{4.40}$$

By comparing the maximum achievable sum-rate of the proposed LR-S-GMI precoding algorithms in (4.36), we conclude that the sum-rate of the proposed LR-S-GMI precoding algorithms will be slightly inferior to that of the BD precoding algorithm at high SNRs. At low SNRs, however, we expect that the achieved sum-rate of the proposed LR-S-GMI precoding algorithms will be better than the performance of the BD precoding algorithm since a regularization factor is employed to mitigate the sum-rate performance degradation by the noise term.

The sum-rate performance of the BD precoding is actually dependent on the power loading scheme being used. Hence, the BD precoding algorithm can achieve its maximum sum-rate performance by allocating the power between streams according to a WF power loading scheme. As pointed out in [106], we do not consider the power loading strategy for the RBD or the proposed LR-S-GMI precoding algorithms for two reasons. One is that it is not easy to identify the optimal power allocation coefficients because of the existence of residual interference. The second reason is that since the minimum MSE condition is already satisfied an allocation of different powers between streams is not needed.

4.4.3 Computational Complexity Analysis

In this section, we use the total number of floating point operations (FLOPs) to measure the computational complexity of the proposed and existing precoding algorithms. It is worth noting that the lattice reduction algorithm has variable complexity, and the average complexity of the CLLL algorithm has been given in FLOPs by [95]. A reduced and fixed complexity lattice reduction structure is proposed in [109], however, we employ the conventional CLLL algorithm for the reason that the lattice reduction algorithm is not the main focus in this work. The number of FLOPs for the complex QR decomposition and the real SVD operation are given in [103]. As shown in [104], the number of FLOPs

required by a $m \times n$ complex SVD operation is equivalent to its extended $2m \times 2n$ real matrix. The total number of FLOPs needed by the matrix operations is summarized below:

- Multiplication of $m \times n$ and $n \times p$ complex matrices: $8mnp - 2mp$;
- QR decomposition of an $m \times n$ $(m \leq n)$ complex matrix: $16(n^2m - nm^2 + \frac{1}{3}m^3)$;
- SVD of an $m \times n$ $(m \leq n)$ complex matrix where only $\boldsymbol{\Sigma}$ and $\boldsymbol{V}$ are obtained: $32(nm^2 + 2m^3)$;
- SVD of an $m \times n$ $(m \leq n)$ complex matrix where $\boldsymbol{U}$, $\boldsymbol{\Sigma}$ and $\boldsymbol{V}$ are obtained: $8(4n^2m + 8nm^2 + 9m^3)$;
- Inversion of an $m \times m$ real matrix using Gauss-Jordan elimination: $4m^3/3$.

We illustrate the required FLOPs for the conventional RBD, S-GMI and LR-S-GMI-MMSE precoding algorithms in Table 4.2, Table 4.3 and Table 4.4, respectively. The complexity of the QR/SVD RBD and LC-RBD-LR-MMSE precoding algorithms is already given in [104]. A system with $N_t = 6$ transmit antennas and $K = 3$ users each equipped with $N_i = 2$ receive antennas is considered; this scenario is denoted as the $(2, 2, 2) \times 6$ case. For the $(2, 2, 2) \times 6$ case, the reduction in the number of FLOPs obtained by the proposed LR-S-GMI-MMSE precoding is 73.6%, 69.5%, 59.1% and 49.9% as compared to the RBD, BD, QR/SVD RBD and LC-RBD-LR-MMSE precoding algorithms, respectively. Clearly, the proposed LR-S-GMI-MMSE precoding algorithm requires the lowest complexity.

In order to further reveal the relationship between the computational complexity and the system dimensions, we first fix the receive antenna configuration and assume that each user is equipped with $N_i = 2$ antennas, so that, the system dimensions change with the number of users K. Similarly, if we fix the number of users to $K = 4$, the system dimensions will change with the variable N_i. The required number of FLOPs of the proposed and existing precoding algorithms are simulated for the above two settings in Figure 4.3 and Figure 4.4, respectively. Figure 4.3 shows that with the receive antenna N_i fixed, the computational complexity of the BD-type precoding algorithms grows relatively

Table 4.2: Computational complexity of conventional RBD

Steps	Operations	Flops	Case $(2,2,2)\times 6$
1	$\overline{\boldsymbol{U}}_i\overline{\boldsymbol{\Sigma}}_i\overline{\boldsymbol{V}}_i^H$	$32K(N_t\overline{N}_i^2+2\overline{N}_i^3)$	21504
2	$(\overline{\boldsymbol{\Sigma}}_i^T\overline{\boldsymbol{\Sigma}}_i+\alpha\boldsymbol{I}_{N_t})^{-\frac{1}{2}}$	$K(18N_t+\overline{N}_i)$	336
3	$\overline{\boldsymbol{V}}_i\overline{\boldsymbol{D}}_i, (\overline{\boldsymbol{D}}_i\leftarrow 2)$	$8KN_t^3$	5184
4	$\boldsymbol{H}_i\boldsymbol{P}_i^a$	$K(8N_i^2N_t-2N_i^2)$	552
5	$\boldsymbol{U}_i\boldsymbol{\Sigma}_i{\boldsymbol{V}_i}^H$	$64K(\frac{9}{8}N_i^3+$ $N_tN_i^2+\frac{1}{2}N_t^2N_i)$	13248 Total 40824

Table 4.3: Computational complexity of S-GMI

Steps	Operations	Flops	Case $(2,2,2)\times 6$
1	$\boldsymbol{H}_{\text{mse}}^{\dagger}$	$(\frac{4}{3}N_r^3+12N_r^2N_t$ $-2N_r^2-2N_rN_t)$	2736
2	$\boldsymbol{Q}_i^{\dagger}\boldsymbol{R}_i^{\dagger}$	$16K(N_t^2N_i-N_tN_i^2+\frac{1}{3}N_i^3)$	2432
3	$\boldsymbol{H}_i\boldsymbol{P}_i^a$	$K(8N_i^2N_t-2N_i^2)$	552
4	$\boldsymbol{U}_i\boldsymbol{\Sigma}_i\boldsymbol{V}_i^H$	$64K(\frac{9}{8}N_i^3+N_tN_i^2+$ $\frac{1}{2}N_t^2N_i)$	13248 Total 18968

faster than the other precoding algorithms with the increase of the number of users K. The same complexity trend of the BD-type precoding is illustrated in Figure 4.4 with the increase of the number of receive antennas N_i with a fixed number of users K. The second aspect we can find from Figure 4.3 and Figure 4.4 is that the S-GMI precoding algorithm

Table 4.4: Computational complexity of LR-S-GMI-MMSE

Steps	Operations	Flops	Case $(2,2,2)\times 6$
1	$\boldsymbol{H}_{\mathrm{mse}}^{\dagger}$	$(\frac{4}{3}N_r^3+12N_r^2N_t$ $-2N_r^2-2N_rN_t)$	2736
2	$\boldsymbol{Q}_i^{\dagger}\boldsymbol{R}_i^{\dagger}$	$16K(N_t^2N_i-N_tN_i^2+\frac{1}{3}N_i^3)$	2432
3	$\boldsymbol{H}_i\boldsymbol{P}_i^a$	$K(8N_i^2N_t-2N_i^2)$	552
4	$\underline{\tilde{\boldsymbol{H}}}_{\mathrm{eff}_i}$	CLLL	4788
5	$\underline{\tilde{\boldsymbol{H}}}_{\mathrm{eff}_i}^{\dagger}$	$K(\frac{4}{3}N_i^3+12N_i^3-4N_i^2)$	272
			Total 10780

can offer a much lower computational complexity than the BD, RBD and QR/SVD RBD precoding algorithms. The reason is that, first, with the number of receive antennas N_i fixed, the number of executions of the first SVD operation of the RBD precoding and the QR decomposition of the S-GMI precoding are dependent on the number of users K but the latter is computed on $\boldsymbol{H}_{i,\mathrm{mse}}$ with a lower dimension $N_i \times N_i$, which is illustrated in Table 4.3. Second, with the number of users K fixed, the SVD operation itself has a higher cost than the channel inversion operation and the QR decomposition [103]. The complexity of the proposed LR-S-GMI-MMSE precoding, however, shows the lowest computational complexity among the analyzed precoding algorithms. The reason is that, we use a less complex LR transformation to replace the second SVD operation in the RBD and S-GMI precoding algorithms. It is worth noting that with the increase of the system dimensions in Figure 4.3 and Figure 4.4, the complexity reduction by the proposed LR-S-GMI-MMSE precoding algorithm becomes more considerable.

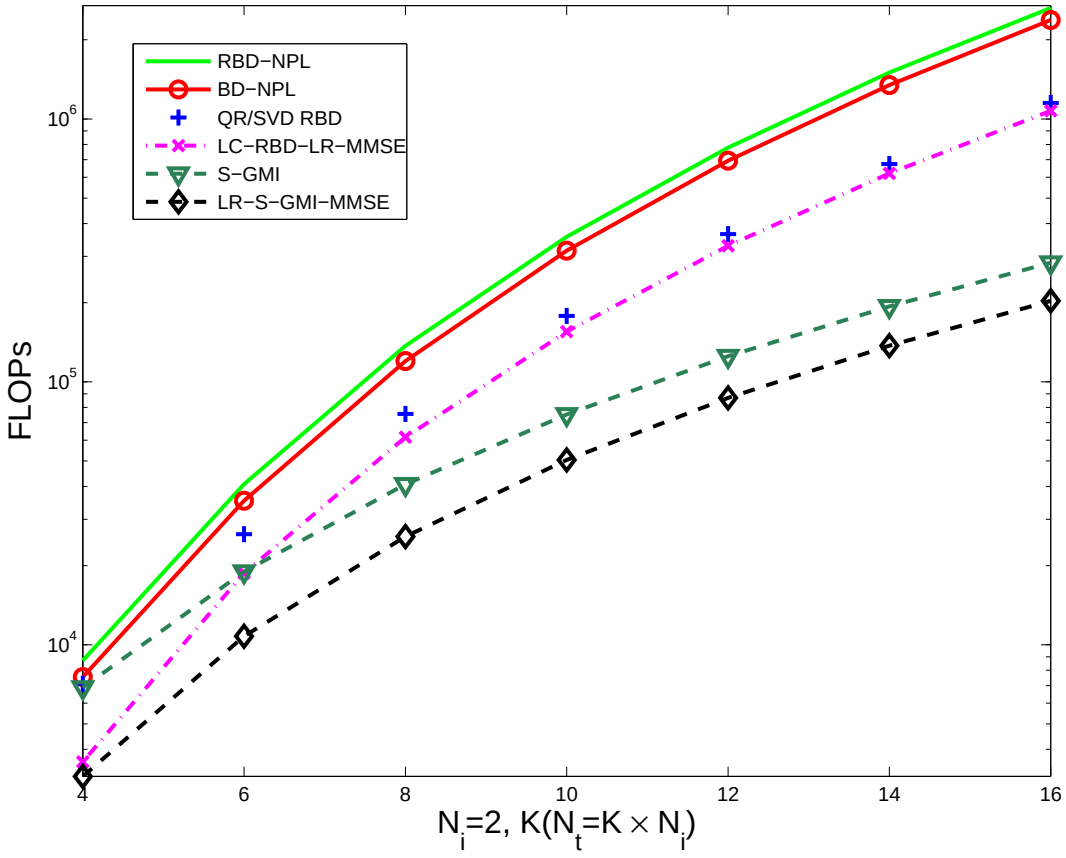

Figure 4.3: Computational Complexity - I Fixed N_i

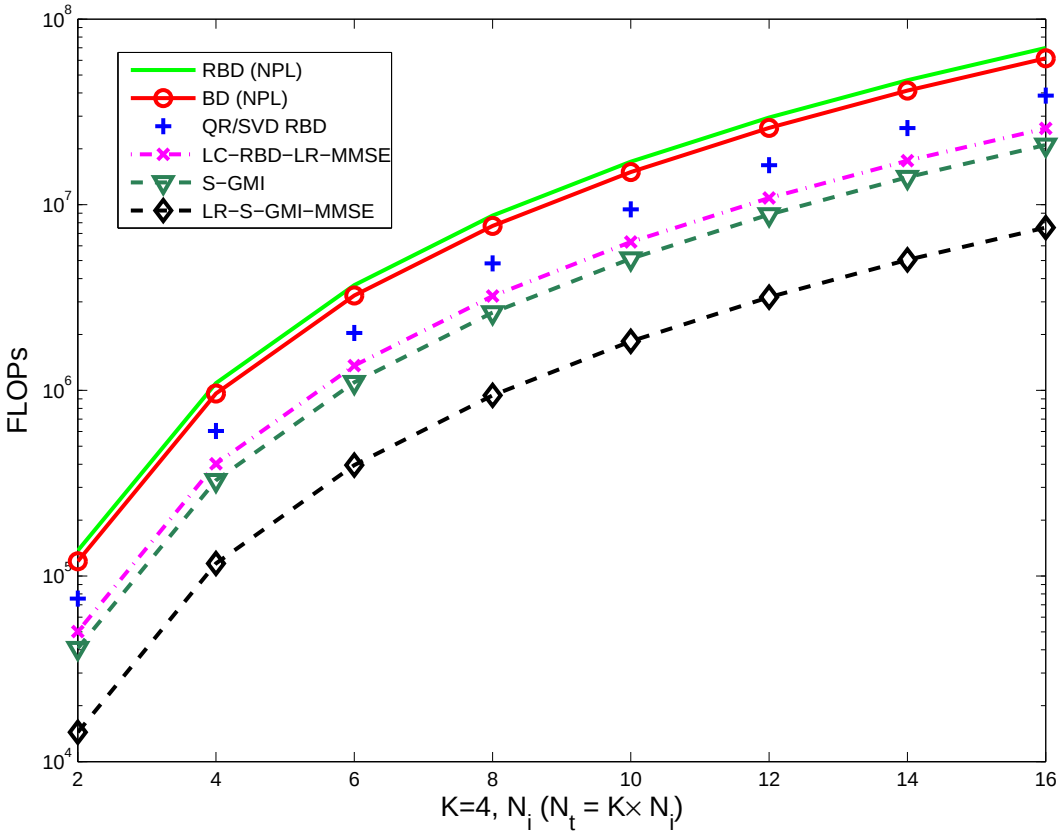

Figure 4.4: Computational Complexity - II Fixed K

4.5 Simulation Results

A system with $N_t = 8$ transmit antennas and $K = 4$ users each equipped with $N_i = 2$ receive antennas is considered; this scenario is denoted as the $(2, 2, 2, 2) \times 8$ case. The vector $\boldsymbol{d}_i$ of the ith user represents the data transmitted with QPSK modulation.

4.5.1 Perfect Channel Scenario

The channel matrix $\boldsymbol{H}_i$ of the ith user is modeled as a complex Gaussian channel matrix with zero mean and unit variance. We assume an uncorrelated block fading channel, that is, the channel is static during each transmit packet and there is no correlation between the antennas. We also assume that the channel estimation is perfect at the receive side and the feedback channel is error free. The number of simulation trials is 10^6 and the packet length is 10^2 symbols. The E_b/N_0 is defined as $E_b/N_0 = \frac{N_r \xi}{N_t M \sigma_n^2}$ with M being the number of transmitted information bits per channel symbol.

Figure 4.5 shows the BER performance of the proposed and existing precoding algorithms. The QR/SVD RBD and GMI precoding algorithms achieve almost the same BER performance as the conventional RBD precoding algorithm. It is clear that the S-GMI precoding scheme has a better BER performance compared to the BD, RBD, QR/SVD RBD and GMI precoding algorithms. The reason is that the residual interference between the users can be suppressed further by the S-GMI precoding scheme as we analyzed in Section V.A. The proposed LR-S-GMI-MMSE precoding algorithm shows the best BER performance in Figure 4.5. At the BER of 10^{-2}, the LR-S-GMI-MMSE precoding has a gain of more than 5.5 dB compared to the RBD precoding. It is worth noting that the RBD precoding is outperformed by the proposed LR-S-GMI-MMSE algorithm in the whole E_b/N_0 range and the BER gains become more significant with the increase of E_b/N_0. From the analysis developed in Section V.A, a better channel quality as measured by the condition number of the effective channel is achieved after the whole precoding process by the proposed LR-S-GMI-MMSE precoding. Therefore, the required transmit power γ_i is reduced and a better BER performance is obtained.

Figure 4.6 illustrates the sum-rate of the proposed and existing precoding algorithms. The

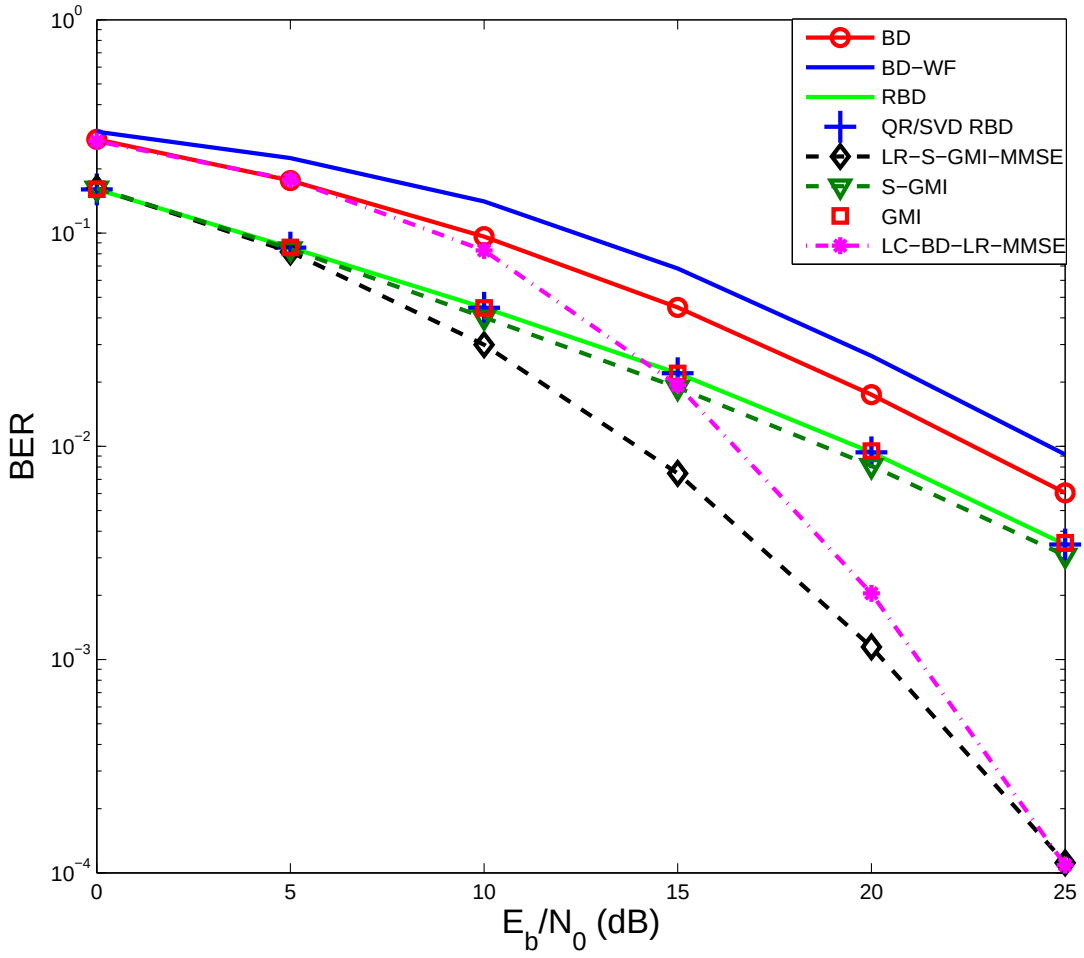

Figure 4.5: BER performance, $(2, 2, 2, 2) \times 8$ *MU-MIMO*

information rate is calculated using [105]:

$$C = \log(\det(\boldsymbol{I} + \sigma_n^{-2}\boldsymbol{H}\boldsymbol{P}\boldsymbol{P}^H\boldsymbol{H}^H)) \ (\text{bits/Hz}). \tag{4.41}$$

The BD precoding with WF power loading shows a better sum-rate performance than the BD precoding without power loading as we mentioned in Section V.B. However, as shown in Figure 4.5, the BER performance is degraded by applying this WF scheme. Similar to the BER figure, the RBD, QR/SVD RBD and GMI precoding algorithms show a comparable sum-rate performance. The S-GMI precoding also achieves the sum-rate performance of the RBD precoding. The proposed LR-S-GMI-MMSE precoding algorithm has almost the same sum-rate as the RBD precoding at low E_b/N_0s. At high E_b/N_0s, however, the sum-rate of LR-S-GMI-MMSE precoding is slightly inferior to that of the RBD precoding and approaches the performance of the BD precoding as we analyzed in Section V. B.

4.5.2 The impact of imperfect channels

From Section 3.6, the estimation errors or feedback errors can be modeled as a complex random Gaussian noise $\boldsymbol{E}$ with i.i.d. entries of zero mean and variance σ_e^2. The imperfect channel matrix $\boldsymbol{H}_e$ is defined as

$$\boldsymbol{H}_e = \boldsymbol{H} + \boldsymbol{E}, \tag{4.42}$$

where, the precoding matrix $\boldsymbol{P}$ has to be designed based on the feedback channel $\boldsymbol{H}_e$ while the physical channel is $\boldsymbol{H}$ during each transmission. Therefore, the BER performance will be degraded by the distortion term $\boldsymbol{E}$.

Figure 4.7 gives the BER performance of the above precoding algorithms with imperfect CSI at $E_b/N_0 = 15$ dB. It is clear that the BER performance gets worse for all the above precoding algorithms with the increase of the distortion noise power σ_e^2. The proposed LR-S-GMI-MMSE precoding algorithm outperforms the RBD precoding algorithm when σ_e^2 is below 0.2, however, the performance of the RBD precoding algorithm decays more slowly. The extra sensitive to channel errors is brought by the lattice reduction since the quality of transformed channel degraded with the imperfect channel information.

We need only to consider the antenna correlation at the transmit side in the MU-MIMO

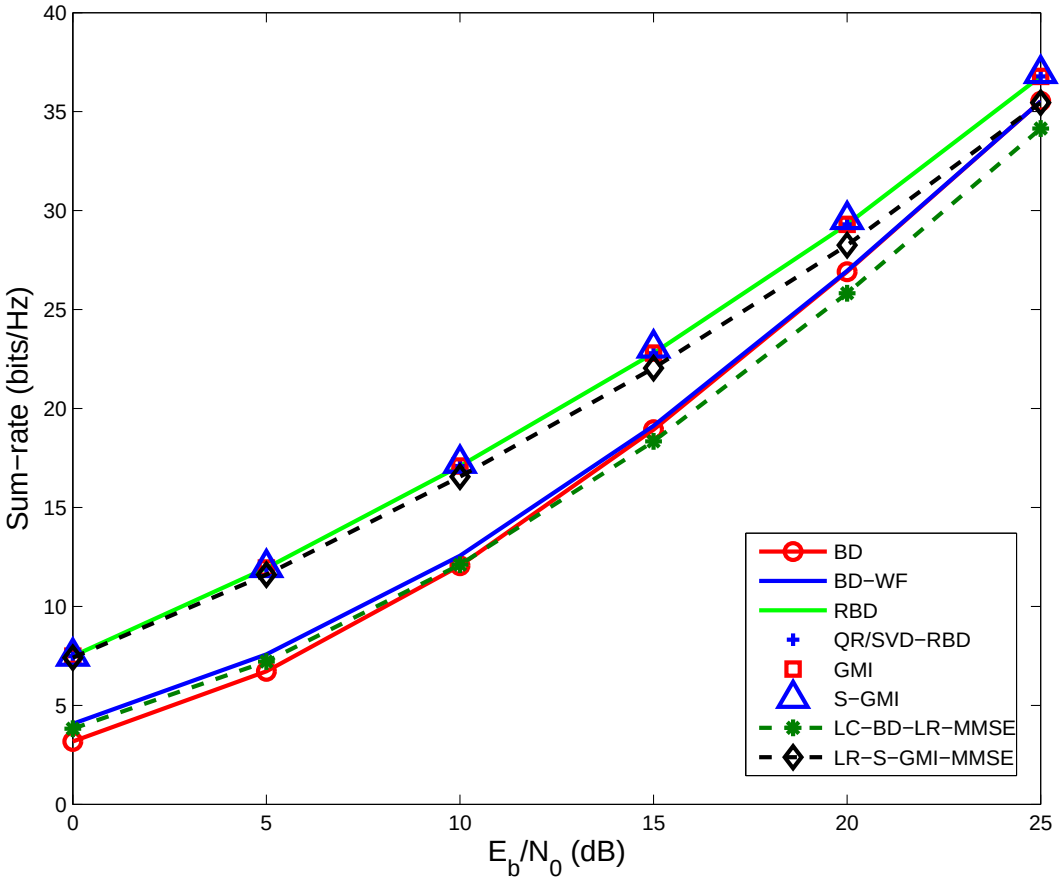

Figure 4.6: Sum-rate performance, $(2, 2, 2, 2) \times 8$ *MU-MIMO*

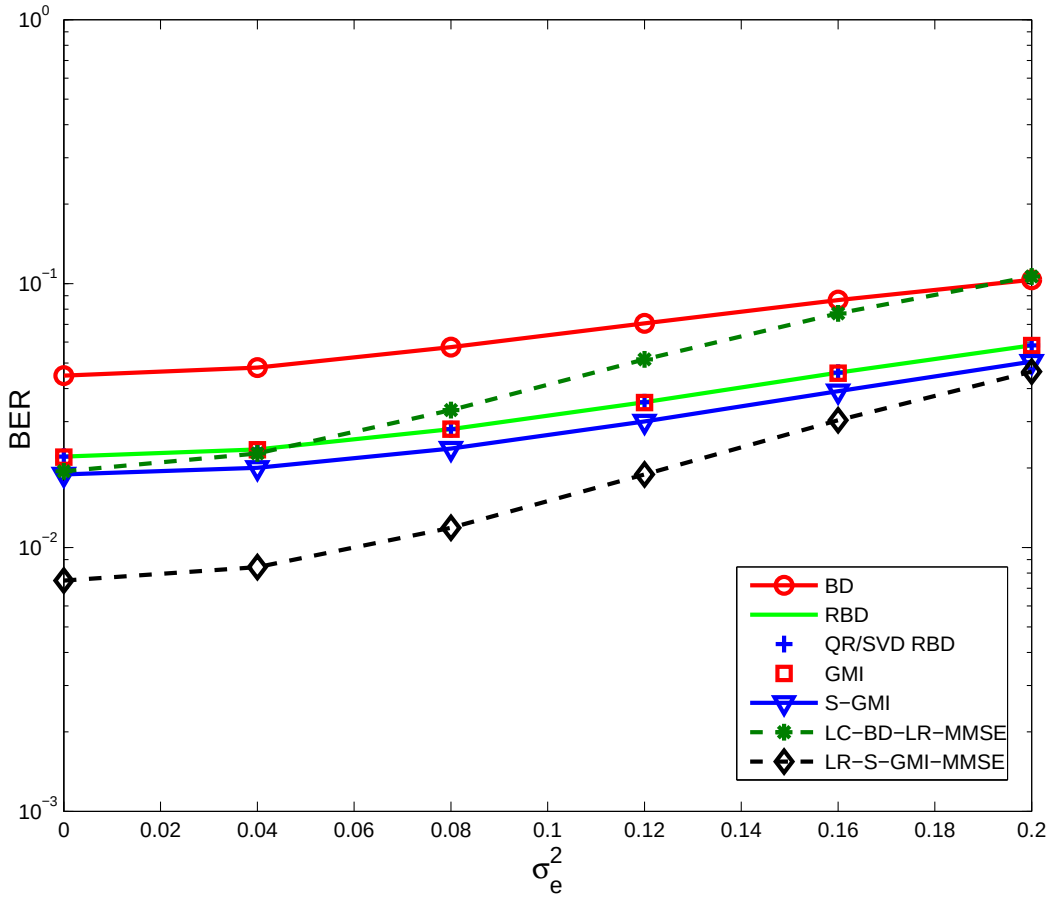

Figure 4.7: BER with σ_e^2 for a fixed E_b/N_0=15 dB

systems due to the users are geographically distributed. The correlated channel model given in Section 2.3.1 is applied in this simulation.

Figure 4.8 and Figure 4.9 display the BER and sum-rate performances of the above precoding algorithms with spatial correlation, respectively. It is clear that both BER and sum-rate performance deteriorate with the increase of the correlation coefficient r. From Figure 4.9, we can verify that the BD precoding degraded more dramatically with the increase of $|r|$ compared to the other precoding algorithms. The sum-rate of the proposed LR-S-GMI-MMSE precoding, however, gradually becomes better compared to the RBD precoding. For example, the sum-rate of the LR-S-GMI-MMSE precoding is better than the RBD precoding when E_b/N_0 below 15 dB with $|r| = 0.7$, which illustrates the robustness of the proposed LR-S-GMI precoding algorithms.

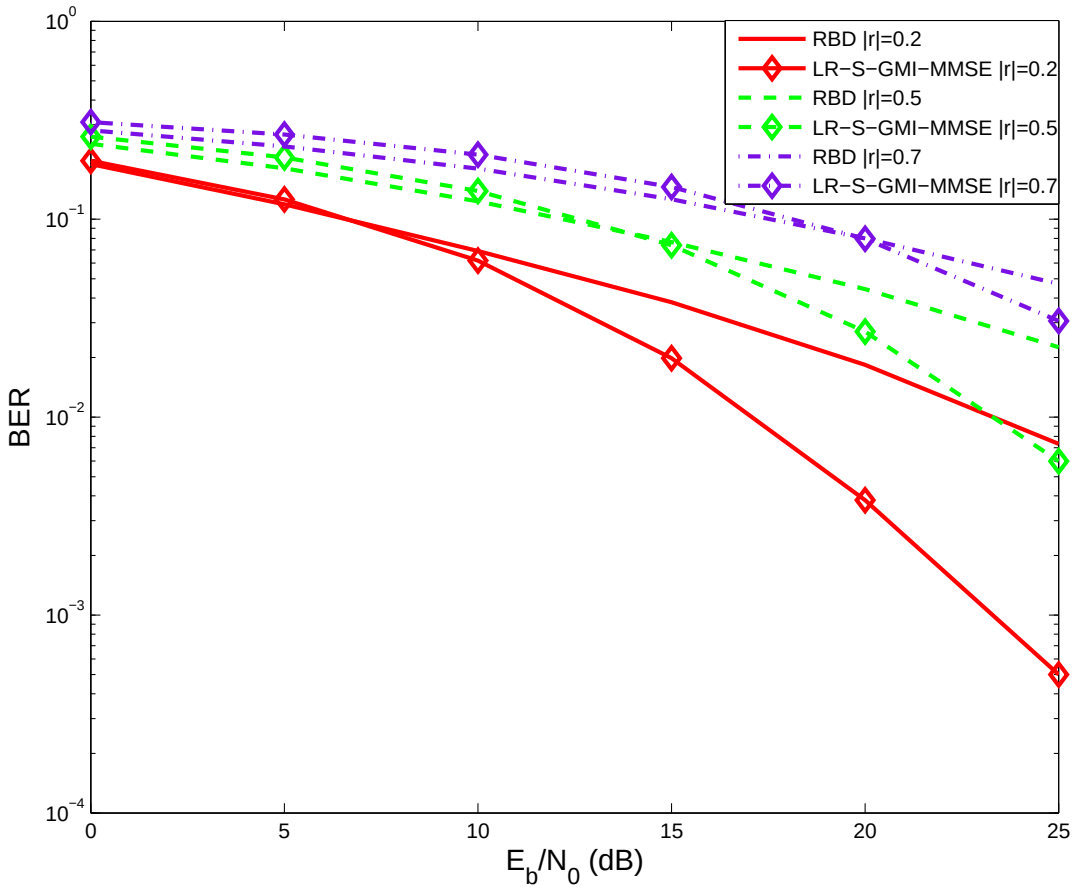

Figure 4.8: BER with spatial correlation

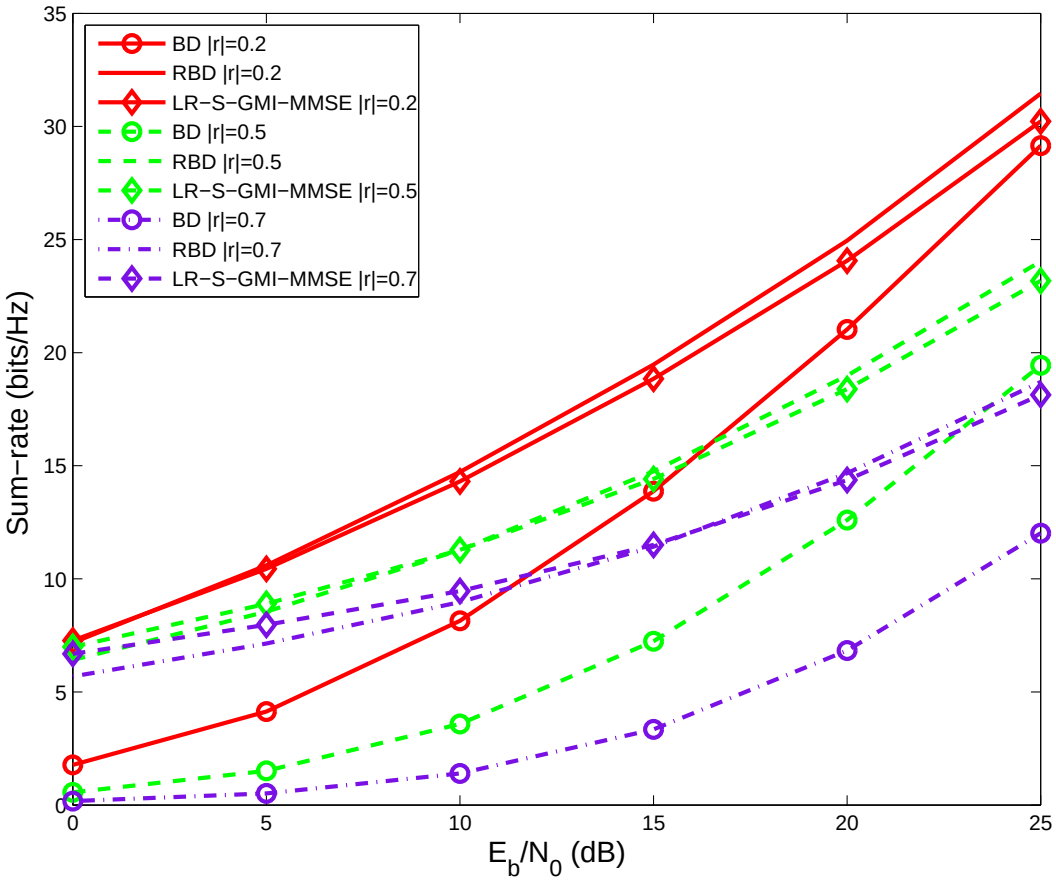

Figure 4.9: Sum-rate with spatial correlation

4.6 Summary

In this Chapter, low-complexity LR-S-GMI precoding algorithms based on a channel inversion technique, QR decompositions, and lattice reductions have been proposed for MU-MIMO systems. The complexity of the precoding process is reduced and a considerable BER gain is achieved by the proposed algorithms at a cost of a slight sum-rate loss at high SNRs. The BER performance, achievable sum-rate and computational complexity of the LR-S-GMI precoding algorithms have been analyzed and compared to existing precoding algorithms. Since the LR-S-GMI precoding algorithms are only implemented at the transmit side, the decoding matrix is not needed anymore at the receive side compared to the BD-type precoding algorithms. Then, the structure of the receiver can be simplified, which is an additional benefit from the proposed LR-S-GMI precoding algorithms.

Chapter 5

Multi-Branch Tomlinson-Harashima Precoding Design

Contents

Tomlinson-Harashima precoding (THP) is a nonlinear processing technique employed at the transmit side and is a dual to the *Successive Interference Cancelation* (SIC) detection at the receive side. Like SIC detection, the performance of THP strongly depends on the ordering of the precoded symbols. The optimal ordering algorithm, however, is impractical for MU-MIMO systems with multiple receive antennas. In this Chapter, we propose a *Multi-Branch THP* (MB-THP) scheme and algorithms that employ multiple transmit processing and ordering strategies along with a selection scheme to mitigate interference in MU-MIMO systems. Two types of MB-THP structures are proposed. The first one employs a decentralized strategy with diagonal weighted filters at the receivers of the users and the second uses a diagonal weighted filter at the transmitter. The MB-MMSE-THP algorithms are also derived based on an extended system model with the aid of an LQ

decomposition, which is much simpler than the conventional MMSE-THP algorithms. Simulation results show that a better BER performance can be achieved by the proposed MB-MMSE-THP precoder with a small computational complexity increase.

5.1 Introduction

MU-MIMO systems are promising for downlink wireless transmissions since they can improve the average user spectral efficiency [21]. When CSI is available at the transmit side, precoding techniques can be employed at the BS to mitigate the multi-user interference. Then, the required computational effort for each user's receiver can be reduced and eventually the receiver structure can be simplified [22]. For these reasons, the design of cost-effective precoders is particularly important for the downlink of MU-MIMO systems.

Linear precoding techniques such as ZF and MMSE precoding [20, 64, 65] are attractive due to their simplicity. However, linear precoding techniques require a higher average transmit power which could result in a reduced BER performance [65]. As a generalization of ZF precoding, BD based precoding algorithms have been proposed in [30, 99] for MU-MIMO systems. However, BD based precoding algorithms only take the MUI into account and thus suffer a performance loss at low SNRs when the noise is the dominant factor. An RBD precoding algorithm which introduces a regularization factor to take the noise term into account has been proposed in [66]. The performance is improved by RBD precoding, but the BD-type precoding algorithms still cannot achieve the maximum transmit diversity. A nonlinear *Vector Perturbation* (VP) approach, which is based on *Sphere Encoding* (SE) to perturb the data, was proposed in [26]. With the perturbation, a near optimal performance is achieved by VP precoding. However, finding the optimal perturbation vector can be a *Nondeterministic Polynomial* (NP) time-hard problem.

Another nonlinear and data-modifying technique is the *Dirty Paper Coding* (DPC) proposed in [18]. It was shown that the capacity of systems with *independent and identically distributed* (i.i.d.) Gaussian interference is equal to that of interference-free systems by utilizing DPC. However, DPC is not suitable for practical use due to the requirement of infinitely long codewords and codebooks [25]. THP [67, 68] is a pre-equalization tech-

nique originally proposed for channels with *Inter-symbol Interference* (ISI). Then, the THP technique was extended from temporal equalization to spatial equalization for MIMO precoding in [69]. Although THP suffers a performance loss compared to DPC as shown in [70], it can work as a cost-effective replacement of DPC in practice [71]. As revealed in [69, 72], the THP structure can be seen as the dual of the SIC detection implemented at the receive side. Like SIC detection, the performance of THP systems strongly depends on the ordering of the precoded symbols.

A V-BLAST like ordering strategy for THP has been studied in [110–112]. The V-BLAST ordering requires multiple calculations of the pseudo inverse of the channel matrix. Therefore, a suboptimal heuristic sorted LQ decomposition algorithm has been extended from the sorted QR decomposition in [61, 63] to THP and a *Tree Search* (TS) algorithm has also been proposed in [108]. Researchers in [113, 114] noticed the importance of the ordering to the THP performance as well, and the best-first ordering approach has been proposed to perform the ordering. Algorithms for finding the near-optimal order are proposed in [115, 116]. The above ordering algorithms, however, assumed that each distributed receiver was equipped with a single antenna. Therefore, the cooperative ordering processing is impractical for receivers with multiple antennas. In [117], a successive optimization THP (SO-THP) algorithm has been proposed for users with multiple antennas, but SO-THP only offers a small BER gain over THP at low SNRs. For high SNRs, the BER performance of SO-THP is comparable to that achieved by THP algorithm. In order to achieve a better BER performance in the whole SNR range, in this Chapter, a novel THP structure is proposed based on a *Multiple Branch* (MB) strategy for MU-MIMO systems with multiple antennas at each receiver.

In the literature, there are two basic THP structures according to the positions of the diagonal weighted filter, decentralized filters located at the receivers or centralized filters deployed at the transmitter, which are denoted as dTHP or cTHP, respectively [73]. Most of the previous research works on THP, however, have only focused on one of the structures. In this Chapter, we develop MB-THP techniques for both of the two basic THP structures. We derive the MMSE precoding filters using an LQ decomposition. Then, we present a design strategy for the transmit patterns that implements an effective ordering of the data streams along with a selection criterion for the best pattern. An analysis

and a comparison between MB-dTHP and MB-cTHP are also illustrated. By utilizing the MB strategy, the transmit diversity gain is maximized for MU-MIMO systems with spatial multiplexing. Therefore, the final BER performance is improved by the proposed MB-THP algorithms. The main contributions of the Chapter can be summarized as

1. Novel MB-THP algorithms are developed based on two basic THP structures.
2. Cost-effective MMSE filters are derived based on the LQ decomposition of an extended matrix along with the design of transmit patterns and a selection procedure.
3. A comprehensive performance analysis is carried out in terms of the error covariance matrix, the sum-rate and the computational complexity.
4. A study of the most relevant precoding algorithms reported in the literature and the proposed MB-THP algorithm is conducted.

5.2 System Model

We consider an uncoded MU-MIMO broadcast channel, with N_t transmit antennas at the BS and N_k receive antennas at the kth user equipment (UE). With K users in the system, the total number of receive antennas is $N_r = \sum_{k=1}^{K} N_k$. When $N_r = N_t$, the channel matrix is a square matrix. When $N_r \geq N_t$, a scheduling procedure is first performed to generate a square equivalent channel matrix [73]. The total number of transmitted streams is denoted by S, and the channel is assumed to be always a square matrix, that is $\boldsymbol{H} = [\boldsymbol{H}_1^T, \boldsymbol{H}_2^T, \cdots, \boldsymbol{H}_K^T]^T \in \mathbb{C}^{S \times S}$ is the combined channel matrix and $\boldsymbol{H}_k \in \mathbb{C}^{N_k \times S}$ is the ith user's channel matrix. Note that power-loading schemes [72] could be used to determine the number of data streams or allocate more power to a weaker user to improve the overall performance. However, for simplicity, we assume that all data streams are active and no power loading between users and streams is used.

5.3 Proposed MB-THP Precoding Algorithm

The structure and filters of the two basic THP precoding algorithms are given in Section 2.5.2. In this section, we first analyze the interference of the two basic THP structures and show that the ordering of the precoded symbols play an important role for both of the two types of THP systems. Based on this analysis, the MB-THP structure is proposed and its performance is illustrated. A cost-effective transmit pattern is especially developed for the MU-MIMO setting with multiple receive antennas, and a selection criterion is also deduced. Finally, since the MMSE-THP structures are the main focus, filters for MB-MMSE-THP are derived based on an extended system model which is much simpler from a computational point of view, as compared to conventional MMSE-THP techniques reported in the literature so far.

5.3.1 Motivation of the Proposed MB-THP Algorithm

As shown in (2.84) and (2.85), the MU-MIMO channel is decomposed into parallel AWGN channels by the successive THP processing as

$$\boldsymbol{r}^{(\mathrm{dTHP})} = \boldsymbol{v} + \boldsymbol{G}\boldsymbol{n}, \tag{5.1}$$

$$\boldsymbol{r}^{(\mathrm{cTHP})} = \boldsymbol{v} + \beta\boldsymbol{n}. \tag{5.2}$$

The modulo processing is equivalent to adding a perturbation vector $\boldsymbol{d}$ to the transmit date $\boldsymbol{s}$, the modified transmit data after the modulo processing is

$$\boldsymbol{v} = \boldsymbol{s} + \boldsymbol{d}. \tag{5.3}$$

With the power and modulo loss ignored, the power of $\boldsymbol{v}$ is approximately equal to that of $\boldsymbol{s}$.

From Section 2.5.2, THP can be implemented by an LQ decomposition. By utilizing an LQ decomposition on the channel matrix $\boldsymbol{H}$, we have

$$\boldsymbol{H} = \boldsymbol{L}\boldsymbol{Q}, \tag{5.4}$$

where $\boldsymbol{L}$ is a lower triangular matrix and $\boldsymbol{Q}$ is a unitary matrix (by unitary we mean

$\boldsymbol{Q}^H\boldsymbol{Q} = \boldsymbol{Q}\boldsymbol{Q}^H = \boldsymbol{I}$). Therefore, the filters for THP algorithm can be obtained as

$$\boldsymbol{F} = \boldsymbol{Q}^H, \tag{5.5}$$

$$\boldsymbol{G} = \mathrm{diag}[l_{1,1}, l_{2,2}, \cdots, l_{S,S}]^{-1}, \tag{5.6}$$

$$\boldsymbol{B}^{(\mathrm{dTHP})} = \boldsymbol{G}\boldsymbol{L}, \boldsymbol{B}^{(\mathrm{cTHP})} = \boldsymbol{L}\boldsymbol{G}, \tag{5.7}$$

where $l_{i,i}$ is the ith diagonal element of the matrix $\boldsymbol{L}$. Then, the error covariance matrices of the effective transmit signal $\boldsymbol{v}$ for dTHP and cTHP schemes are respectively given by

$$\boldsymbol{\Phi}_{\mathrm{dTHP}} = \mathrm{diag}(\sigma_n^2/l_{1,1}^2, \cdots, \sigma_n^2/l_{S,S}^2), \tag{5.8}$$

$$\boldsymbol{\Phi}_{\mathrm{cTHP}} = \mathrm{diag}(\sigma_n^2 \sum_{i=1}^{S}(1/l_{i,i}^2), \cdots, \sigma_n^2 \sum_{i=1}^{S}(1/l_{i,i}^2)). \tag{5.9}$$

From (5.8) and (5.9), we can verify that the error covariance matrices are different among layers for dTHP while they are equal for cTHP. Therefore, for each layer, the SNR is inversely proportional to $1/l_{i,i}^2$ for dTHP, while it is inversely proportional to $\sum_{i=1}^{S}(1/l_{i,i}^2)$ for cTHP. Due to the lower triangular structure of the feedback matrix $\boldsymbol{B}$, the interference from transmit data $s_1, s_2, \cdots, s_S$ is canceled out from s_1 to s_S in dTHP. That is, the layer precoded first will interfere with the layer precoded afterwards. Then, the performance of dTHP will be dominated by the layer with the minimum SNR. For cTHP, the sum of $\sum_{i=1}^{S}(1/l_{i,i}^2)$ can be influenced by reordering the rows of $\boldsymbol{H}$ during the LQ decomposition. In particular, the ordering of the precoded symbols plays an important role in the performance of THP systems. Thus, considerable research efforts have been spent on the development of various ordering methods, however, they all focused on SU-MIMO or MU-MIMO with single receive antenna systems. For MU-MIMO with multiple receive antennas, these cooperative ordering algorithms are impractical due to the geographically distributed users. In addition, most of the ordering algorithms only consider one THP structure, either cTHP or dTHP. In this work, an efficient MB-THP structure, which is especially suited for the users equipped with multiple antennas, is proposed based on the two basic THP structures.

5.3.2 Structure of the Proposed MB-THP

The idea of *multi-branch* (MB) processing has been first proposed in [118] as the parallel arbitrated branches to improve the performance of *Decision Feedback* (DF) receivers. A

MB-SIC detector has been proposed in [119] to exploit diversity gains in MIMO systems. In [97], the authors applied the MB strategy to generate interleaving patterns for DS-CDMA systems. Inspired by these research works, the MB-THP algorithms for the MU-MIMO downlink are developed and proposed. The structures of the proposed MB-THP schemes are illustrated in Figure 5.1.

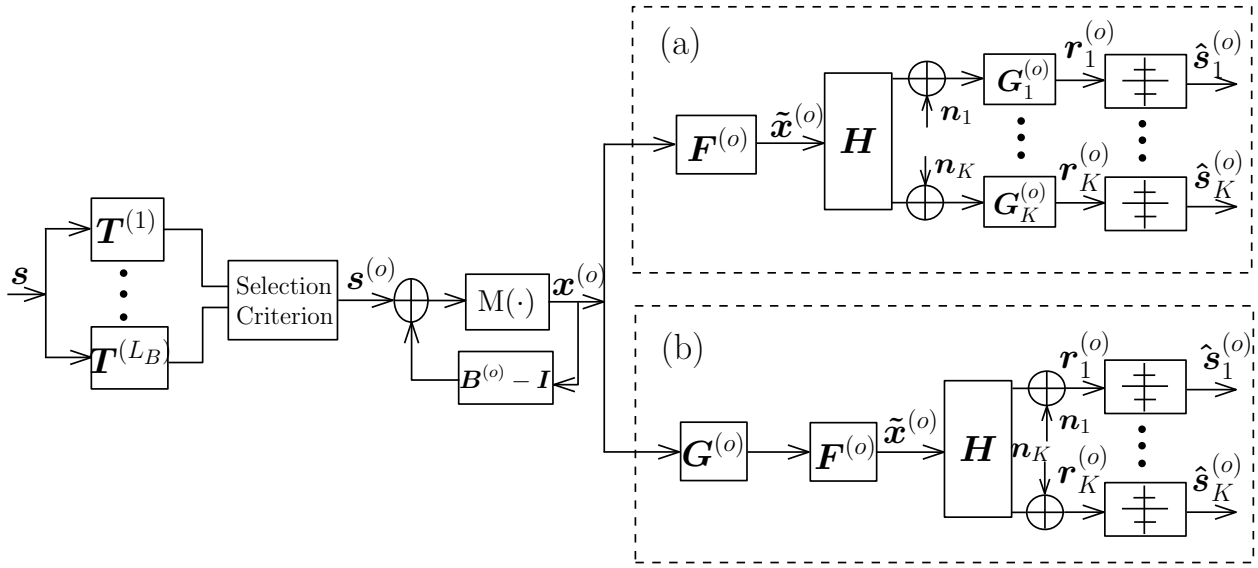

Figure 5.1: The proposed MB-THP structures (a) MB-dTHP (b) MB-cTHP

The matrices $\boldsymbol{T}^{(l)} \in \mathbb{C}^{N_r \times N_r}$ $(l = 1, \cdots, L_B)$ are the transmit patterns used to generate multiple parallel candidate branches, where L_B is the total number of branches. A proper selection metric is employed to choose the optimal branch to transmit the data streams. Then, the matrices $\boldsymbol{B}^{(o)}$, $\boldsymbol{F}^{(o)}$ and $\boldsymbol{G}^{(o)}$ represent the feedback, feedforward and scaling filters for the selected branch.

5.3.3 Design of the Transmit Patterns

The main concern of the transmit pattern design is to be effective but simple in this work. Observing the formulation in (5.8) and (5.9), the SNR performance of dTHP and cTHP can be influenced by $\boldsymbol{\Phi}_{\mathrm{dTHP}}$ and $\boldsymbol{\Phi}_{\mathrm{cTHP}}$. An ordering of the rows of $\boldsymbol{H}$ will lead to a corresponding change of $\boldsymbol{L}$ and $\boldsymbol{\Phi}$. Therefore, different ordering patterns can be employed to generate multiple branches for exploiting extra transmit diversity gains. Based on these

motivations, we pre-store the designed transmit patterns both at the transmitter and the receivers, which means that they are known permutations. Drawing upon previous design methods in [118] and [119], and considering the nature of distributed users in MU-MIMO scenarios, the design of transmit patterns is developed in three steps.

As the total number of users is K, we first obtain the different ordering patterns $\boldsymbol{T}_u^{(i)}$ between multiple users by

$$\boldsymbol{T}_u^{(1)} = \boldsymbol{I}_K, \tag{5.10}$$

$$\boldsymbol{T}_u^{(i)} = \begin{bmatrix} \boldsymbol{I}_p & \boldsymbol{0}_{p,K-p} \\ \boldsymbol{0}_{K-p,p} & \boldsymbol{\Pi}_{K-p} \end{bmatrix}, \ 2 \leq i \leq K, \tag{5.11}$$

where $p = (i-2)$ and $\boldsymbol{\Pi}_{K-p}$ denotes the exchange matrix of size $(K-p) \times (K-p)$ with ones on the reverse diagonal and the superscript i in $\boldsymbol{T}_u^{(i)}$ is termed as the ordering state. For the $K = 3$ case, we have

$$\boldsymbol{T}_u^{(1)} = \begin{bmatrix} 1\,0\,0 \\ 0\,1\,0 \\ 0\,0\,1 \end{bmatrix}, \boldsymbol{T}_u^{(2)} = \begin{bmatrix} 0\,0\,1 \\ 0\,1\,0 \\ 1\,0\,0 \end{bmatrix}, \boldsymbol{T}_u^{(3)} = \begin{bmatrix} 1\,0\,0 \\ 0\,0\,1 \\ 0\,1\,0 \end{bmatrix}. \tag{5.12}$$

Next, in order to make the branches as non-contiguous as possible, we shuffle the streams for each user in a similar way. The ordering patterns for the ith user equipped with N_{k_i} receive antennas is given by

$$\boldsymbol{T}_{k_i}^{(1)} = \boldsymbol{I}_{N_{k_i}}, \tag{5.13}$$

$$\boldsymbol{T}_{k_i}^{(j)} = \begin{bmatrix} \boldsymbol{I}_q & \boldsymbol{0}_{q,N_{k_i}-q} \\ \boldsymbol{0}_{N_{k_i}-q,q} & \boldsymbol{\Pi}_{N_{k_i}-q} \end{bmatrix}, \ 2 \leq j \leq J, \tag{5.14}$$

where $q = (j-2)$ and J is the maximum number of ordering states. Assuming that the first, second, and third user are equipped with 2, 2, and 3 receive antennas, respectively, then, we have

$$\boldsymbol{T}_{k_1}^{(1)} = \boldsymbol{T}_{k_2}^{(1)} = \begin{bmatrix} 1\,0 \\ 0\,1 \end{bmatrix}, \boldsymbol{T}_{k_1}^{(2)} = \boldsymbol{T}_{k_2}^{(2)} = \begin{bmatrix} 0\,1 \\ 1\,0 \end{bmatrix},$$

$$\boldsymbol{T}_{k_3}^{(1)} = \begin{bmatrix} 1\,0\,0 \\ 0\,1\,0 \\ 0\,0\,1 \end{bmatrix}, \boldsymbol{T}_{k_3}^{(2)} = \begin{bmatrix} 0\,0\,1 \\ 0\,1\,0 \\ 1\,0\,0 \end{bmatrix}, \boldsymbol{T}_{k_3}^{(3)} = \begin{bmatrix} 1\,0\,0 \\ 0\,0\,1 \\ 0\,1\,0 \end{bmatrix}. \tag{5.15}$$

Unlike the ordering states in $\boldsymbol{T}_u^{(i)}$, the total number of ordering states in $\boldsymbol{T}_{k_i}^{(j)}$ for each user is not uniform. In order to maximize the retention of ordering states, we choose $J = \mathrm{Max}_{k_i}(N_{k_i})$ but we note that different strategies for choosing J are possible. For the case that total ordering states N_{k_i} of the ith user is less than the maximum ordering states J, we simply repeat from the ith user's first ordering pattern to fill the gap.

Finally, we need to package the two ordering patterns $\boldsymbol{T}_u^{(i)}$ and $\boldsymbol{T}_{k_i}^{(j)}$ together to generate the resulting transmit pattern $\boldsymbol{T}^{(l)}$. The packaging scheme is that for each ordering state i, we increment the ordering state j by 1 until J. Inside each $(\boldsymbol{T}_u^{(i)}, \boldsymbol{T}_{k_i}^{(j)})$th packaging process, in order to put $\boldsymbol{T}_{k_i}^{(j)}$ in the right position, we locate the row indices of the nonzero entries in the sparse matrix $\boldsymbol{T}_u^{(i)}$. Then, we put the ordering pattern $\boldsymbol{T}_{k_i}^{(j)}$ to its corresponding nonzero element in the sparse matrix $\boldsymbol{T}_u^{(i)}$ and preserve the original sparse pattern. Taking the combination of $(\boldsymbol{T}_u^{(2)}, \boldsymbol{T}_k^{(2)})$ for example, the resulting transmit pattern is

$$\boldsymbol{T}^{(2)} = \begin{bmatrix} \mathbf{0} & \mathbf{0} & \boldsymbol{T}_{k_3}^{(2)} \\ \mathbf{0} & \boldsymbol{T}_{k_2}^{(2)} & \mathbf{0} \\ \boldsymbol{T}_{k_1}^{(2)} & \mathbf{0} & \mathbf{0} \end{bmatrix}. \tag{5.16}$$

For the users equipped with the same number of receive antennas, the total number of ordering states for each user is the same and $\boldsymbol{T}_{k_1}^{(j)} = \boldsymbol{T}_{k_2}^{(j)} = \boldsymbol{T}_{k_3}^{(j)}$. Then, we use $\boldsymbol{T}_k^{(j)}$ to denote the ordering patterns for the users and the packaging strategy is simplified by directly implementing the Kronecker product between $\boldsymbol{T}_u^{(i)}$ and $\boldsymbol{T}_{k_i}^{(j)}$

$$\boldsymbol{T}^{(l)} = \boldsymbol{T}_u^{(i)} \otimes \boldsymbol{T}_{k_i}^{(j)},\ 1 \leq l \leq L_B. \tag{5.17}$$

With the transmit patterns, a list of transmission branches are constructed. Then, a proper selection criterion is developed below to find the branch with minimum sum of errors among all the branches. The corresponding equivalent channel matrix for a chosen transmit pattern is denoted as $\boldsymbol{H}^{(o)} = \boldsymbol{T}^{(o)}\boldsymbol{H}$. Since we employ the MB strategy to generate extra branches for selection, the BER performance of the proposed MB-THP algorithms will keep same or better than the conventional THP algorithms.

The maximum number of branches L_B can be equal to $K!J!$, however, we restrict the total number of branches to no more than $K \cdot J$ here from the two steps of ordering patterns design and the packing process. And thus, a reasonable system complexity is maintained. It is also not necessary to set L_B equal to the maximum number of branches. Only with

2 or 4 branches, the MB-cTHP and MB-dTHP can approach its performance with full branches as illustrated in the simulation part.

5.3.4 Selection Criterion for the MB-THP

From the analysis followed after (5.8) and (5.9), the multiplication of different transmit patterns $\boldsymbol{T}^{(l)}$ to the row vectors of the channel matrix $\boldsymbol{H}$ resulted in different error covariance matrices for MB-cTHP and MB-dTHP. For each layer of MB-dTHP, its SNR is inversely proportional to $1/l_{i,i}^2$. For MB-cTHP, it is inversely proportional to $\sum_{i=1}^{S}(1/l_{i,i}^2)$. Thus, a minimum error selection criterion (MESC) is developed for both MB-cTHP and MB-dTHP to select the best branch according to

$$l^{(o)} = \arg \min_{1 \le l \le L_B} \sum_{1 \le i \le S} (1/l_{i,i}^{(l)})^2, \tag{5.18}$$

where $l^{(o)}$ is the selected branch. Then, the received signal $\boldsymbol{r}^{(o)}$ is obtained by

$$\boldsymbol{r}^{(o)^{(\mathrm{dTHP})}} = \boldsymbol{G}^{(o)}(\boldsymbol{H}^{(o)}\boldsymbol{F}^{(o)}\boldsymbol{x}^{(o)} + \boldsymbol{n}), \tag{5.19}$$

$$\boldsymbol{r}^{(o)^{(\mathrm{cTHP})}} = \beta(\boldsymbol{H}^{(o)} \cdot \frac{1}{\beta}\boldsymbol{F}^{(o)}\boldsymbol{G}^{(o)}\boldsymbol{x}^{(o)} + \boldsymbol{n}). \tag{5.20}$$

Since the transmit patterns are pre-stored and known both at the transmit and receive terminals, the transmitter can inform the receiver about the index of the selected pattern or the receiver can search for the best pattern. Then, the ordered signal $\boldsymbol{r}^{(o)}$ is transformed back to $\boldsymbol{r}$ by $\boldsymbol{T}^{(o)^T}$ at each receive terminal. Next, the transformed signal $\boldsymbol{r}$ is passed through the modulo processing to remove the offset by the perturbation vector $\boldsymbol{d}^{(o)}$, and a quantization function is followed to slice the symbols to the nearest points of the constellation as

$$\hat{\boldsymbol{s}} = \mathrm{Q}(\mathrm{M}(\boldsymbol{r})), \tag{5.21}$$

where $\mathrm{Q}(\cdot)$ is the slicing function and $\mathrm{M}(\cdot)$ is implemented element-wise as in (8).

5.3.5 Derivation of Filters for the MB-MMSE-THP

It is well-known that MMSE based algorithms always have a better performance than ZF based algorithms. Based on the MMSE design the filters of cTHP are deduced from an optimization problem in [111, 112], which results in a high computational complexity since

multiple calculations of matrix inverses are required. The orthogonality principle is utilized in [113] to obtain the filters of MMSE-dTHP. In [108], the filters of MMSE-cTHP are derived from an extended system model, which is simpler and more effective compared to the above two methods because the LQ decomposition is utilized. The receive model for MMSE-cTHP based on the extended matrix, however, is not given in [26]. In this work, we derive the filters of the proposed MB-MMSE-cTHP and MB-MMSE-dTHP based on the extended matrix and their corresponding receive models are also described.

Define the $N_r \times (N_r + N_t)$ extended channel matrix $\underline{\boldsymbol{H}}$ for the MB-MMSE precoding schemes as

$$\underline{\boldsymbol{H}}^{(l)} = \left[\begin{array}{cc} \boldsymbol{H}^{(l)}, & \sigma_n \boldsymbol{I}_{N_r} \end{array} \right], \tag{5.22}$$

where $\boldsymbol{H}^{(l)} = \boldsymbol{T}^{(l)}\boldsymbol{H}$. Then, the linear precoding MMSE filter can be rewritten as $\boldsymbol{P}_{\mathrm{MMSE}}^{(l)} = \boldsymbol{A}\underline{\boldsymbol{H}}^{(l)^H}(\underline{\boldsymbol{H}}^{(l)}\underline{\boldsymbol{H}}^{(l)^H})^{-1}$, where $\boldsymbol{A} = [\boldsymbol{I}_{N_t},\ \boldsymbol{0}_{N_t,N_r}]$. By implementing the LQ decomposition of the extended channel matrix $\underline{\boldsymbol{H}}^{(l)}$ we have

$$\underline{\boldsymbol{H}}^{(l)} = \underline{\boldsymbol{L}}^{(l)}\underline{\boldsymbol{Q}}^{(l)} = \underline{\boldsymbol{L}}^{(l)} \left[\begin{array}{cc} \boldsymbol{Q}_1^{(l)}, & \boldsymbol{Q}_2^{(l)} \end{array} \right], \tag{5.23}$$

where $\underline{\boldsymbol{L}}^{(l)}$ is a $N_r \times N_r$ lower triangular matrix and the $N_r \times (N_r + N_t)$ matrix $\underline{\boldsymbol{Q}}^{(l)}$ with orthogonal columns can be partitioned into the $N_r \times N_t$ matrix $\boldsymbol{Q}_1^{(l)}$ and the $N_r \times N_r$ matrix $\boldsymbol{Q}_2^{(l)}$. From (5.22) and (5.23), the following relations hold

$$\boldsymbol{H}^{(l)} = \underline{\boldsymbol{L}}^{(l)}\boldsymbol{Q}_1^{(l)}, \tag{5.24}$$

$$\underline{\boldsymbol{L}}^{(l)^{-1}} = \frac{1}{\sigma_n}\boldsymbol{Q}_2^{(l)}, \tag{5.25}$$

$$\boldsymbol{A}\underline{\boldsymbol{Q}}^{(l)^H} = \boldsymbol{Q}_1^{(l)^H}. \tag{5.26}$$

Therefore, the filters for the MB-MMSE-cTHP and the MB-MMSE-dTHP schemes can be obtained as

$$\boldsymbol{F}^{(l)} = \underline{\boldsymbol{Q}}^{(l)^H}, \tag{5.27}$$

$$\boldsymbol{G}^{(l)} = \mathrm{diag}[\underline{l}_{1,1}^{(l)}, \underline{l}_{2,2}^{(l)}, \cdots, \underline{l}_{N_t,N_t}^{(l)}]^{-1}, \tag{5.28}$$

$$\boldsymbol{B}^{(l)^{(\mathrm{dTHP})}} = \boldsymbol{G}^{(l)}\underline{\boldsymbol{L}}^{(l)}, \tag{5.29}$$

$$\boldsymbol{B}^{(l)^{(\mathrm{cTHP})}} = \underline{\boldsymbol{L}}^{(l)}\boldsymbol{G}^{(l)}, \tag{5.30}$$

where $\underline{l}_{ii}^{(l)}$ are the diagonal elements of $\underline{\boldsymbol{L}}^{(l)}$. The received signal for the lth branch is

$$\boldsymbol{r}^{(l)^{(\mathrm{dTHP})}} = \boldsymbol{G}^{(l)}(\boldsymbol{H}^{(l)}\boldsymbol{A}\boldsymbol{F}^{(l)}\boldsymbol{x}^{(l)} + \boldsymbol{n}), \tag{5.31}$$

$$\boldsymbol{r}^{(l)^{(\mathrm{cTHP})}} = \beta(\boldsymbol{H}^{(l)} \cdot \frac{1}{\beta}\boldsymbol{A}\boldsymbol{F}^{(l)}\boldsymbol{G}^{(l)}\boldsymbol{x}^{(l)} + \boldsymbol{n}). \tag{5.32}$$

It is worth noting that the multiplication by $\boldsymbol{A}$ will not result in transmit power amplification since $\boldsymbol{A}\boldsymbol{A}^H = \boldsymbol{I}_{N_t}$ ($\boldsymbol{A}$ is unitary). The implementation steps of the MB-MMSE-THP algorithms are summarized in Table 5.1.

5.4 Performance Analysis

In this section, we consider a performance analysis in terms of error covariance, sum-rate and computational complexity.

5.4.1 Performance Analysis of the Error Covariance Matrix

The autocorrelation matrices of the interference-plus-noise power in ZF-dTHP and ZF-cTHP have been given in [73], however, the comparison has not been done. In this section, we illustrate the BER performances in terms of error covariance. For the comparison between ZF-dTHP and ZF-cTHP, we assume i is an arbitrary layer, then we have

$$\frac{\boldsymbol{\Phi}^{l^{(o)}}_{\mathrm{ZF-cTHP}_{i,i}}}{\boldsymbol{\Phi}^{l^{(o)}}_{\mathrm{ZF-dTHP}_{i,i}}} = 1 + {l^{(o)}_{i,i}}^2 \sum_{j\neq i}^{S}(1/{l^{(o)}_{j,j}}^2). \tag{5.33}$$

That is, $\forall\ i:\ \boldsymbol{\Phi}^{l^{(o)}}_{\mathrm{ZF-cTHP}_{i,i}} > \boldsymbol{\Phi}^{l^{(o)}}_{\mathrm{ZF-dTHP}_{i,i}}$. Since the BER performance is largely related to the error covariance matrix, we expect a better BER performance of ZF-dTHP over ZF-cTHP. This is also verified by the simulation result in [73], from which a slightly better BER performance of ZF-dTHP over ZF-cTHP is reported.

The comparison between MMSE-dTHP and MMSE-cTHP, however, has not been analyzed nor simulated in the literature so far. Substituting (5.24), (5.26), (5.27) and (5.29) into (5.31), we can get the error covariance matrix for MMSE-dTHP as

$$\boldsymbol{\Phi}^{(l)}_{\mathrm{MMSE-dTHP}} = \mathrm{diag}(\sigma_n/\underline{l}^{(l)}_{1,1}, \cdots, \sigma_n/\underline{l}^{(l)}_{S,S})^2. \tag{5.34}$$

Table 5.1: Proposed MB-MMSE-THP Algorithms

Steps	Operations
	Compute the extended channel matrix for the lth branch
(1)	$\underline{\boldsymbol{H}}^{(l)} = \left[\begin{array}{cc} \boldsymbol{T}^{(l)}\boldsymbol{H}, & \sigma_n \boldsymbol{I}_S \end{array} \right]$
	Implement the LQ decomposition
(2)	$\underline{\boldsymbol{H}}^{(l)} = \underline{\boldsymbol{L}}^{(l)}\underline{\boldsymbol{Q}}^{(l)}$
	Obtain the filters for MB-cTHP and MB-dTHP
(3)	$\boldsymbol{F}^{(l)} = \underline{\boldsymbol{Q}}^{(l)^H}, \boldsymbol{G}^{(l)} = \mathrm{diag}[\underline{l}_{1,1}^{(l)}, \underline{l}_{2,2}^{(l)}, \cdots, \underline{l}_{N_t,N_t}^{(l)}]^{-1}$, $\boldsymbol{B}^{(l)^{(\mathrm{cTHP})}} = \underline{\boldsymbol{L}}^{(l)}\boldsymbol{G}^{(l)}$, $\boldsymbol{B}^{(l)^{(\mathrm{dTHP})}} = \boldsymbol{G}^{(l)}\underline{\boldsymbol{L}}^{(l)}$
	The MESC selection criterion
(4)	for j = 1 : L_B[‡]
(5)	$\mathrm{MESC}(j) = \sum_{i=1}^{S}(1/l_{i,i}^2)$
(6)	end
(7)	$l^{(o)\ddagger} = \mathrm{Min}(\mathrm{MESC})$
	The successive cancelation process
(8)	for i = 1 : S
(9)	$x^{(o)}(i) = s_i - \sum_{j\neq i}^{S} b_{i,j}x^{(o)}(j)$
(10)	$x^{(o)}(i) = \mathrm{M}(x^{(o)}(i))$
(11)	end
	The received signal
(12)	$\beta = \frac{\mathrm{E}\|\boldsymbol{FGx}\|}{\mathrm{E}\|\boldsymbol{s}\|}$
(13)	$\boldsymbol{r}^{(o)^{(\mathrm{cTHP})}} = \beta(\boldsymbol{H}^{(o)} \cdot \frac{1}{\beta}\boldsymbol{F}^{(o)}\boldsymbol{G}^{(o)}\boldsymbol{x}^{(o)} + \boldsymbol{n})$
(14)	$\boldsymbol{r}^{(o)^{(\mathrm{dTHP})}} = \boldsymbol{G}^{(o)}(\boldsymbol{H}^{(o)}\boldsymbol{F}^{(o)}\boldsymbol{x}^{(o)} + \boldsymbol{n})$
(15)	$\hat{\boldsymbol{s}}^{(\mathrm{cTHP})} = \mathrm{Q}(\mathrm{M}(\boldsymbol{T}^{(o)^T}\boldsymbol{r}^{(o)^{(\mathrm{cTHP})}}))$
(16)	$\hat{\boldsymbol{s}}^{(\mathrm{dTHP})} = \mathrm{Q}(\mathrm{M}(\boldsymbol{T}^{(o)^T}\boldsymbol{r}^{(o)^{(\mathrm{dTHP})}}))$
	% ‡ L_B is the total number of branches
	% ‡ $l^{(o)}$ is the selected optimal branch

For the MMSE-cTHP we start from the calculation of β for a more accurate expression

by

$$\beta^2 = \frac{\mathrm{E}\|\boldsymbol{A}\boldsymbol{F}^{(l)}\boldsymbol{G}^{(l)}\boldsymbol{x}^{(l)}\|^2}{\sigma_s^2}, \tag{5.35}$$

where $\sigma_s^2 = \mathrm{E}\|\boldsymbol{s}\|^2$. Since $\boldsymbol{x}^{(l)} = \boldsymbol{B^{(l)}}^{-1}\boldsymbol{v}^{(l)}$, $\boldsymbol{B}^{(l)} = \underline{\boldsymbol{L}}^{(l)}\boldsymbol{G}^{(l)}$ and $\underline{\boldsymbol{L}}^{(l)^{-1}} = \frac{1}{\sigma_n}\boldsymbol{Q}_2^{(l)}$, the multiplication $\boldsymbol{A}\boldsymbol{F}^{(l)}\boldsymbol{G}^{(l)}\boldsymbol{x}^{(l)}$ is obtained as

$$\boldsymbol{A}\boldsymbol{F}^{(l)}\boldsymbol{G}^{(l)}\boldsymbol{x}^{(l)} = \frac{1}{\sigma_n}\boldsymbol{A}\boldsymbol{F}^{(l)}\boldsymbol{Q}_2^{(l)}\boldsymbol{v}^{(l)}. \tag{5.36}$$

Then, by applying the equivalence $\mathrm{tr}(\boldsymbol{A}\boldsymbol{B}\boldsymbol{C}) = \mathrm{tr}(\boldsymbol{C}\boldsymbol{A}\boldsymbol{B})$, the normalization factor β can be expressed as

$$\beta^2 = \frac{{\sigma_v^{(l)}}^2}{\sigma_n^2\sigma_s^2}, \tag{5.37}$$

where the quantity ${\sigma_v^{(l)}}^2$ is the variance of $\boldsymbol{v}^{(l)}$. Therefore, the error covariance matrix for MMSE-cTHP is obtained as

$$\boldsymbol{\Phi}_{\mathrm{MMSE-cTHP}}^{(l)} = \mathrm{diag}\left(\frac{{\sigma_v^{(l)}}^2}{\sigma_s^2}, \cdots, \frac{{\sigma_v^{(l)}}^2}{\sigma_s^2}\right). \tag{5.38}$$

Since the noise term is taken into account in MMSE-cTHP, we expect a better BER performance of MMSE-cTHP over MMSE-dTHP. By changing the transmit signal order, different perturbation vectors $\boldsymbol{d}^{(l)}$ are obtained in MB-MMSE-cTHP. The multi-branch processing is actually used to select the one with the minimum ${\sigma_v^{(l)}}^2$ among all the L_B branches in MB-MMSE-cTHP algorithms. For the comparison between MB-MMSE-dTHP and MMSE-dTHP, we have the proposition below.

Proposition: The trace of the error covariance matrix for the proposed MB-MMSE-dTHP technique is upper bounded by that of the conventional MMSE-dTHP scheme, i.e.,

$$\mathrm{tr}(\boldsymbol{\Phi}_{\mathrm{MB-MMSE-dTHP}}) \leq \mathrm{tr}(\boldsymbol{\Phi}_{\mathrm{MMSE-dTHP}}). \tag{5.39}$$

Proof: From the MESC selection criterion in (5.18), the selected branch $l^{(o)}$ corresponds to the sum of the elements associated with the smallest value, i.e.,

$$\mathrm{tr}(\boldsymbol{\Phi}_{\mathrm{MB-MMSE-dTHP}}) = \sum_{1\leq i\leq S}(1/\underline{l}_{i,i}^{(o)})^2, \tag{5.40}$$

With the MESC selection criterion, we have

$$\sum_{1\leq i\leq S}(1/\underline{l}_{i,i}^{(o)})^2 \leq \sum_{1\leq i\leq S}(1/\underline{l}_{i,i}^{(l)})^2, l = 1, 2, \cdots, L_B. \tag{5.41}$$

By writing the above quantities without the sum, we get

$$\left(\frac{1}{\underline{l}_{1,1}^{(o)}}\right)^2 + \cdots + \left(\frac{1}{\underline{l}_{S,S}^{(o)}}\right)^2 \leq \left(\frac{1}{\underline{l}_{1,1}^{(l)}}\right)^2 + \cdots + \left(\frac{1}{\underline{l}_{S,S}^{(l)}}\right)^2,$$
$$\left[\left(\frac{1}{\underline{l}_{1,1}^{(o)}}\right)^2 - \left(\frac{1}{\underline{l}_{1,1}^{(l)}}\right)^2\right] + \cdots + \left[\left(\frac{1}{\underline{l}_{S,S}^{(o)}}\right)^2 - \left(\frac{1}{\underline{l}_{S,S}^{(l)}}\right)^2\right] \leq 0. \tag{5.42}$$

If we choose $\underline{l}_{i,i}^{(o)}$ to be identical to $\underline{l}_{i,i}^{(l)}$ then we prove the equality $\mathrm{tr}(\mathbf{\Phi}_{\mathrm{MB-MMSE-dTHP}}) = \mathrm{tr}(\mathbf{\Phi}_{\mathrm{MMSE-dTHP}})$. If we choose at least one element $\underline{l}_{i,i}^{(o)} > \underline{l}_{i,i}^{(l)}$ or $\underline{l}_{i,i}^{(o)} - \underline{l}_{i,i}^{(l)} = \epsilon$ while keeping the others identical $\underline{l}_{j,j}^{(o)} = \underline{l}_{j,j}^{(l)}$, $j \neq i$ then we prove the inequality $\mathrm{tr}(\mathbf{\Phi}_{\mathrm{MB-MMSE-dTHP}}) < \mathrm{tr}(\mathbf{\Phi}_{\mathrm{MMSE-dTHP}})$, where ϵ is a small real positive value.

For MMSE-cTHP, the overall SNR performance is influenced by the sum of each layer, then from (5.38) we have

$$\mathrm{tr}(\mathbf{\Phi}_{\mathrm{MMSE-cTHP}}) = \frac{K{\sigma_v^{(l)}}^2}{\sigma_s^2}, \tag{5.43}$$
$$\mathrm{tr}(\mathbf{\Phi}_{\mathrm{MB-MMSE-cTHP}}) = \frac{K{\sigma_v^{(o)}}^2}{\sigma_s^2}.$$

Because of the MESC selection process, we have obtained that $\forall\, l : {\sigma_v^{(o)}}^2 \leq {\sigma_v^{(l)}}^2$. Thus, it is straightforward to conclude that

$$\mathrm{tr}(\mathbf{\Phi}_{\mathrm{MB-MMSE-cTHP}}) \leq \mathrm{tr}(\mathbf{\Phi}_{\mathrm{MMSE-cTHP}}). \tag{5.44}$$

Therefore, we expect that a better BER performance can be achieved by the proposed MB-dTHP and MB-cTHP, respectively, as compared to their original counterparts.

5.4.2 Sum-Rate Performance Analysis

From the analysis illustrated in Section III, the MU-MIMO channel is decomposed into parallel AWGN channels in the THP systems. Therefore, the ith SNR for the lth branch transmit signal of MB-ZF-THP is given by

$${\gamma_i}^{(l)(\mathrm{MB-ZF-dTHP})} = \frac{\sigma_s^2}{\sigma_n^2(1/{l_{i,i}^{(l)}}^2)}, \tag{5.45}$$
$${\gamma_i}^{(l)(\mathrm{MB-ZF-cTHP})} = \frac{\sigma_s^2}{\sigma_n^2 \sum_{i=1}^{S}(1/{l_{i,i}^{(l)}}^2)}. \tag{5.46}$$

Then, the achieved sum-rate for the lth branch of MB-ZF-dTHP and MB-ZF-cTHP is

$$C^{(l)}_{(\mathrm{MB-ZF-dTHP})} = \sum_{i=1}^{S} \log\Big(1 + \frac{\sigma_s^2 {l^{(l)}_{i,i}}^2}{\sigma_n^2}\Big), \tag{5.47}$$

$$C^{(l)}_{(\mathrm{MB-ZF-cTHP})} = S \log\left(1 + \frac{\sigma_s^2}{\sigma_n^2 \sum_{i=1}^{S} (1/{l^{(l)}_{i,i}}^2)}\right). \tag{5.48}$$

For MB-MMSE-THP, the achieved sum-rate of dTHP and cTHP can be expressed as follows

$$C^{(l)}_{(\mathrm{MB-MMSE-dTHP})} = \sum_{i=1}^{S} \log\Big(1 + \frac{\sigma_s^2 {l^{(l)}_{i,i}}^2}{\sigma_n^2}\Big), \tag{5.49}$$

$$C^{(l)}_{(\mathrm{MB-MMSE-cTHP})} = S \log\left(1 + \frac{\sigma_s^4}{{\sigma_v^{(l)}}^2}\right). \tag{5.50}$$

From (5.47) and (5.49), the difference of the overall average SNR for the lth branch is small. Thus, we expect that MB-MMSE-dTHP with different branches shares a similar sum-rate performance. For MB-MMSE-cTHP, the ${\sigma_v^{(o)}}^2$ of the selected $l^{(o)}$th branch has the minimum value among all the branches because of the multi-branch and the selection processing, that is

$${\sigma_v^{(o)}}^2 \leq {\sigma_v^{(l)}}^2,\ l = 1, \cdots, L_B, \tag{5.51}$$

Thus, we have

$$C^{(o)}_{(\mathrm{MB-MMSE-cTHP})} \geq C_{(\mathrm{MMSE-cTHP})}, \tag{5.52}$$

which means the sum-rate of MMSE-cTHP can be improved by the proposed MB-MMSE-cTHP algorithm.

5.4.3 Complexity Analysis

In this section we use the total number of floating point operations (FLOPs) to measure the computational complexity of the proposed and existing algorithms. The number of FLOPs for the LQ decomposition is obtained by assuming that the LQ decomposition is computed by using the Householder transformation given in [103]. We summarize the total number of FLOPs needed for the matrix operations below:

- Multiplication of $m \times n$ and $n \times p$ complex matrices: $8mnp - 2mp$;
- LQ decomposition of an $m \times n$ $(m \leq n)$ complex matrix: $8m^2(n - \frac{1}{3}m)$;
- Pseudo-inversion of an $m \times n$ complex matrix: $(\frac{4}{3}m^3 + 7m^2n - m^2 - 2mn)$.

The number of FLOPs needed for BD and RBD can be found in [120]. The computational complexity of MMSE-THP based on multiple matrix inversions in [111] has been given in [121]. The complexity reported in [121], however, is only computed in terms of the number of multiplications and additions. For the complex multiplications and additions, it respectively needs 6 and 2 FLOPs. Thus, the number of FLOPs needed by MMSE-THP in [111] is at least $24N_r^4 + 48N_r^3 + N_tN_r$. For MMSE-THP based on the Cholesky factorization in [121], the number of FLOPs needed is at least $\frac{20}{3}N_r^3 + 8N_r^2N_t$. The ZF-VP in [26] and MMSE-VP in [80] are implemented by using the SE algorithm which is employed for sphere encoding. The complexity of SD is associated with the constellation size M and the radius d which is chosen to be a scaled version of the noise variance [27]. The required multiplications and additions of SD are given in [122].

For simplicity, we assume that the number of transmit antennas N_t and the number of receive antennas N_r are equal to n. From the above derivation, MB-MMSE-dTHP and MB-MMSE-cTHP share the same computational complexity. The number of FLOPs for the above precoding algorithms are listed in Table 5.2, where n_i is the number of antennas of the ith user, and $\bar{n}_i = N_r - n_i$. In case of system dimension $n = 6$, number of users $K = 3$, each user equipped with $N_i = 2$ receive antennas and number of branches $L_B = 2$, the required number of FLOPs of MB-ZF-THP and MB-MMSE-THP is much lower than the BD, RBD, conventional MMSE-THP in [111] and VP algorithms.

The required number of FLOPs of the proposed and existing algorithms is simulated for different system dimensions and the results are depicted in Figure 5.2. From Figure 5.2, it is clear that VP shows the highest complexity. The computational cost of BD, RBD, and MMSE-THP in [64] is relatively high compared to the proposed MB-MMSE-THP algorithms due to multiple SVD or matrix inversion operations are implemented. Moreover, the proposed MB-MMSE-THP with $L_B = 2$ and $L_B = 4$ branches have a complexity that is slightly higher than the ZF-THP, MMSE, and MMSE-THP algorithms especially when the system dimension is below 10.

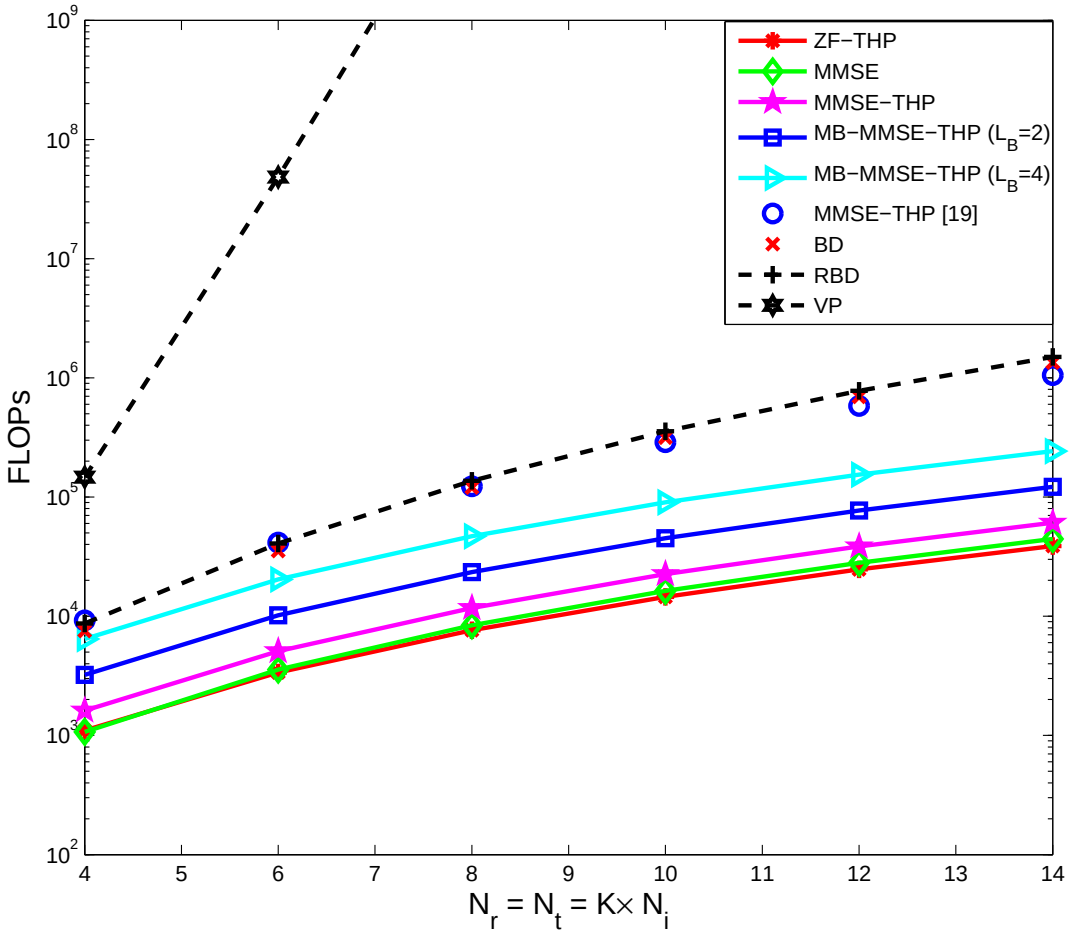

Figure 5.2: Complexity Analysis

Table 5.2: Comparison of the complexity

Algorithm	FLOPs	Case $(2,2,2)\times 6$
ZF	$16n^3+3n^2-2n$	3552
MMSE	$16n^3+3n^2$	3564
BD	$K(72n_i^3+72n_i^2n+32n_in^2$ $-2n_i^2+32n\bar{n}_i^2+64\bar{n}_i^3)$	35304
RBD	$K(72n_i^3+72n_i^2n+32n_in^2-2n_i^2$ $+8n^3+18n+\bar{n}_i+32n\bar{n}_i^2+64\bar{n}_i^3)$	40824
ZF-THP	$\frac{40}{3}n^3+10n^2+22n$	3372
MMSE-THP [64]	$24n^4+48n^3+n^2$	41508
MMSE-THP	$\frac{64}{3}n^3+10n^2+22n$	5100
MB-ZF-THP	$L_B(\frac{40}{3}n^3+10n^2+22n)$	6744
MB-MMSE-THP	$L_B(\frac{64}{3}n^3+10n^2+22n)$	10200
ZF-VP/MMSE-VP [26, 27]	$8\sum_{k=1}^{n}\frac{Mk\pi^{\frac{k}{2}}}{\Gamma(k/2+1)}d^k$ $+16n^2-2n+4$	$4.8\cdot 10^7$

5.5 Simulation Results

In this section, we assess the performance of the proposed MB-THP algorithms. A system with $N_t=8$ transmit antennas and $K=4$ users each equipped with $N_i=2$ receive antennas is considered; this scenario is denoted as the $(2,2,2,2)\times 8$ case. The quantity E_b/N_0 is defined as $E_b/N_0=\frac{N_rE_s}{N_tN\sigma_n^2}$ with N being the number of information bits

transmitted per channel symbol. Uncoded QPSK and 16-QAM modulation schemes are employed in the simulations. The channel matrix $\boldsymbol{H}$ is assumed to be a complex i.i.d. Gaussian matrix with zero mean and unit variance. The number of branches employed for MB-MMSE-THP is $L_B = 2, 4, 6, 8$, respectively. The number of simulation trials is 10^6 and the packet length is 10^2 symbols.

5.5.1 Perfect Channel State Information Scenario

As illustrated in Figure 5.3, the BER performance of the BD and RBD precoding algorithms is worse than that of the THP algorithms. For the THP algorithms, a better BER performance is offered by ZF-dTHP over ZF-cTHP, and a much better BER performance is achieved by MMSE-cTHP than MMSE-dTHP, which verifies the analysis developed in Section IV.

The comparison among nonlinear precoding algorithms with 16-QAM is displayed in Figure 5.4. The same phenomenon is also observed for the two types of THP with 16-QAM. A slightly better BER performance is offered by ZF-dTHP over ZF-cTHP, whereas, the situation is reversed for MMSE-THP. The THP with successive BD implementation (SO-THP) algorithm in [117] shows a slightly better performance than ZF-cTHP at low E_b/N_0s, however, its performance is almost the same as ZF-dTHP and ZF-cTHP at high E_b/N_0s. The maximum transmit diversity order is achieved by ZF-VP and MMSE-VP algorithms.

The BER performance of the proposed MB-MMSE-cTHP with 16-QAM and QPSK are shown in Figure 5.5 and Figure 5.6, respectively. From Figure 5.5, the proposed MB-MMSE-cTHP with $L_B = 2, 4, 8$ branches has a gain of more than 2 dB, 3 dB, and 3.4 dB as compared to the conventional MMSE-cTHP and the performance gap between MB-MMSE-cTHP with $L_B = 4$ and MMSE-VP is only 2 dB at the BER of 10^{-3}. For the QPSK modulation in Figure 5.6, the BER performance of MB-MMSE-cTHP with $L_B = 4$ is better than MMSE-VP at low E_b/N_0s and is very close to that of MMSE-VP at the BER of 10^{-3} but requires a much lower computational complexity.

Figure 5.7 displays the BER performance of the proposed MB-MMSE-dTHP algorithms. For the proposed MB-MMSE-dTHP with $L = 2, 4, 8$ branches, there is a gain of more

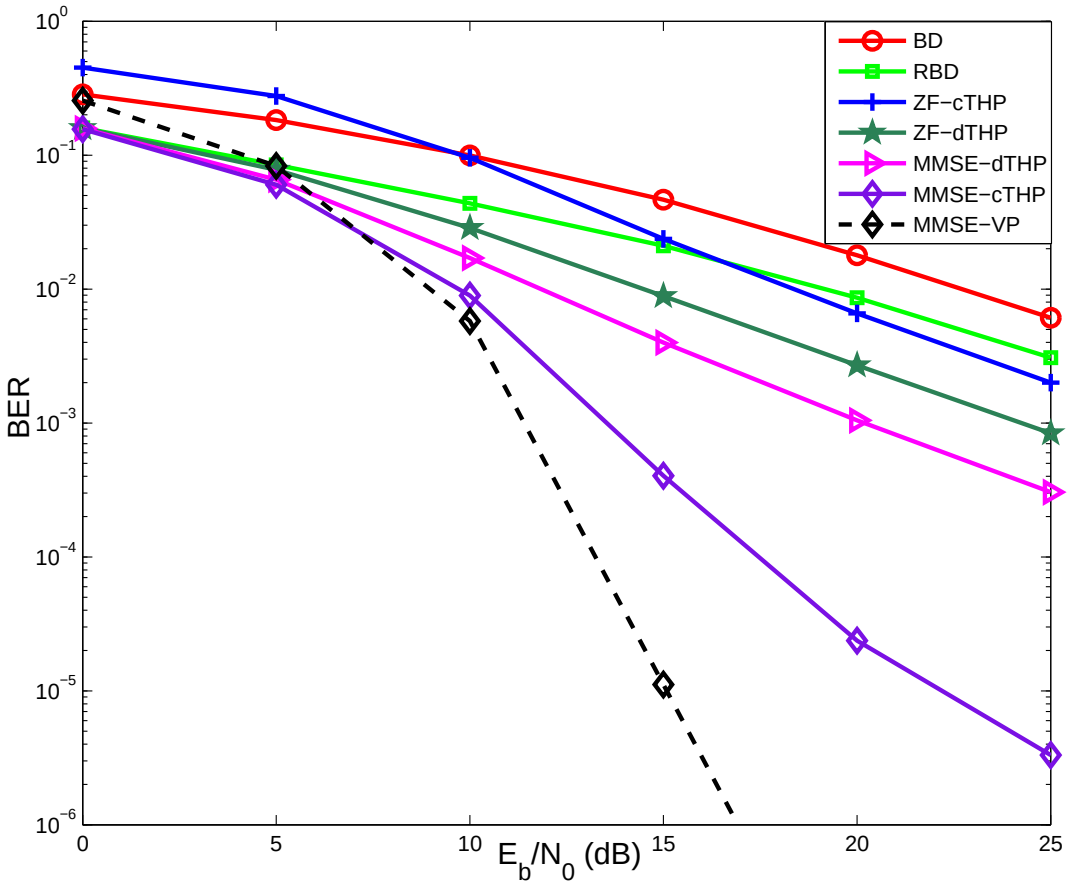

Figure 5.3: BER performance of THP, QPSK.

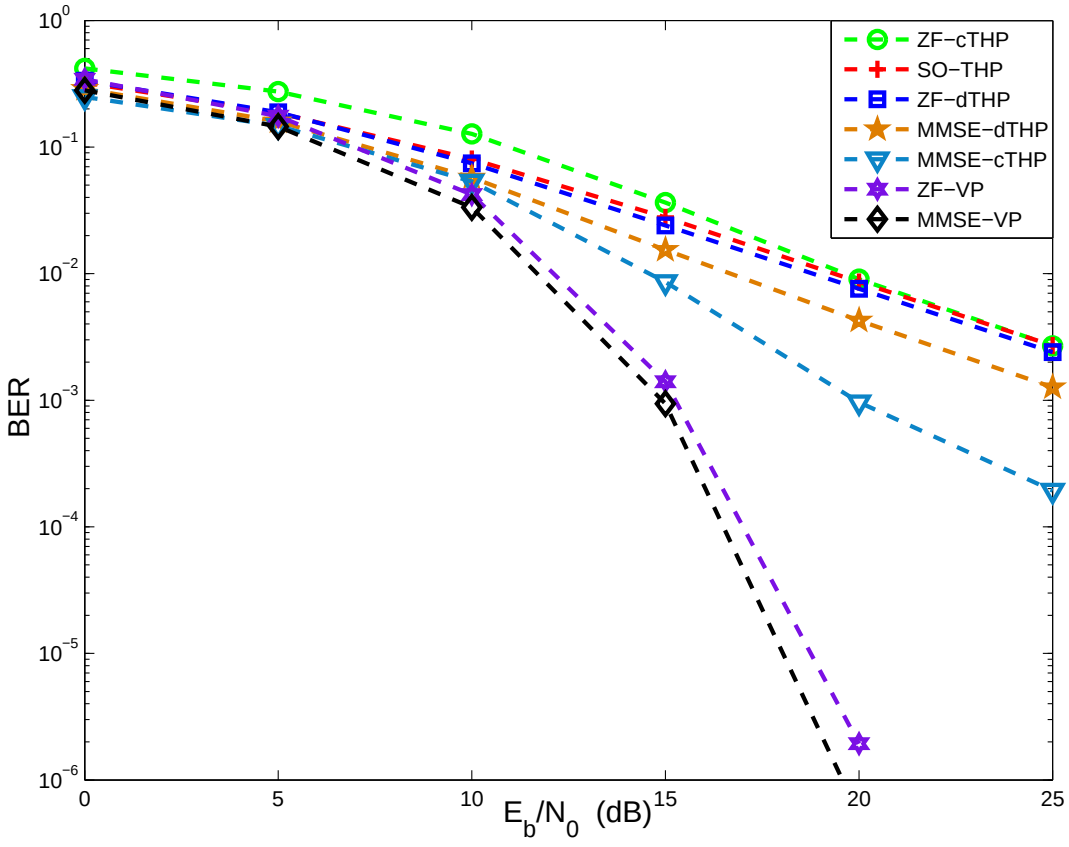

Figure 5.4: BER performance of THP, 16-QAM.

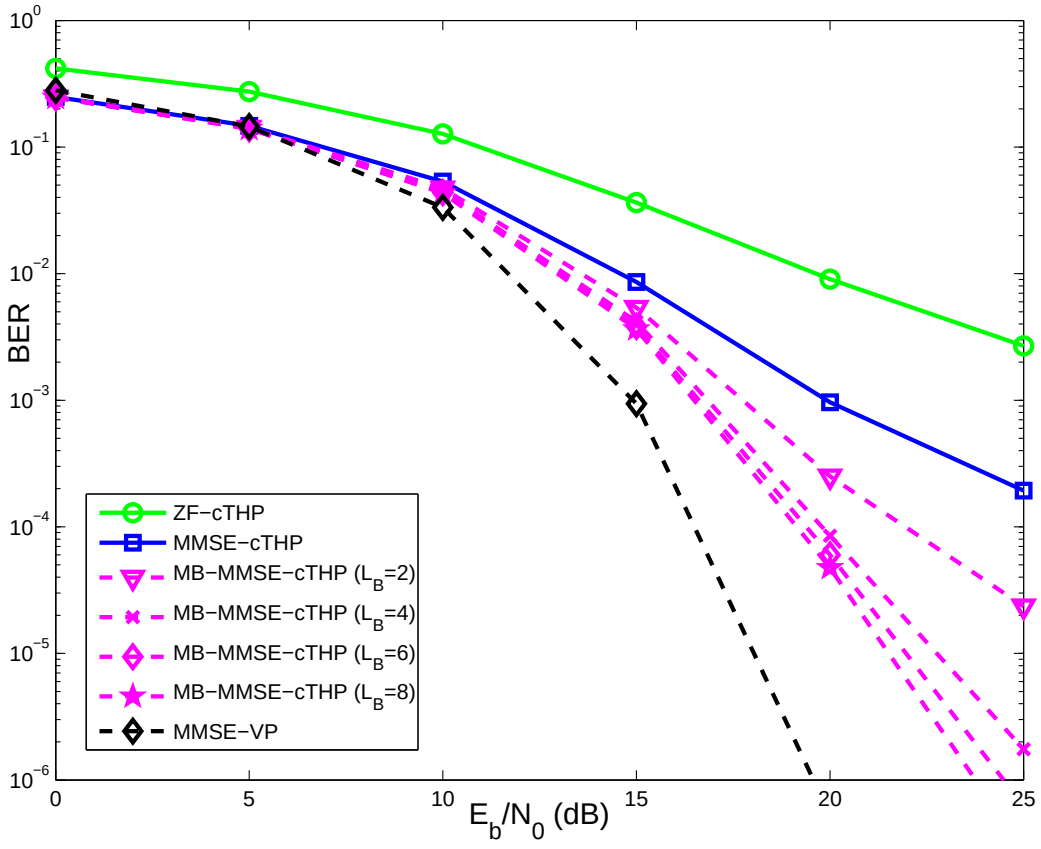

Figure 5.5: BER performance of cTHP, 16-QAM.

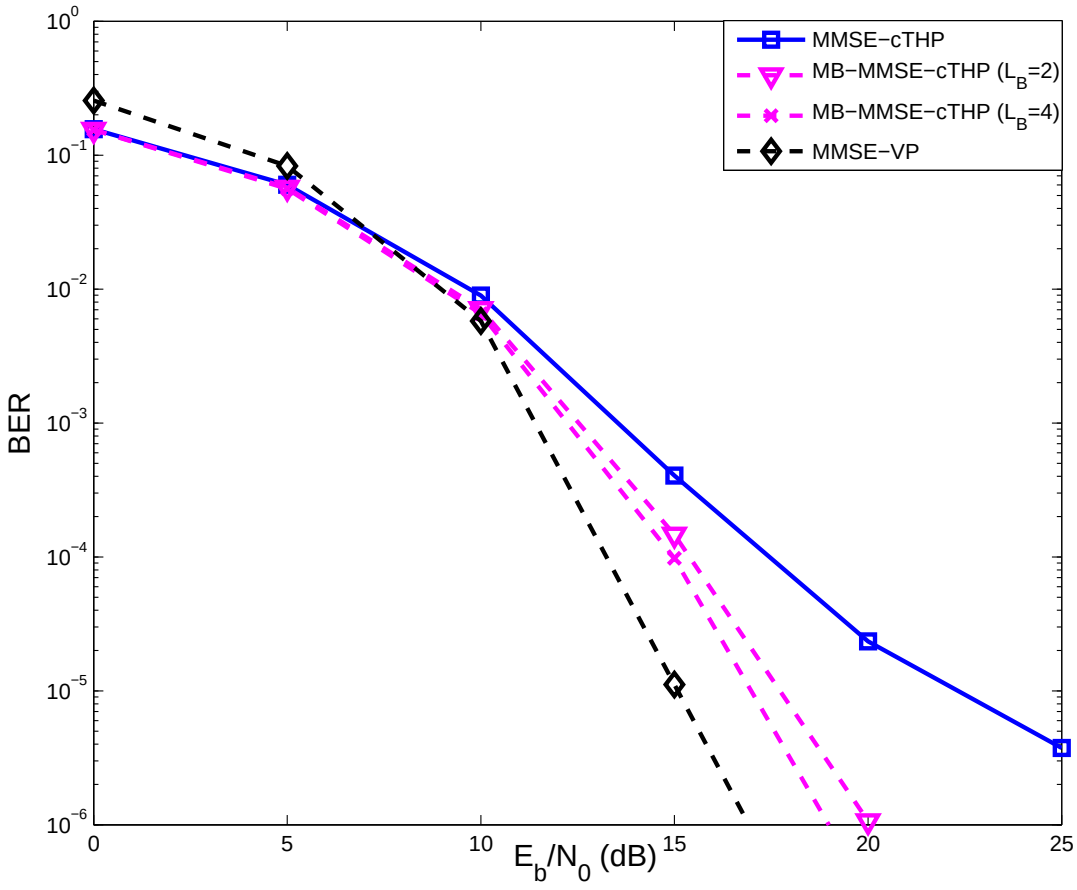

Figure 5.6: BER performance of cTHP, QPSK.

than 3.6 dB, 6 dB, and 7 dB as compared to the conventional MMSE-dTHP at BER 10^{-3}, respectively. It is worth noting that for both MB-MMSE-dTHP and MB-MMSE-cTHP with only 2 branches, there is a considerable performance improvement and their BER performances with 4 branches can approach the one with 8 branches. Especially for MB-MMSE-cTHP, its BER performance with only 4 branches is not far from MMSE-VP with fixed computational complexity.

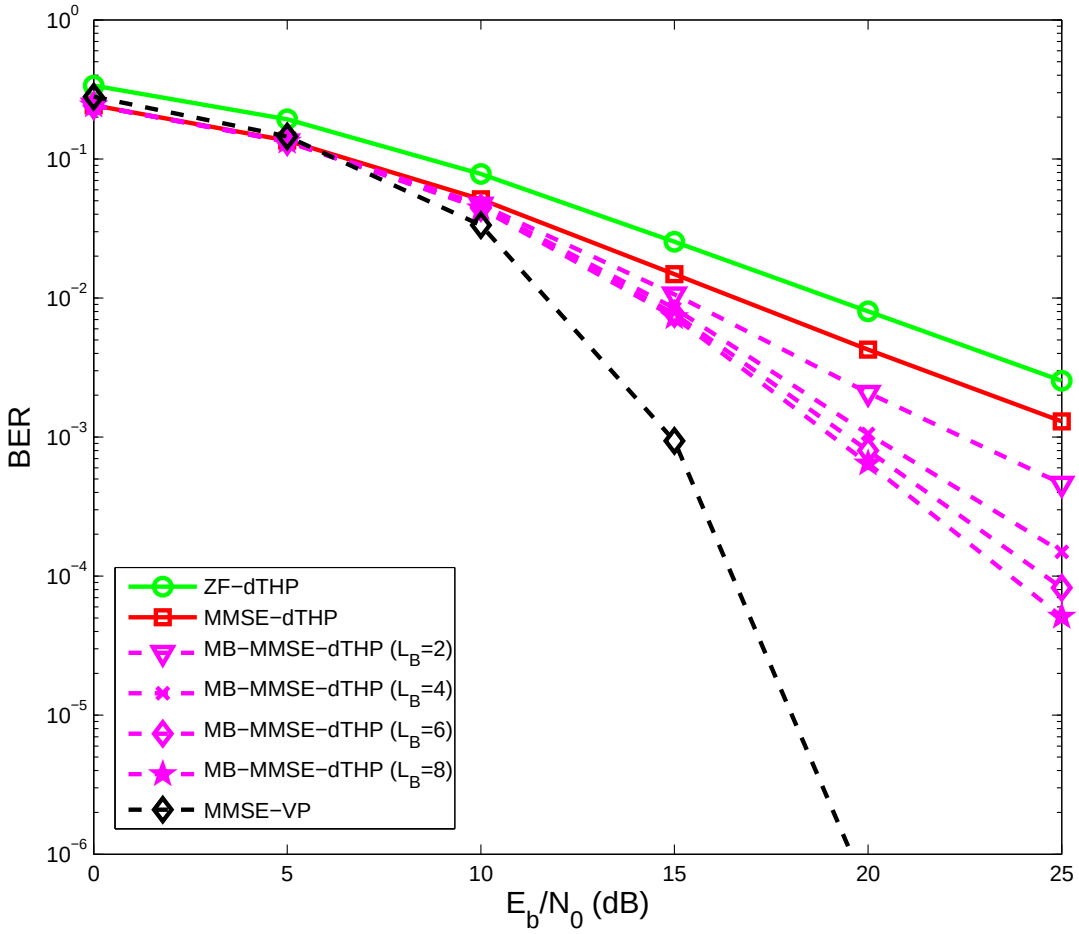

Figure 5.7: BER performance of MB-dTHP, QPSK.

Figure 5.8 and Figure 5.9 display the sum-rate performance of the proposed MB-MMSE-cTHP and MB-MMSE-dTHP algorithms, respectively. From Figure 5.8 , we can find that the sum-rate of MB-MMSE-cTHP is improved with the increase of L_B. When L_B is increased to 4, it can achieve almost the same sum-rate performance as with 8 branches.

The SO-THP in [117] has shown a better sum-rate performance than MB-MMSE-cTHP algorithms for high values of E_b/N_0. For MB-MMSE-dTHP, however, they share almost the same sum-rate performance with different branches. This phenomenon confirms the analysis developed in Section 5.4.2. Another interesting phenomenon can be observed by comparing these two figures is that the sum-rate performance of MB-MMSE-cTHP is better than MB-MMSE-dTHP at low values of E_b/N_0, while MB-MMSE-dTHP offers a very good performance at high values of E_b/N_0.

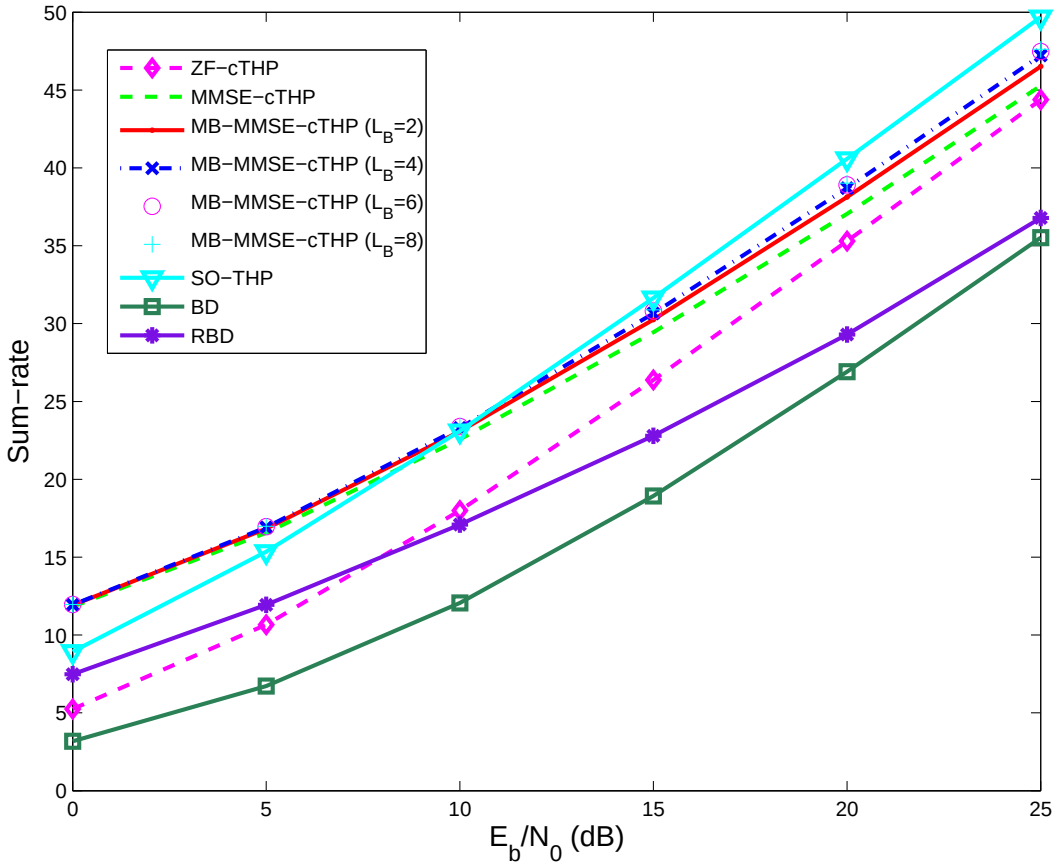

Figure 5.8: Sum-rate performance of MB-cTHP.

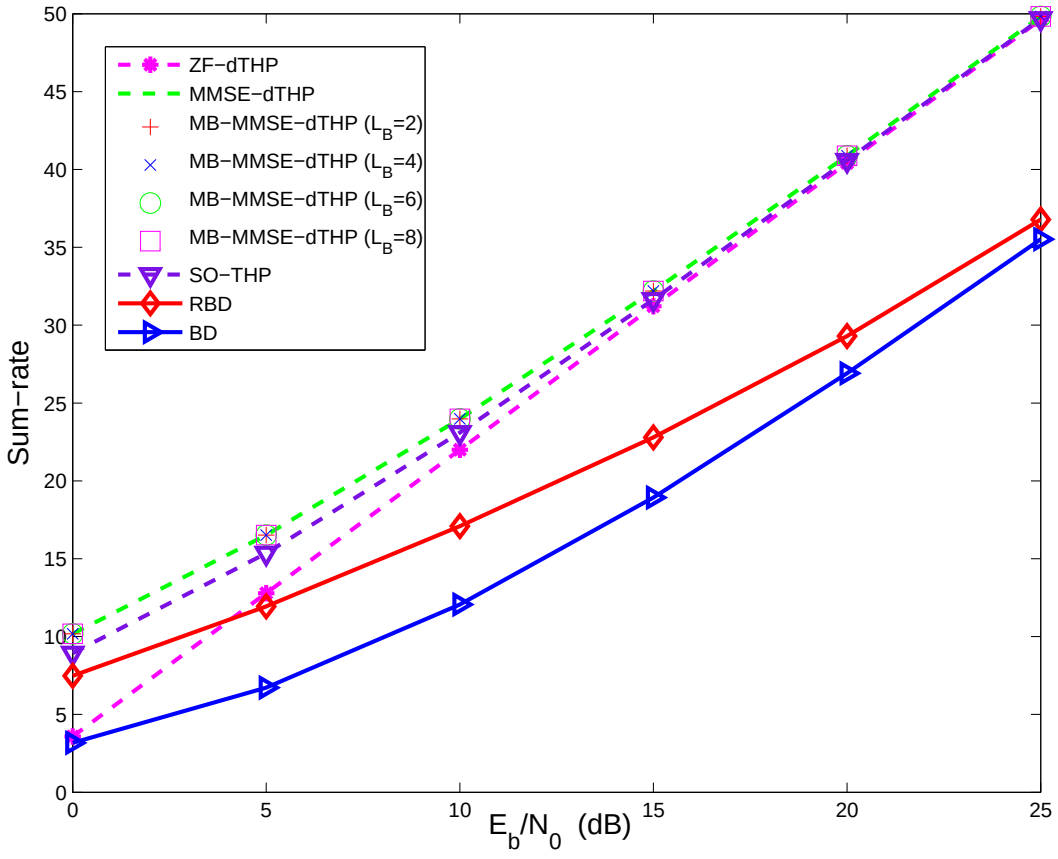

Figure 5.9: Sum-rate performance of MB-dTHP.

5.5.2 Correlated Channel State Information Scenario

In the following Figure 5.10 and Figure 5.11, we examine the performance of the proposed MB-MMSE-THP algorithms with correlation coefficient $|r| = 0.2$. The simulation results show that with the spatial correlation, the proposed MB-MMSE-THP algorithms still offer a better performance compared to their conventional counterparts.

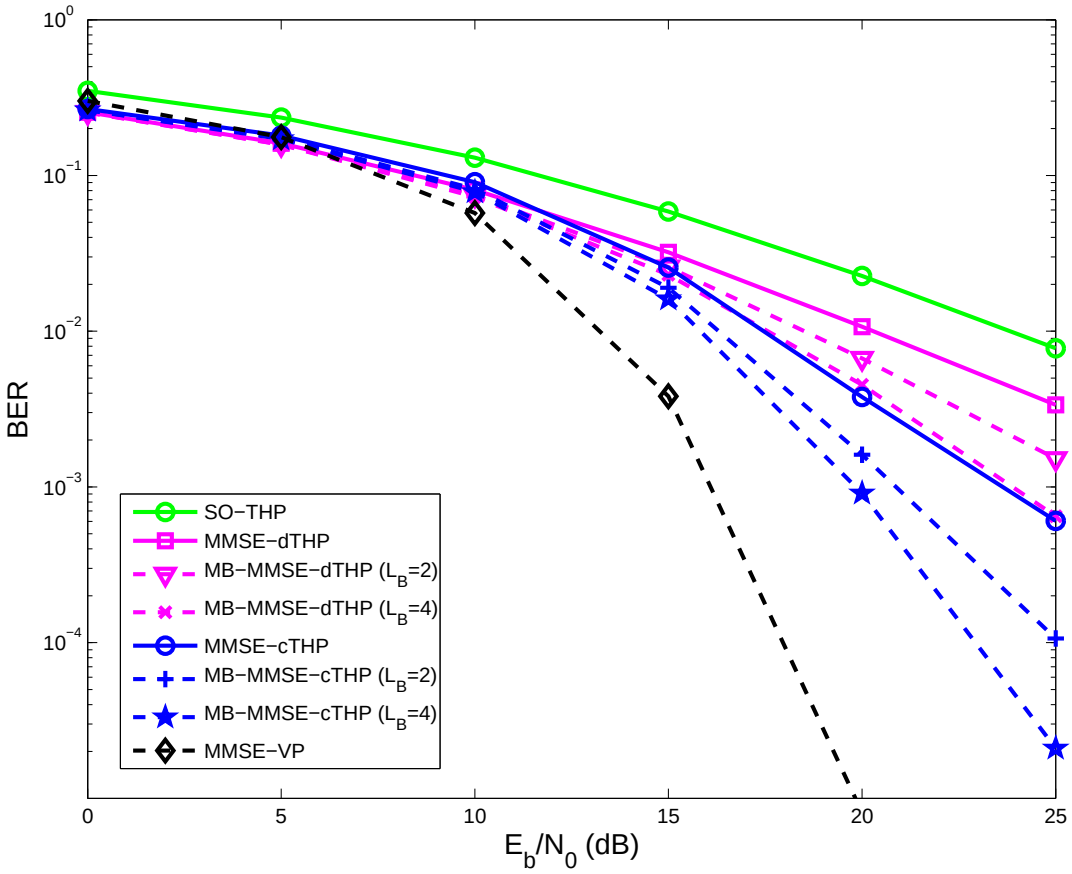

Figure 5.10: BER with spatial correlation.

5.5.3 The impact of imperfect channels

Figure 5.12 illustrates the BER performance of the above precoding algorithms with imperfect CSI at $E_b/N_0 = 20$ dB. The BER performance gets worse for all the precoding

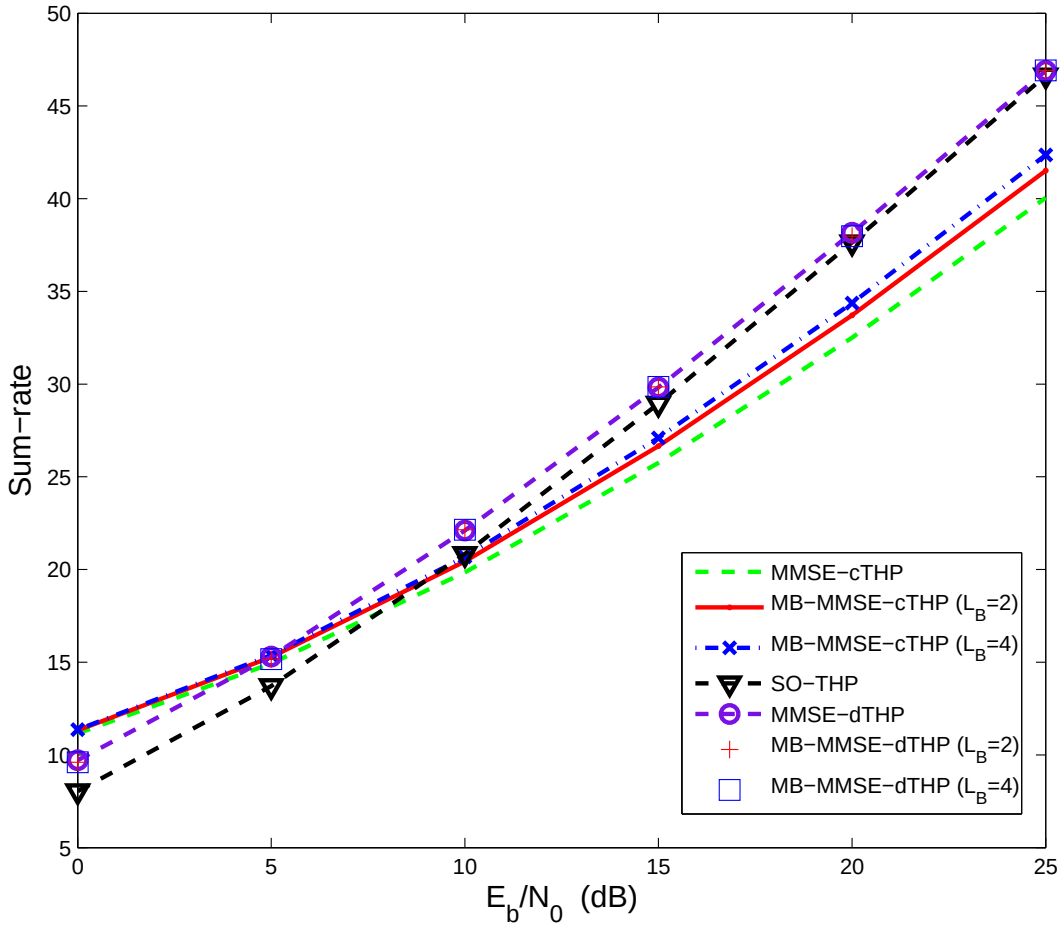

Figure 5.11: Sum-rate with spatial correlation.

algorithms with the increase of σ_e^2. The performance advantage of the proposed MB-MMSE-THP algorithms are not changed at low values of σ_e^2, while the performance of all the precoding algorithms in Figure 5.12 degrades to approximately the same level of BER at higher values of σ_e^2.

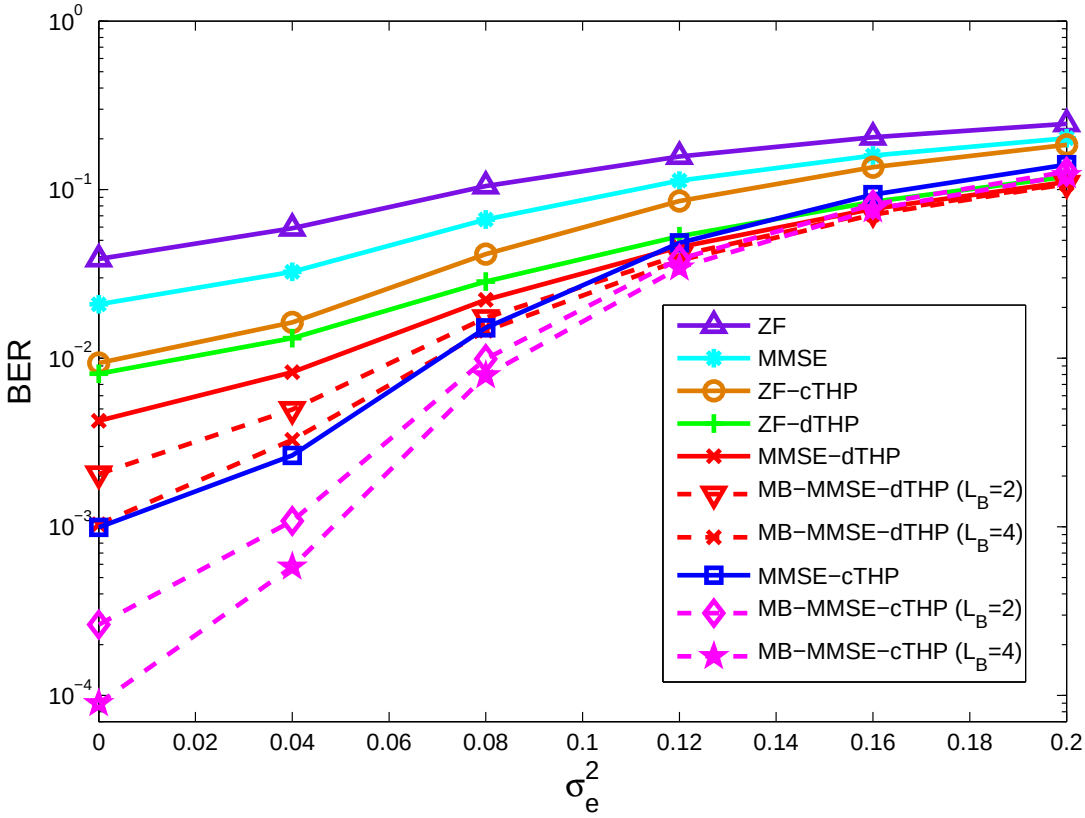

Figure 5.12: BER with σ_e^2 for a fixed E_b/N_0, 16-QAM

It is worth noting that the MMSE-cTHP loses its BER performance advantage to MMSE-dTHP from $\sigma_e^2 = 0.14$, which illustrates the cTHP structure is more sensitive to the impact of imperfect channel. Therefore, more feedback bits are needed by the cTHP than dTHP in realistic systems. A robust optimization of THP based on mean-squared-error (MSE) has been developed in [75] to alleviate the impact of CSI errors, while we leave the robust optimizations under the MB-cTHP and MB-dTHP framework as a future extension.

Although less feedback information required for the dTHP in practice, the corresponding scaling matrix needs to be informed to each distributed receiver, which requires an extra

control overhead or additional feedforward information. Since feedback issue is not the main focus of this work, we leave it for further research.

For the MB-MMSE-cTHP and MB-MMSE-dTHP, we have found that

- A better BER performance is obtained by MB-MMSE-cTHP compared to MB-MMSE-dTHP.
- MB-MMSE-dTHP can lead to a larger system sum-rate and more flexible sub-channel management, while the sum-rate of MB-MMSE-cTHP can be improved with the increase of the number of branches.
- MB-MMSE-cTHP is more sensitive to CSI than MB-MMSE-dTHP but a simplified receiver structure for MB-MMSE-cTHP has been proposed here.

5.6 Summary

In this Chapter, MB-MMSE-cTHP and MB-MMSE-dTHP algorithms have been proposed for MU-MIMO systems with multiple receive antennas. The proposed MB-MMSE-THP algorithms increase the degrees of freedom for transmission by constructing a list of branches, which results in extra transmit diversity gains. Moreover, the required computational complexity is still reasonable since the filters of MB-MMSE-THP are derived based on an LQ decomposition. A comprehensive performance analysis has been carried out and a wide range of comparisons have been conducted with the existing precoding algorithms, including the BD, RBD, THP, SO-THP, and VP algorithms. The simulation results have illustrated that a considerable improvement is achieved with only 2 or 4 branches, which reveals the value of the proposed MB-MMSE-THP algorithms for practical applications.

Chapter 6

Conclusions and Future Work

Contents

This thesis has described wireless techniques following a system perspective and has proposed novel precoding algorithms that can offer an improved performance while requiring a lower complexity than existing methods. This final Chapter summarizes the contributions of the thesis and outlines some directions for future work. Conventionally, for the algorithm design, there is always a dilemma between performance and computational complexity. In order to achieve an optimal performance a design often requires a higher computational complexity, whilst if the goal is an easy implementation and efficiency this is inevitably associated with a loss in performance. In this thesis, we have explored the art of novel efficient precoding algorithms with a comparable performance as the optimal one but which require much less computational complexity. In what follows, a summary of contributions is given along with a brief discussion on possibilities for future work.

6.1 Summary of Contributions

1. A low-complexity precoding algorithm (LC-RBD-LR) based on multiple LQ decompositions and lattice reduction is developed in Chapter 3. The two SVD operations and the decoding matrix for each user in the conventional RBD precoding algorithm are no longer required in the proposed LC-RBD-LR type algorithms. Therefore, the computational complexity is reduced considerably (more than half) as compared to that of the conventional RBD precoding, while almost the same sum-rate performance as RBD and substantial BER performance gains are achieved by the proposed LC-RBD-LR type algorithms.

2. Another class of low-complexity precoding algorithms (LR-S-GMI) based on one channel inversion, QR decompositions and lattice reductions are derived in Chapter 4. Based on this channel inversion scheme, the multiple LQ decompositions in LC-RBD-LR are avoided. The reduction of computational complexity by the proposed LR-S-GMI-MMSE algorithm is more than 70% and 50% as compared to the RBD and LC-RBD-LR precoding algorithms, respectively. In addition, a comparable sum-rate performance as BD-type precoding algorithms and a considerable BER performance improvement are obtained by the proposed LR-S-GMI type precoding algorithms. By implementing the proposed LC-RBD-LR and LR-S-GMI type precoding algorithms solely at the transmit side, not only the receiver structure is simplified but also it becomes easier to implement these techniques in practical MU-MIMO systems because the decoding matrices of each user required by the BD-type precoding algorithms are not needed anymore.

3. The performance of THP strongly depends on the ordering of the precoded symbols, however, most of the ordering schemes in the literature are applied to SU-MIMO systems or simply assume that each user is equipped with a single receive antenna. In addition, there are two basic THP structures according to the positions of the diagonal weighted filter, decentralized filters located at the receivers or centralized filters deployed at the transmitter, which are denoted as dTHP or cTHP, respectively. In Chapter 5, novel MB-THP algorithms are developed based on these two structures for MU-MIMO and especially for situations in which the receiver is equipped

with multiple antennas, which fills an important gap in the literature since most of the previous research works on THP have only focused on one of the structures. A comprehensive analysis is carried out in terms of the error covariance matrix, the sum-rate and the computational complexity to illustrate the performance of MB-THP algorithms. The results of simulations indicate that with only 2 or 4 branches, the MB-THP algorithm can achieve a comparable performance with that of VP.

6.2 Future Work

Based on the contributions of this thesis, some suggestions for future work are given in the following:

1. According to Chapter 2 it is not difficult to find that, the wireless MIMO channel models we assumed in the following Chapters are flat fading channels. The fast fading channel based precoding techniques have not been addressed in this thesis. In order to make this research work more valuable, the more complicated fast fading channel situations should be considered.

2. The imperfect channel scenarios with correlation and feedback errors are simulated in Chapter 3, Chapter 4, and Chapter 5. The proposed LC-RBD-LR, LR-S-GMI, and MB-THP precoding algorithms suffer a performance loss under the imperfect channel environment. Therefore, robust designs of the proposed algorithms worth our further researching work to improve the performance in the context of imperfect CSI.

3. The low-complexity precoding algorithms proposed in this thesis are derived for MIMO systems with the dimensions that include antenna array with less than 20 antenna elements. Basically, the more antennas the transmitter/receiver is equipped with, and the more degrees of freedom that the propagation channel can provide, the better the performance in terms of data rate or link reliability can be achieved [24]. Currently, the concept of *massive MIMO* or *large MIMO* is drawing considerable interest in the research community because of the potential to improve data rates dramatically and to scale down transmit power drastically. The number of antennas

considered in the large MIMO is usually hundreds or more, which is much more than the system configurations we discussed in this thesis. Problems like a pilot contamination produced by the massive number of antennas will require designers to develop low-complexity and high-performance precoding algorithms for large MIMO systems. This is a very challenging topic that will keep researchers busy in the future.

4. The MIMO technique has become more and more mature, and the research focus on MIMO systems has moved from the MU-MIMO to the multi-cell system, network MIMO, MIMO systems with relays, etc. As we revealed in this thesis, the MU-MIMO scenario is so different from the SU-MIMO scenario (due to the fact that multiple users are geographically distributed) that we have to derive different algorithms or strategies to deal with the specific challenges. The same principle applies to these new scenarios. New design approaches or specific precoding algorithms need to be developed for these new systems.

Some other interesting topics are also worth further studying, for example scheduling, channel estimation, since these strategies are highly relevant to the core research topics of this thesis.

Bibliography

[1] David. G, *Introduction to electrodynamics*, Prentice Hall, third edition, 1999.

[2] A. Paulraj, R. Nabar, and D. Gore, *Introduction to space-time wireless communications*, Cambridge University Press, 2003.

[3] Cisco and/or its affiliates, "Cisco Visual Networking Index: Global Mobile Data Traffic Forecast Update, 20122017", Tech. Rep., Cisco Systems, Inc., January 2013.

[4] C. Lim, T. Yoo, B. Clerckx, and B. Lee, "Recent trend of multiuser MIMO in LTE-Advanced", *IEEE Communications Magazine*, pp. 127–135, March 2013.

[5] J. Hoydis, M. Kobayashi, and M. Debbah, "Green small-cell networks", *IEEE Vehicular Technology Magazine*, pp. 37–43, March 2011.

[6] H. Yanikomeroglu, "The building blocks of the 5th generation (5G) wireless networks for affordable and ubiquitous", Tech. Rep., BCWS Seminar Series, Carleton University, 2011.

[7] L. Thiele, M. Kurras, M. Olbrich, and T. Haustein, "Boosting 4G networks with spatial interference management under feedback constraints: a noncooperative downlink transmission scheme", *IEEE Vehicular Technology Magazine*, pp. 40–48, March 2013.

[8] NTT DOCOMO, "DOCOMO and Tokyo Institute of Technology Achieve World's First 10 Gbps Packet Transmission in Outdoor Experiment", www.nttdocomo.co.jp/english, 2013.

[9] B. Sklar, *Digital communications: fundamentals and applications*, Prentice Hall PTR, 2nd edition, 2002.

[10] J. G. Proakis and M. Salehi, *Digital Communications*, McGraw-Hill, 5th edition, 2007.

[11] IEEE Standards Association, "IEEE 802.11n-2009 Amendment 5: Enhancements for Higher Throughput", Tech. Rep., Institute of Electrical and Electronics Engineers (IEEE), January 2011.

[12] Working Group on Broadband Wireless Access Standards, "Air Interface for Fixed and Mobile Broadband Wireless Access System", Tech. Rep., Institute of Electrical and Electronics Engineers (IEEE), January 2011.

[13] Institute of Electrical and Electronics Engineers (IEEE), "Wireless LAN medium access control (MAC) and physical layer (PHY) specifications: enhancements for very high throughput for operation in bands below 6GHz", Tech. Rep., IEEE P802.11ac/D1.0 Standard, January 2011.

[14] 3GPP, "TR 36.913 Requirements for further advancements for E-UTRA (LTE-Advanced)", Tech. Rep., 3GPP, 2011.

[15] N. Jindal, S. Vishwanath, and A. Goldsmith, "On the duality of Gaussian multiple-access and broadcast channels", *IEEE Transactions on Information Theory*, vol. 50, no. 5, pp. 768–783, May 2004.

[16] J. Winters, "On the capacity of radio communication systems with diversity in a Rayleigh fading environment", *IEEE Journal on Selected Areas in Communications*, vol. 5, no. 5, pp. 871–878, June 1987.

[17] A. Goldsmith, S. Jafar, N. Jindal, and S. Vishwanath, "Capacity limits of MIMO channels", *IEEE Journal on Selected Areas in Communications*, vol. 21, no. 5, pp. 684–702, June 2003.

[18] M. Costa, "Writing on dirty paper", *IEEE Transaction on Information Theory*, vol. 29, no. 3, pp. 439–441, May 1983.

[19] A. Kurve, "Multi-user MIMO systems: The future in the making", *IEEE Potentials*, pp. 2–6, December 2009.

[20] C. Windpassinger, *Detection and precoding for multiple input multiple output channels*, PhD thesis, University Erlangen-Nurnberg, Germany, 2004.

[21] L. Liu, R. Chen, S. Geirhofer, K. Sayana, Z. Shi, and Y. Zhou, "Downlink MIMO in LTE-Advanced: SU-MIMO vs. MU-MIMO", *IEEE Communications Letters*, vol. 50, no. 2, pp. 140–147, Feburary 2012.

[22] D. Tse and P. Viswanath, *Fundamentals of wireless communications*, Cambridge University Press, 2005.

[23] C. Chiu, J. Yan, and R. Murch, "24-Port and 36-Port antenna cubes suitable for MIMO wireless communications", *IEEE Transaction on Antennas and Propagation*, vol. 56, no. 4, pp. 1170–1176, April 2008.

[24] F. Rusek, D. Persson, B. Lau, E. Larsson, T. Marzetta, O. Edfors, and F. Tufvesson, "Scaling up MIMO: opportunities and challenges with very large arrays", *IEEE Signal Processing Magazine*, vol. 30, no. 1, pp. 40–60, January 2013.

[25] A. Khina and U. Erez, "On the Robustness of Dirty Paper Coding", *IEEE Transactions on Communications*, vol. 58, no. 5, pp. 1437–1446, May 2010.

[26] B. M. Hochwald, C. B. Peel, and A. L. Swindlehurst, "A vector-perturbation technique for near capacity multiantenna multiuser communication - Part II: Perturbation", *IEEE Transaction on Communications*, vol. 53, no. 3, pp. 537–544, March 2005.

[27] B. Hassibi and H. Vikalo, "On the sphere decoding algorithm: Part I the expected complexity", *IEEE Transaction on Signal Processing*, vol. 53, no. 8, pp. 2806–2818, August 2005.

[28] H. Vikalo and B. Hassibi, "On the sphere decoding algorithm: Part II generalizations, second-order statistics, and applications to communications", *IEEE Transaction on Signal Processing*, vol. 53, no. 8, pp. 2819–2834, August 2005.

[29] Q. H. Spencer, A. L. Swindlehurst, and M. Haardt, "Zero-forcing methods for downlink spatial multiplexing in multiuser MIMO channels", *IEEE Communicaitons Magazine*, vol. 52, no. 2, pp. 461–471, February 2004.

[30] L. U. Choi and R. D. Murch, "A transmit preprocessing technique for multiuser MIMO systems using a decomposition approach", *IEEE Transactions on Wireless Communications*, vol. 3, no. 1, pp. 20–24, January 2004.

[31] G. J. Foschini, "Layered space-time architecture for wireless communication in a fading environment when using multi-element antennas", *Bell Labs Technical Journal*, vol. 1, no. 2, pp. 41–59, Autumn 1996.

[32] E. Telatar, "Capacity of multi-antenna Gaussian channels", *European Transaction Telecommunications*, vol. 10, no. 6, pp. 585–595, Novermber 1999.

[33] S. M. Alamouti, "A simple transmitter diversity technique for wireless communications", *IEEE Journal on Selected Areas in Communications*, vol. 16, no. 8, pp. 141–1458, October 1998.

[34] V. Tarokh, H. Jafarkhani, and A. R. Calderbank, "Space-time block coding for wireless communications: performance results", *IEEE Journal on Selected Areas in Communications*, vol. 17, no. 3, pp. 451–460, March 1999.

[35] P. W. Wolniansky, G. J. Foschini, G. D. Golden, and R. A. Valenzuela, "V-BLAST: Architecture for realizing very high data rates over the rich-scattering wireless channel", in *Proceedings of URSI International Symposium on Signals, Systems and Electronics*, September 1998, pp. 295–300.

[36] D. N. C. Tse and L. Zheng, "Diversity and multiplexing: a fundamental trade-off in multiple antenna channels", *IEEE Transactions on Information Theory*, vol. 49, no. 5, pp. 1073–1096, May 2003.

[37] W. Jakes, "Diversity Techniques", in *Microwave Mobile Communications*. Wiley-IEEE Press, 1974.

[38] Y. Okumura, E. Ohmuri, T. Kawano, and K. Fukuda, "Field strength and its variability in VHF and UHF land mobile radio service", *Rev. ECL*, vol. 16, pp. 825–873, 1968.

[39] M. Hata and T. Nagatsu, "Mobile location using signal strength measurements in cellular systems", *IEEE Transaction on Vehicular Technology*, vol. 29, no. 2, pp. 245–251, 1980.

[40] COST-231 TD(973) 119-REV 2 (WG2), "Urban transmission loss models for mobile radio in 900- and 1800-MHz bands", Tech. Rep., September 1991.

[41] V. Erceg, L. Greenstein, S. Tjandra, S. Parkoff, A. Gupta, B. Kulic, A. Julius, and R. Bianchi, "An empirically based path loss model for wireless channels in suburban environments", *IEEE Journal on Selected Areas in Communications*, vol. 17, no. 7, pp. 1205–1211, 1999.

[42] M. Nakagami, "The m distribution: a general formula of intensity distribution of rapid fading", in *Statistical Methods in Radio Wave Propagation*, pp. 3–36. Pergamon Press, 1960.

[43] 3GPP, "TR 25.996 V10.0 Spatial channel model for Multiple Input Multiple Output (MIMO) simulations", Tech. Rep., 3GPP, 2011.

[44] J. Kermoal, L. Schumacher, K. Pedersen, P. Mogensen, and F. Frederiksen, "A stochastic MIMO radio channel model with experimental validation", *IEEE Journal on Selected Areas in Communications*, vol. 20, no. 8, pp. 1211–1226, 2002.

[45] M. T. Ivrlac, W. Utschick, and J. A. Nossek, "Fading correlations in wireless MIMO communicaitons systems", *IEEE Journal of Selected Areas in Communications*, vol. 21, no. 5, pp. 819–828, June 2003.

[46] S. L. Loyka, "Channel capacity of MIMO architecture using the exponential correlation matrix", *IEEE Communications Letters*, vol. 5, no. 9, pp. 369–371, September 2001.

[47] S. Sandhu and A. Paulaj, "Space-time block codes: A capacity perspective", *IEEE Communicaitons Letters*, vol. 4, no. 12, pp. 384–386, December 2000.

[48] Emre Telatar, *Capacity and mutual information of wideband multipath fading channels*, Electronics Research Laboratory, University of California, 1999.

[49] T. Cover and J. Thomas, *Elements of Information Theory*, Wiley, 1991.

[50] C. Chuah, D. Tse, J. Kahn, and R. Valenzuela, "Capacity scaling in MIMO wireless systems under correlated fading", *IEEE Transaction on Information Theory*, vol. 48, no. 3, pp. 637–650, March 2002.

[51] R. Ahlswede, "Multi-wav communication channels", in *IEEE International Symposium on Information Theory*, Tsaghkadsor, Armenian S.S.R., 1973, pp. 23–52.

[52] C. E. Shannon, "Two-way communication channels", in *Proceedings of Berkeley Symposium on Mathematical Statistics and Probability*, Berkeley, USA, 1961, pp. 611–644.

[53] H. Huang, C. B. Papadias, and S. Venkatesan, *MIMO communication for celluare networks*, Springer, 2012.

[54] H. Viswanathan, S. Venkatesan, and H. Huang, "Downlink capacity evaluation of cellular networks with known-interference cancellation", *IEEE Journal on Selected Areas in Communications*, vol. 51, no. 5, pp. 802–811, June 2003.

[55] G. Caire and S. Shamai, "On the achievable throughput of a multiantenna Gaussian broadcast channel", *IEEE Transaction on Information Theory*, vol. 43, no. 7, pp. 1691–1706, July 2003.

[56] P. Vishwanath and D. Tse, "Sum capacity of the vector Gaussian broadcast channel and uplink-downlink duality", *IEEE Transaction on Information Theory*, vol. 49, no. 8, pp. 1912–1921, August 2003.

[57] S. Vishwanath, N. Jindal, and A. Goldsmith, "Duality, achievable rates, and sum capacity of Gaussian MIMO broadcast channels", *IEEE Transaction on Information Theory*, vol. 49, no. 10, pp. 2658–2668, October 2003.

[58] F. Shayegh and M. R. Soleymani, "Low complexity implementations of sphere decoding for MIMO detection", in *Proceedings of Canadian Conference on Electrical and Computer Engineering*, Ontario, Canada, May 2008, pp. 821–826.

[59] H. Blcskei, D. Gesbert, C. B. Papadias, and A. J. van der Veen, *Space-time wireless systems: From array processing to MIMO communications*, Cambridge University Press, 2008.

[60] H. Vikalo, B. Hassibi, and T. Kailath, "Iterative decoding for MIMO channels via modified sphere decoding", *IEEE Transaction on Wireless Communications*, vol. 3, no. 6, pp. 2299–2311, November 2004.

[61] D. Wübben, R. Böhnke, V. Kühn, and K. Kammeyer, "MMSE extension of V-BLAST based on sorted QR decomposition", in *Proceedings of IEEE Vehicular Technology Conference(VTC)*, Orlando, USA,, October 2003, pp. 399–405.

[62] R. C. de Lamare, R. Sampaio-Neto, and A. Hjrungnes, "Joint iterative interference cancellation and parameter estimation for CDMA systems", *IEEE Communications Letters*, vol. 11, no. 12, pp. 916–918, December 2007.

[63] D. Wübben, J. Rinas, R. Böhnke, V. Kühn, and K. Kammeyer, "Efficient algorithm for detecting layered space-time codes", in *Proceedings of ITG Conference on Source and Channel Coding (SCC)*, Berlin, Germany, January 2002, pp. 399–405.

[64] M. Joham, W. Utschick, and J. A. Nossek, "Linear transmit processing in MIMO communications systems", *IEEE Transaction on Signal Processing*, vol. 53, no. 8, pp. 2700–2712, August 2005.

[65] C. B. Peel, B. M. Hochwald, and A. L. Swindlehurst, "A vector-perturbation technique for near capacity multiantenna multiuser communication - Part I: Channel inversion and regularization", *IEEE Transaction on Communications*, vol. 52, no. 1, pp. 195–202, January 2005.

[66] V. Stankovic and M. Haardt, "Generalized design of multi-user MIMO precoding matrices", *IEEE Transactions on Wireless Communications*, vol. 7, no. 3, pp. 953–961, March 2008.

[67] M. Tomlinson, "New automatic equaliser employing modulo arithmetic", *Electronic Letters*, vol. 7, no. 5, pp. 138–139, March 1971.

[68] H. Harashima and H. Miyakawa, "Matched-transmission technique for channels with intersymbol interference", *IEEE Transactions on Communications*, vol. 20, no. 4, pp. 774–780, August 1972.

[69] R. Fischer, C. Windpassinger, A. Lampe, and J. Huber, "Space-time transmission using Tomlinson-Harashima precoding", in *Proceedings of ITG Conference on Source and Channel Coding (SCC)*, Berlin, Germany, January 2002, pp. 139–147.

[70] W. Yu, D. Varodayan, and J. Cioffi, "Trellis and convolutional precoding for transmitter based interference presubtracion", *IEEE Transactions on Communications*, vol. 53, no. 7, pp. 1220–1230, July 2005.

[71] U. Erez, S. Shamai, and R. Zamir, "Capacity and lattice strategies for canceling known interference", *IEEE Transactions on Information Theory*, vol. 51, no. 11, pp. 3820–3833, November 2005.

[72] C. Windpassinger, R. Fischer, T. Vencel, and J. Huber, "Precoding in multiantenna and multiuser communications", *IEEE Transactions on Wireless Communications*, vol. 3, no. 4, pp. 1305–1306, July 2004.

[73] M. Huang, S. Zhou, and J. Wang, "Analysis of Tomlinson-Harashima precoding in multiuser MIMO systems with imperfect channel state information", *IEEE Transactions on Vehicular Technology*, vol. 57, no. 5, pp. 2856–2867, September 2008.

[74] D. Shiu and J. M. Kahn, "Layered space-time codes for wireless communications using multiple transmit antennas", in *Proceedings of IEEE International Conference on Communications (ICC)*, Vancouver, Canada, June 1999, pp. 436–440.

[75] F. Dietrich, P. Breun, and W. Utschick, "Robust Tomlinson-Harashima precoding for the wireless broadcast channel", *IEEE Transaction on Signal Processing*, vol. 55, no. 2, pp. 631–644, Feburary 2007.

[76] R. Müller, D. Guo, and A. L. Moustakas, "Vector precoding for wireless MIMO systems and its replica analysis", *IEEE Journal on Selected Area in Communications*, vol. 26, no. 3, pp. 530–540, April 2008.

[77] B. Hassibi and H. Vikalo, "On the expected complexity of integer least-squares problems", in *Proceedings of IEEE Acoustics, Speech, and Signal Processing (ICASSP)*, Orlando, USA, May 2002, pp. 1497–1500.

[78] M. Damen, H. Gamal, and G. Caire, "On maximum-likelihood detection and the search for the closest lattice point", *IEEE Transactions on Information Theory*, vol. 49, no. 10, pp. 2389–2402, October 2003.

[79] W. H. Mow, "Universal lattice decoding: a review and some recent results", in *Proceedings of IIEEE International Conference on Communications*, Paris, France, June 2004, pp. 2842–2846.

[80] D. A. Schmidt, M. Joham, and W. Utschick, "Minimum mean square error vector precoding", *European Transaction on Telecommunications*, vol. 19, no. 3, pp. 219–231, June 2008.

[81] D. J. Love, R. W. Heath, V. Lau, D. Gesbert, B. Rao, and M. Andrews, "An overview of limited feedback in wireless communication systems", *IEEE Journal on Selected Areas in Communications*, vol. 26, no. 8, pp. 1341–1365, October 2008.

[82] Y. H. Gan, C. Ling, and W. H. Mow, "Complex lattice reduction algorithm for low-complexity full-diversity MIMO detection", *IEEE Transaction on Signal Processing*, vol. 57, no. 7, pp. 2701–2710, July 2009.

[83] V. Lau, Y. Liu, and T. Chen, "On the design of MIMO blockfading channels with feedback-link capacity constraint", *IEEE Transaction on Communications*, vol. 52, no. 1, pp. 62–70, Janurary 2004.

[84] D. J. Love, R. W. Heath, and T. Strohmer, "Grassmannian beamforing for multiple-input multiple-output wireless systems", *IEEE Transaction on Information Theory*, vol. 49, no. 10, pp. 2735–2747, October 2003.

[85] W. Stantipach and M. L. Honig, "Asymptotic performance of MIMO wireless channels with limited feedback", in *IEEE Military Communications Conference*, Monterey, Canada, October 2003, pp. 141–146.

[86] D. J. Love, "Duplex distortion models for limited feedback MIMO communication", *IEEE Transaction on Signall Processing*, vol. 54, no. 2, pp. 766–774, Feburary 2006.

[87] A. Mukherjee and H. M. Kwon, "Sum-rate distortion in MIMO broadcast channels with irregular limited feedback", in *IEEE Global Telecommunications Conference*, Washington D. C, USA, November 2007, pp. 3205–3209.

[88] C. Steger and A. Sabharwal, "Two-way fading channels: Training protocol and diversity-multiplexing performance", in *IEEE Asilomar Conference on Signals, Systems, and Computers*, Asilomar, USA, November 2007, pp. 1941–1945.

[89] H. Yao and G. Wornell, "Lattice-reduction-aided detectors for MIMO communication systems", in *Proceedings of IEEE Globecom*, Taipei, Taiwan, November 2002, pp. 424–428.

[90] D. Wbben, R. Bhnke, V. Khn, and K. Kammeyer, "Near-maximum-likelihood detection of MIMO systems using MMSE-based lattice-reduction", in *Proceedings of IEEE International Conference on Communications (ICC)*, Paris, France, June 2004, pp. 798–802.

[91] C. Windpassinger and R. Fischer, "Low-complexity near-maximum likelihood detection and precoding for MIMO systems using lattice reduction", in *Proceedings of IEEE Information Theory Workshop*, Paris, France, March 2003, pp. 345–348.

[92] A. K. Lenstra, H. W. Lenstra, and L. Lovász, "Factoring polynomials with rational coefficients", *Math. Ann*, vol. 261, pp. 515–534, March 1982.

[93] A. Korkine and G. Zolotareff, "Sur les formes quadratiques", *Math. Annalen*, vol. 6, pp. 366–389, 1873.

[94] C. P. Schnorr and M. Euchner, "Lattice basis reduction: improved practical algorithms and solving subset sum problems", *Math Programming*, vol. 66, pp. 181–191, 1994.

[95] Y. H. Gan, C. Ling, and W. H. Mow, "Complex lattice reduction algorithm for low-complexity full-diversity MIMO detection", *IEEE Transaction on Signal Processing*, vol. 57, no. 7, pp. 2701–2710, July 2009.

[96] C. Windpassinger, R. Fischer, and J. Huber, "Lattice reduction aided broadcast precoding", *IEEE Transactions on Communications*, vol. 52, no. 12, pp. 2057–2060, December 2004.

[97] Y. Cai, R. C. de Lamare, and R. Fa, "Switched interleaving techniques with limited feedback for interference mitigation in DS-CDMA systems", *IEEE Transactions on Communications*, vol. 59, no. 7, July 2011.

[98] Y. Cai, R. C. De Lamare, and D. Le Ruyet, "Transmit Processing Techniques Based on Switched Interleaving and Limited Feedback for Interference Mitigation in Multiantenna MC-CDMA Systems", *IEEE Transactions on Vehicular Technology*, vol. 60, no. 4, pp. 1559–1570, May 2011.

[99] Q. Spencer, C. Peel, A. Swindlehurst, and M. Haardt, "An introduction to the multi-user MIMO downlink", *IEEE Communicaitons Magazine*, vol. 42, no. 10, pp. 60–67, October 2004.

[100] C. B. Chae, S. Shim, and R. W. Heath, "Block diagonalized vector perturbation for multiuser MIMO systems", *IEEE Transactions on Wireless Communications*, vol. 7, no. 11, pp. 4051–4057, November 2008.

[101] H. Wang, L. Li, L. Song, and X. Gao, "A linear precoding scheme for downlink multiuser MIMO precoding systems", *IEEE Communications Letters*, vol. 15, no. 6, pp. 653–655, June 2011.

[102] J. Li, R. Chen, and W. Liu, "Lattice reduction aided robust detection and precoding for MIMO systems with imperfect CSI", in *Proceedings of 5th International ICST Conference*, Beijing, China, August 2010, pp. 1–6.

[103] G. Golub and C. V. Loan, *Matrix computaitons*, The Johns Hopkins University Press, 1996.

[104] K. Zu, R. C. de Lamare, and M. Haardt, "Lattice reduction-aided regularized block diagonalization for multiuser MIMO systems", in *Proceedings of IEEE Wireless Communications and Networking Conference (WCNC)*, Paris, France, April 2012, pp. 131–135.

[105] S. Vishwanath, N. Jindal, and A. J. Goldsmith, "On the capacity of multiple input multiple output broadcast channels", in *Proceedings of IEEE International Conference on Communications (ICC)*, New York, USA, April 2002, pp. 1444–1450.

[106] H. Sung, S. Lee, and I. Lee, "Generalized channel inversion methods for multiuser MIMO systems", *IEEE Transactions on Communications*, vol. 57, no. 11, pp. 3489–3409, November 2009.

[107] D. Wbben, D. Seethaler, J. Jaldn, and G. Matz, "Lattice reduction: a survey with applications in wireless communications", *EEE Signal Processing Magazine*, vol. 28, no. 3, pp. 70–91, May 2011.

[108] R. Habendorf and G. Fettweis, "On ordering optimization for MIMO systems with decentralized receivers", in *Proceedings of IEEE Vehicular Technology Conference(VTC)*, Melbourne, Australia, May 2006, pp. 1844–1848.

[109] H. Vetter, V. Ponnampalam, M. Sandell, and P. A. Hoeher, "Fixed complexity LLL algorithm", *IEEE Transaction on Signal Processing*, vol. 57, no. 4, pp. 1634–1637, April 2009.

[110] C. Windpassinger, T. Vencel, and R. Fischer, "Precoding and loading for BLAST-like system", in *Proceedings of IEEE Iternational Conference on Communications (ICC)*, Alaska, USA, May 2003, pp. 3061–3065.

[111] M. Joham, J. Brehmer, and W. Utschick, "MMSE approaches to multiuser spatio-temporal Tomlinson-Harashima precoding", in *Proceedings of ITG Conference Source and Channel Coding*, Germany, January 2004, pp. 208–215.

[112] M. Joham and W. Utschick, "20 Ordered spatial Tomlinson-Harashima precoding", in *Smart antennas state-of-the-art*, vol. 3. New York: EURASIP, Hindawi Publishing Corporation, 2005.

[113] J. Liu and W. Krzymień, "Improved Tomlinson-Harashima precoding for the downlink of multi-user MIMO systems", *Canadian Journal of Electrical and Computer Engineering*, vol. 32, no. 3, pp. 133–144, Summer 2007.

[114] J. Liu and W. Krzymień, "A Novel nonlinear joint transmitter-receiver processing algorithm for the downlink of multiuser MIMO systems", *IEEE Transactions on Vechicular Technology*, vol. 57, no. 4, pp. 2189–2204, July 2008.

[115] C. Fung, W. Yu, and T. Lim, "Precoding for the multiantenna downlink: multiuser SNR gap and optimal user ordering", *IEEE Transactions on Communications*, vol. 55, no. 1, pp. 188–197, January 2007.

[116] N. Dào and Y. Sun, "User-selection algorithms for multiuser precoding", *IEEE Transactions on Vehicular Technology*, vol. 59, no. 7, pp. 3617–3622, September 2010.

[117] V. Stankovic and M. Haardt, "Successive optimization Tomilinson-Harashima precoding (SO-THP) for multi-user MIMO systems", in *Proceedings of IEEE International Conference on Acoustics, Speech, and Signal Processing (ICASSP)*, Philadelphia, USA, March 2005, pp. 1117–1120.

[118] R. C. de Lamare and R. Sampaio-Neto, "Minimum mean squared error iterative successive parallel arbitrated decision feedback detectors for DS-CDMA systems", *IEEE Transaction on Communications*, vol. 56, no. 5, pp. 778–789, May 2008.

[119] R. Fa and R. C. de Lamare, "Multi-branch successive interference cancellation for MIMO spatial multiplexing systems: design, analysis and adaptive implementation", *IET Communications*, vol. 5, no. 4, pp. 484–494, May 2010.

[120] K. Zu and R. C. de Lamare, "Low-complexity lattice reduction-aided regularized block diagonalization for MU-MIMO systems", *IEEE Communication Letters*, vol. 16, no. 6, pp. 925–928, June 2012.

[121] K. Kusume, M. Joham, W. Utschick, and G. Bauch, "Cholesky factorization with symmetric permutation applied to detecting and precoding spatially multiplexed data streams", *IEEE Transactions on Signal Processing*, vol. 55, no. 6, pp. 3089–3103, June 2007.

[122] K. Zu and R. C. de Lamare, "Pre-sorted multiple-branch successive interference cancelation detection for high-dimensional MIMO systems", in *ITG/IEEE Workshop on Smart Antennas*, Dresden, Germany, March 2012, pp. 36–40.